

**DEVELOPMENT OF AN ANALYTICAL MODEL FOR THE
ANALYSIS OF PULLOUT CAPACITY OF ANCHORS
EMBEDDED IN FRICTIONAL SOILS**

by

Azmayeen Rafat Shahriar

A thesis submitted to the Department of Civil Engineering,
Bangladesh University of Engineering and Technology, Dhaka,
in partial fulfillment of the degree of
Master of Science in Civil and Geotechnical Engineering



**DEPARTMENT OF CIVIL ENGINEERING
BANGLADESH UNIVERSITY OF ENGINEERING AND TECHNOLOGY**

MARCH, 2018

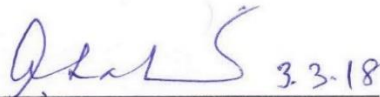
The thesis titled “Development of an Analytical Model for the Analysis of Pullout Capacity of Anchors Embedded in Frictional Soils”, submitted by Azmayeen Rafat Shahriar, Student Number- 0416042203P and session April/2016 has been accepted as satisfactory in partial fulfillment of the requirement for the degree of Master of Science (Civil and Geotechnical Engineering) on 3 March, 2018.

BOARD OF EXAMINERS



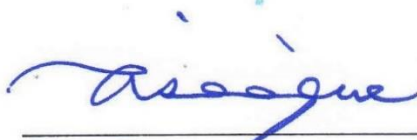
Dr. Mohammad Shariful Islam
Professor
Department of Civil Engineering
BUET, Dhaka-1000

Chairman
(Supervisor)

 3.3.18

Dr. Ahsanul Kabir
Professor and Head
Department of Civil Engineering
BUET, Dhaka-1000

Member
(Ex-Officio)



Dr. Abu Siddique
Professor
Department of Civil Engineering
BUET, Dhaka-1000

Member



Dr. Md. Shahin Hossain
Professor
Department of Civil and Environmental Engineering
Islamic University of Technology (IUT)
Board Bazar, Gazipur-1704

Member
(External)

DECLARATION

I certify that, although I have conferred with others in preparing the thesis and drawn upon a range of sources cited in this work, the content and concept of this thesis is my original work. Neither the thesis nor any part has been submitted to or is being submitted elsewhere for any other purposes.



Azmayeen Rafat Shahriar

TABLE OF CONTENTS

DECLARATION.....	iii
TABLE OF CONTENTS.....	iv
LIST OF FIGURES	vii
LIST OF TABLES	xi
NOTATIONS.....	xii
ACKNOWLEDGEMENT	xv
ABSTRACT.....	xvi
CHAPTER 1: INTRODUCTION.....	1
1.1 General	1
1.2 Background	1
1.3 Research Objectives	2
1.4 Organization of the Thesis	3
CHAPTER 2: LITERATURE REVIEW.....	4
2.1 General	4
2.2 Anchor	4
2.3 Classification of Anchor.....	4
2.3.1 Shallow Anchor.....	5
2.3.2 Intermediate Anchor	5
2.3.3 Deep Anchor	6
2.4 Studies on Anchor Based on Analysis Technique.....	6
2.4.1 Displacement Finite Element Method (DFEM).....	7
2.4.2 Upper Bound Analysis	8
2.4.3 Lower Bound Analysis.....	8
2.4.4 Limit Equilibrium Analysis	9

2.5 Studies on Anchor Based on Analysis Mode	10
2.5.1 Previous Experimental Investigations	10
2.5.2 Previous Analytical Investigations	11
2.5.3 Previous Numerical Investigations	23
2.6 Summary	24
CHAPTER 3: THEORY OF THE PROPOSED MODEL.....	26
3.1 General	26
3.2 Problem Notation	26
3.3 Description of the Proposed Method.....	26
3.4 Idealization of the Failure Mechanism.....	27
3.4.1 Failure Surface in Passive Side	28
3.4.2 Failure Surface in Active Side.....	35
3.4.3 Pressure Distribution on the Failure Surface.....	37
3.4.4 Load Displacement Curve	39
3.4.5 Anchor-soil Interface.....	41
3.4.6 Formation of Side Flanks	44
3.5 Summary	47
CHAPTER 4: DEVELOPMENT OF THE MATHEMATICAL MODEL.....	48
4.1 General	48
4.2 Analysis Technique	48
4.3 Passive Pressure Calculation	48
4.3.1 Passive Pressure in Logarithmic Spiral Surface.....	48
4.3.2 Passive Pressure in Plane Surface	58
4.4 Active Pressure Calculation	61
4.5 Friction Forces around the Anchor.....	63

4.6 Equilibrium of the Anchor 63

4.7 Contribution from the Side Flanks 63

4.8 Summary 74

CHAPTER 5: RESULTS AND DISCUSSIONS 75

5.1 General 75

5.2 Comparison with Experimental Studies 75

5.3 Comparison with Theoretical Studies 83

5.4 Parametric Studies 87

5.4.1 Effect of Friction Angle on Pullout Capacity 87

5.4.2 Effect of Aspect Ratio on Pullout Capacity 88

5.4.3 Effect of Active Pressure Components on Pullout Capacity 89

5.4.4 Effect of Side Flank on Pullout Capacity 92

5.4.5 Effect of Angle of Wall Friction on Pullout Capacity 93

5.5 Why this Model? 96

5.6 Summary 97

CHAPTER 6: CONCLUSIONS AND RECOMMENDATIONS 98

6.1 General 98

6.2 Conclusions 98

6.3 Recommendations for Future Study 99

REFERENCES 101

APPENDIX A 107

APPENDIX B 112

APPENDIX C 126

LIST OF FIGURES

Figure 2.1	Schematic view of a shallow anchor (H = embedment depth, B = height of anchor, P_u = pullout capacity)	5
Figure 2.2	Schematic view of an intermediate anchor.....	6
Figure 2.3	Schematic view of a deep anchor	7
Figure 2.4	Force components assumed by Ovesen and Stromann (1972) for analysis of continuous vertical anchor in frictional soil	13
Figure 2.5	Variation of $K_p \cos \delta'$ with $K_p \sin \delta'$ (Ovesen and Stromann, 1972).....	14
Figure 2.6	Notations adopted by Ovesen and Stromann (1972) for (a) strip anchors, (b) row anchors	15
Figure 2.7	Variation of $(B_e - L)/(H + B)$ with $(S' - L)/(H + B)$ for anchors in frictional soil (Ovesen and Stromann, 1972).....	15
Figure 2.8	Effect of anchor location on pullout capacity of anchor according to NAVFAC DM (1986).....	16
Figure 2.9	Failure wedge geometry for continuous anchor located between Rankine failure surface and slope ϕ' according to NAVFAC DM (1986).....	16
Figure 2.10	Anchor design parameters for (a) continuous wall and (b) individual anchor assumed by NAVFAC DM (1986).....	18
Figure 2.11	Complete set of forces acting on anchor block as per the assumptions of Bowles (1997).....	20
Figure 2.12	Free body diagram of anchor based on the assumptions of Naser (2006)..	21
Figure 2.13	Idealized failure pattern in front of single anchor with acting forces in one face of the wedge according to Jadid et al. (2018) (β = angle subtended by central flank with the vertical, β' = angle subtended by side flank with the vertical, F_{sf} = friction force at the side of the wedge, F_{sn} = normal force at the side of the wedge).....	22
Figure 3.1	Problem notation.....	27
Figure 3.2	Failure surface in the passive side as assumed by Ovesen (1964).	28
Figure 3.3	Failure surface in the passive side as observed by Dickin and Leung (1985) when (a) $H/B = 3$, (b) $H/B = 5$	29
Figure 3.4	Failure surface in the passive side as assumed by NAVFAC DM (1986)...	30
Figure 3.5	Failure surface in the passive side as observed by Choudhury and Dash (2016) when (a) $H/B = 1$, (b) $H/B = 5$	31
Figure 3.6	Failure mechanism idealization by Neely's (1973) surcharge method	32

Figure 3.7	Failure mechanism idealization by Neely's (1973) equivalent free surface method	33
Figure 3.8	Geometry of the passive failure wedge developed in front of (a) a shallow anchor, and (b) an intermediate anchor as assumed in the present study ...	34
Figure 3.9	Failure surface in the active side as per the assumption of Ovesen (1964) and Kame et al. (2012a,b).....	36
Figure 3.10	Failure surface in the active side as per the assumption of Merifield and Sloan (2006)	36
Figure 3.11	Geometry of the active failure wedge developed at the back of anchor as assumed in the present study	37
Figure 3.12	Pressure distribution on the failure surface	38
Figure 3.13	Typical load-deflection curves depicting anchor failure criteria.....	39
Figure 3.14	Design chart to estimate anchor deformation at failure, developed by Neely et al. (1973).....	40
Figure 3.15	Movement of the anchor-soil system due to pullout in (a) a light structure, (b) a heavy structure	43
Figure 3.16	Plan view of the side flank formation during anchor pullout and consideration of equivalent rectangle to replace two triangles.....	47
Figure 4.1	Free body diagram showing the forces acting in logarithmic spiral zone ..	49
Figure 4.2	Free body diagram showing the forces acting in planar zone	58
Figure 4.3	Free body diagram showing passive resistance forces acting on the failure surface.....	60
Figure 4.4	Free body diagram showing the wedge block in active side	62
Figure 4.5	Free body diagram showing the forces acting on anchor	64
Figure 4.6	Formation of side flanks due to pullout force exerted from the tie rod (a) plan view, (b) sectional view	66
Figure 4.7	Schematic view of Zone <i>ODE</i> to estimate the enclosed area	67
Figure 4.8	Geometry of the failure surface in passive side to estimate some anchor parameters.....	68
Figure 4.9	Estimation of the centroid of Zone <i>ODE</i>	69
Figure 4.10	Integration volume to obtain the weight enclosed within the failure surface in side flanks	71
Figure 5.1	Comparison of breakout factors with Neely et al. (1973)	76

Figure 5.2	Comparison of breakout factors with Akinmusuru (1978) and Hoshiya and Mandal (1984)	77
Figure 5.3	Comparison of breakout factors with Dickin and Leung (1983).....	78
Figure 5.4	Comparison of breakout factors with Dickin and Leung (1985).....	79
Figure 5.5	Comparison of breakout factors with existing theoretical prediction techniques with the experimental force coefficients reported in Dickin and Leung (1985) corresponding to 50 mm high anchor	81
Figure 5.6	Comparison of breakout factors with existing theoretical prediction techniques with the experimental force coefficients reported in Dickin and Leung (1985) corresponding to 25 mm high anchor	82
Figure 5.7	Comparison of breakout factors with Merifield and Sloan (2006), and Neely (1973).....	84
Figure 5.8	Comparison of breakout factors with Meyerhof (1973).....	85
Figure 5.9	Comparison of breakout factors with Merifield and Sloan (2006), and Basudhar and Singh (1994)	87
Figure 5.10	Effect of friction angle on the force coefficient for an anchor with a height of 50 mm.....	88
Figure 5.11	Effect of aspect ratio on the force coefficient for an anchor with a height of 50 mm	90
Figure 5.12	Effect of active pressure components on the breakout factor.....	91
Figure 5.13	Effect of active pressure components on the force coefficient.....	92
Figure 5.14	Effect of consideration of fide flanks on the force coefficient	94
Figure 5.15	Change of δ/φ' with H/B and L/B for a typical concrete anchor	95
Figure 5.16	Evaluation of different methods with respect to reliability and MAPE	96
Figure B-1	Variation of K with the change of φ' and γ for a 0.1m high anchor	112
Figure B-2	Variation of K with the change of φ' and γ for a 0.2m high anchor	113
Figure B-3	Variation of K with the change of φ' and γ for a 0.3m high anchor	114
Figure B-4	Variation of K with the change of φ' and γ for a 0.4m high anchor	115
Figure B-5	Variation of K with the change of φ' and γ for a 0.5m high anchor	116
Figure B-6	Variation of K with the change of φ' and γ for a 0.6m high anchor	117
Figure B-7	Variation of K with the change of φ' and γ for a 0.7m high anchor	118

Figure B-8	Variation of K with the change of φ' and γ for a 0.8m high anchor.....	119
Figure B-9	Variation of K with the change of φ' and γ for a 0.9m high anchor.....	120
Figure B-10	Variation of K with the change of φ' and γ for a 1.0m high anchor.....	121
Figure B-11	Variation of K with the change of φ' and γ for a 2.0m high anchor.....	122
Figure B-12	Variation of K with the change of φ' and γ for a 3.0m high anchor.....	123
Figure B-13	Variation of K with the change of φ' and γ for a 4.0m high anchor.....	124
Figure B-14	Variation of K with the change of φ' and γ for a 5.0m high anchor.....	125

LIST OF TABLES

Table 2.1 Model tests and field tests on vertical anchor plate in frictional soil.....	12
Table 2.2 Model tests and field tests on vertical anchor block in frictional soil.	12
Table 2.3 Analytical studies on vertical anchors in frictional soil.....	13
Table 2.4 Anchor design methodology as per NAVFAC DM (1986)	17
Table 2.5 Numerical studies on vertical anchors in frictional soil	23
Table C-1 Integrals and k value corresponding to a given ϕ'	126

NOTATIONS

The following symbols are used in this thesis:

B	height of the anchor
B_e	equivalent length of anchor
F_b	friction force at the bottom of the anchor
F_{bf}	friction force at the bottom of the wedge
F_{bn}	normal force at the bottom of the wedge
F_s	friction force at two sides of the anchor
F_{sf}	friction force at the side of the wedge
F_{sn}	normal force at the side of the wedge
F_t	friction force at the top of the anchor
F_δ	anchor roughness coefficient
H	depth of embedment of the anchor
K_a	coefficient of active lateral earth pressure
K_o	coefficient of lateral earth pressure at rest
K_p	coefficient of passive lateral earth pressure
L	width of the anchor
$M_{\gamma q}$	anchor force coefficient
M	passive resistance coefficient
m	mobilization factor
N_b	normal force at the bottom of the anchor
N_γ	anchor breakout factor
P	pressure at any point on the logarithmic spiral surface
P_{AH}	horizontal component of resultant active thrust
P_{AV}	vertical component of resultant active thrust
P_E	pressure at point E on the failure surface
P_F	pressure at point F on the failure surface
P_P	pressure at point P on the failure surface
P_R	pressure at point R on the failure surface
P_i	pullout capacity at any instant

P_{PH}	horizontal component of resultant passive thrust
P_{PV}	vertical component of resultant passive thrust
P_u	ultimate pullout capacity from plane strain condition
$P_{u_{side}}$	pullout capacity from side flanks
$P_{ultimate}$	ultimate pullout capacity
R_{AP}	reactive active force acting on plane surface
R_{APH}	horizontal component of reactive active force on plane surface
R_{APV}	vertical component of reactive active force on plane surface
R_{PL}	reactive passive force acting on logarithmic spiral surface
R_{PLH}	horizontal component of reactive passive force acting on logarithmic spiral surface
R_{PLV}	vertical component of reactive passive force acting on logarithmic spiral surface
R_{PP}	reactive passive force acting on plane surface
R_{PPH}	horizontal component of reactive passive force acting on plane surface
R_{PPV}	vertical component of reactive passive force acting on plane surface
q	surcharge pressure
$q_{u(rough)}$	ultimate pullout capacity for rough anchors
$q_{u(smooth)}$	ultimate pullout capacity for smooth anchors
r	instantaneous radius of log-spiral surface
r_o	starting radius of logarithmic spiral surface
r_1	maximum radius of logarithmic spiral surface
S'	centre to centre distance between two anchors
t	thickness of the anchor block
u	horizontal anchor displacement at any instant
V	total volume of soil contained within the failed surface
W	weight of the wedge block within the failure surface in side flanks
W_a	weight of soil contained within plane surface in active side
W_b	weight of the anchor
W_l	weight of soil contained within logarithmic spiral surface
W_p	weight of soil contained within plane surface in passive side
φ'	angle of internal friction of soil

φ_{cp}	critical state friction angle
φ_{ps}	peak plane strain angle
ψ'	dilatancy angle of soil
γ	unit weight of soil
γ'_b	effective unit weight of anchor material
α'	angle of side flanks of the wedge
δ_{max}	maximum angle of friction between soil and anchor
δ_t	angle of friction between soil and top surface of the anchor
δ_b	angle of friction between soil and bottom surface of the anchor
δ_s	angle of friction between soil and side surface of the anchor
δ_p	angle of friction between soil and anchor in the passive side
δ_a	angle of friction between soil and anchor in the active side
δ'	angle of wall friction
θ	spiral angle
θ_m	maximum spiral angle
α	inclination of tangent at the point of interest with the horizontal
σ	effective normal stress
u	allowable anchor deflection
Δ_u	anchor deformation at failure

ACKNOWLEDGEMENT

The author would like to express his sincere gratitude to Dr. Mohammad Shariful Islam, Professor, Department of Civil Engineering, BUET for his sincere supervision, comprehensive discussions, encouraging comments, stimulating working enthusiasm and valuable suggestions throughout the research work. His devotion for guidance and constant encouragement strongly supported me to complete the present research work in this manner. It was a great honor for me to get the opportunity to work under his supervision and it was quite impossible for me to complete the entire study without his unremitting guidance and inspirations. He often went beyond the call of duty in encouraging and supporting the goals of the research and providing his expertise.

The author would like to express his heartfelt thanks to Dr. Ahsanul Kabir, Professor and Head, Department of Civil Engineering, BUET, for the valuable time he provided as member of my advisory committee. The author would also like to take the opportunity of expressing sincere appreciation to Dr. Abu Siddique, Professor, Department of Civil Engineering, BUET, for supporting me whenever I asked for any help to focus on my research work. The author is indebted to Dr. Md. Shahin Hossain, Professor, Department of Civil and Environmental Engineering, Islamic University of Technology (IUT) for his kind consent to be the member of my advisory committee. His co-operation and essential suggestions helped me to prepare the thesis in a more refined way. Author also expresses his sincere thanks to Mr. Shohel Ahmed, Assistant Professor, Department of Mathematics, BUET for his cooperation during the development of the model.

I greatly appreciate my wife for her continuous inspiration and support during my research work. I also acknowledge my family members especially my mother and brothers for their blessing and love which provided me the courage to complete the work. Lastly, I want to dedicate this work in the memory of my late father, who used to keep belief and faith in my capabilities.

ABSTRACT

Anchors, made of steel, pre-cast or cast-in-place concrete, timber are generally designed and constructed to resist outwardly directed loads imposed on the foundation of a structure. Depending on the placement, it may be horizontal, vertical or inclined. The aim of the present study is to develop an analytical model for the estimation of pullout capacity of vertical anchors embedded in frictional soils. The analytical model can consider more realistic variations in pullout capacity due to installation at a wider range of embedment depth. The model is based on the principle of limit equilibrium. The predictions from the developed analytical expression were compared to the available experimental and numerical investigations.

Results show that the present model can predict the pullout capacity of shallow and intermediate anchors with more accuracy and reliability compared to the available pullout capacity prediction models. In addition, a comprehensive parametric study is also presented. It is found that with the increase of friction angle (φ'), pullout capacity increases significantly, the effect being higher at high friction angles ($\varphi' > 30^\circ$). The demarcation aspect ratio (ratio of anchor length to height) between single and continuous anchor is 10 rather than 5, which was proposed by Das (1990). Parametric studies further reveal that the active pressure components although play an insignificant role at an embedment depth ratio of less than 2.5, the effect is substantial thereafter. It appears that omission of contribution from side flanks results in a discrepancy of as much as 37% in highly frictional soils at an embedment depth ratio (H/B) greater than 3. Finally, it is observed that a constant value of δ/φ' assumed in most pullout capacity prediction models for all the range of H/B and L/B to analyze the pullout capacity is not actually valid. The present study suggests a cautious selection of δ/φ' parameter for square anchors and anchors laid at $H/B < 4$.

Chapter 1

INTRODUCTION

1.1 General

The design of geotechnical structures, such as sheet pile walls, bulkheads, bridge abutments, and retaining walls requires foundation systems which can withstand horizontal pullout forces. In such circumstances, internally stabilized foundation systems, like soil anchoring, can provide an efficient and economical design solution. These anchors are usually tied to the retaining structure and are buried deep enough that they can safely withstand pullout forces (Merifield and Sloan, 2006). However, before the mid of nineteenth century, stabilizing structures using anchoring techniques was quite unthinkable. Recently, anchors are used to stabilize structures like suspension bridges, transmission towers, radar towers, aircraft moorings, submerged pipelines and tunnels. Anchors are now embedded not only in frictional soils but also in cohesive soils and rocks. Research showed that the use of anchors in a retaining structure may reduce the construction cost as much as 43 to 64% (Khan and Sikder, 2004). Nevertheless, inadequate anchorage systems constitute most of the causes of failure of retaining structures (Daniel and Olson, 1982).

1.2 Background

Anchor plates, anchor blocks, tie backs, and anchor beams supported by batter pile are some of the common types of anchors used for soil reinforcement. An anchor is a precast or cast-in-place member that may be rectangular, square or circular in shape, with necessary geometry and depth to mobilize adequate passive pressure (Bowles, 1997). Installation of an anchor requires excavation of the ground to the required depth, placement of the anchor, and backfilling with suitable soil (Merifield and Sloan, 2006). While used for retaining waterfront structure, or sheet pile walls, anchors are attached to tie rods either by driving or placing through augured holes. This type of anchor is of prime interest in the present study.

Literature reveals that many researches have been conducted on the capacity of vertical anchors especially for anchor plate including that by Hueckel (1957), Ovesen and

Stromann (1972), Neely et al. (1973), Das (1975), Akinmusuru (1978), Rowe and Davis (1982), Murray and Geddes (1989), Ghaly (1997), Merifield and Sloan (2006), and Chowdhary and Dash (2016) etc. On the contrary, Bowles (1997), Duncan and Mokwa (2001), Naser (2006), Khan et al. (2017) conducted research on anchor block (limited aspect ratio). It is to be noted that the theoretical methods of calculating pullout capacity of vertical anchor plate are commonly employed for anchor block as well.

The majority of past research has been experimental based and, as a result, current design practices are largely based on empiricism. In contrast, very few thorough theoretical and numerical analyses have been performed to determine the ultimate pullout loads of anchor. Of the numerical studies that have been presented in the literature, few can be considered as rigorous.

From the existing research state, it seems that analytical studies to assess the pullout capacity of anchors are very few. Consequently, the present research work aims to propose an analytical model to estimate the ultimate pullout capacity of a vertical anchor embedded in frictional soil utilizing the principle of limit equilibrium. The analytical model will be capable to capture more realistic variations in pullout capacity due to installation at a wider range of embedment depth. In the meantime, reliability and stability of the model would be observed through comparison with the existing laboratory and field test data. The differences in inherent assumptions among the pullout capacity prediction models will be discussed while comparing to the model of the present study. The comparison is useful, because in the daily practice of geotechnical engineering many discussions arise on the choice of model at any particular set of conditions. Finally, conclusions will be drawn from the presented results.

1.3 Research Objectives

The present study aims to achieve the following objectives:

- i) To propose a new closed form analytical model to predict the ultimate pullout capacity of an anchor embedded at shallow and intermediate depth in the frictional soil utilizing the principle of limit equilibrium.
- ii) To quantify the contribution of side flanks developed due to pullout force exerted from the retaining structure via attachment to a rebar, thus providing a clear distinction between conventional plane strain case and actual 3-D

situation.

- iii) To validate the proposed model with the laboratory and full-scale model tests available in the present state of literature.
- iv) To conduct an extensive parametric study and observe the influencing parameters on which the ultimate pullout capacity depends.

1.4 Organization of the Thesis

The thesis consists of six chapters. A brief introduction on each chapter will now follow.

Chapter 1 contains an introduction that includes the problem statement, background and objective of this study along with the thesis organization.

Chapter 2 presents the literature review including the experimental, theoretical and numerical studies conducted on anchor block and plate. In addition, discrepancies among the assumptions in existing pullout capacity prediction models are discussed.

Chapter 3 introduces the theory and the basic assumptions of the proposed model. The idealization of failure mechanism is clearly expressed in the chapter.

Chapter 4 provides an elaborate mathematical insight into the analytical model to estimate the pullout capacity of an anchor embedded at shallow and intermediate depth.

Chapter 5 shows the comparison of the proposed model with the existing experimental and theoretical studies. After that a parametric study is also presented.

Finally, in Chapter 6, the main conclusions drawn from the study are pointed out. In addition to that some recommendations for future work are also provided.

Chapter 2

LITERATURE REVIEW

2.1 General

This chapter presents a summary of research into vertical anchor plate or block behavior in order to provide a satisfactory background of subsequent discussions. A comprehensive overview on the topic of anchors is given by Das (1990). As the research work aims to focus on the analysis of an anchor embedded in frictional soil, a brief summary of existing research on relevant topic herein has been presented. Author took an attempt to present a selective overall summary of research into the behavior of anchors embedded in frictional soils.

2.2 Anchor

Anchors are generally designed and constructed to resist outwardly directed loads imposed on the foundation of a structure (Das, 1990). These loads are transmitted to soil by earth anchors. These are generally made of steel, pre-cast or cast-in-place concrete, timber etc. Depending on the placement, it may be horizontal, vertical or inclined. Anchors are generally installed by excavating up to the desired depth, then placing the anchor and finally backfilling with good quality soil. If such technique is adopted, then, it is referred to as backfilled anchors. In this study backfilled vertical anchor will be discussed.

2.3 Classification of Anchor

The ratio of the distance between existing ground surface and the bottom of the anchor, H to the height of the anchor, B is termed as embedment depth ratio. This is a very significant parameter in identification of the behavior of an anchor. Depending on the embedment depth ratio, an anchor can be classified as (i) shallow, (ii) intermediate, or (iii) deep. A brief description of each of the classification is presented in subsequent discussions.

2.3.1 Shallow Anchor

Das (1990) suggested that when the embedment depth ratio (H/B) is less than 3, the anchor is considered to be shallow. However, Terzaghi (1948) suggested that this ratio should be up to 2, for an anchor to be shallow. Dickin and Leung (1985) observed that the resistance of such shallow anchors is primarily governed by the anchor roughness and weight. Das (1990) and Merifield and Sloan (2006) suggested that neglecting the active force generated on the back side of the anchor might lead to significant error for such anchors. In case of shallow anchors, the failure plane reaches the ground surface at limit equilibrium condition. Figure 2.1 shows schematic view of a shallow anchor.

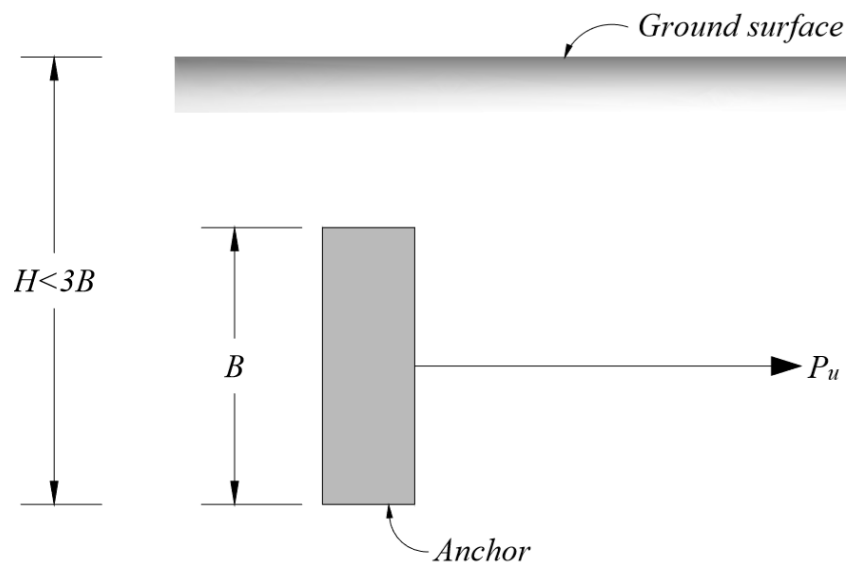


Figure 2.1 Schematic view of a shallow anchor (H = embedment depth, B = height of anchor, P_u = pullout capacity)

2.3.2 Intermediate Anchor

Although in some literature (Kame et al. 2012a; Choudhary and Dash, 2016), intermediate anchors are also classified as shallow anchors, Dickin and Leung (1985) observed that for a range of embedment depth ratio, consideration of smooth anchor (angle of wall friction = 0) provided strong agreement with the experimental results. Consequently, another classification named intermediate anchor was added. For such anchors, H/B varies from 3 to 8. Although, in some studies it was observed that the failure surface reached the ground surface for anchors laid at such depths, however, no conclusive evidence was found to support the observation undoubtedly. Chowdhary and Dash (2016) did observe both the phenomena to occur at intermediate depth. However,

density of the soil might have played an important role in identifying the failure pattern. Figure 2.2 shows schematic view of an intermediate anchor.

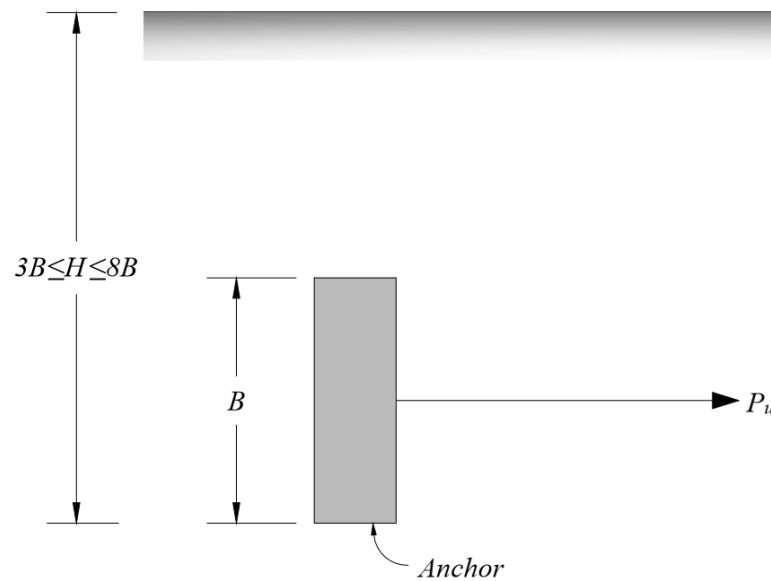


Figure 2.2 Schematic view of an intermediate anchor

2.3.3 Deep Anchor

Biarez et al. (1965) suggested that if the embedment depth increases beyond 8, then the failure mechanism changes. The failure becomes localized in such cases; thus, failure is termed as rotational failure (Figure 2.3). They derived an equation considering the couple required for the rotation of the cylinder of soil on front of the anchor which provides close agreement with experimental data. The relation can be expressed as-

$$M_{\gamma q} = 4\pi \left(\frac{H}{B} - 1 \right) \tan \varphi' \quad (2.1)$$

Where, $M_{\gamma q}$ = anchor force coefficient, H = embedment depth of anchor, B = height of anchor and φ' = angle of internal friction of the soil in which the anchor was embedded.

2.4 Studies on Anchor Based on Analysis Technique

At present, there are a number of techniques available for use by geotechnical practitioners and researchers when analyzing geotechnical problems. Depending on the analysis technique, the total researches on anchor can be classified into four categories. These are-

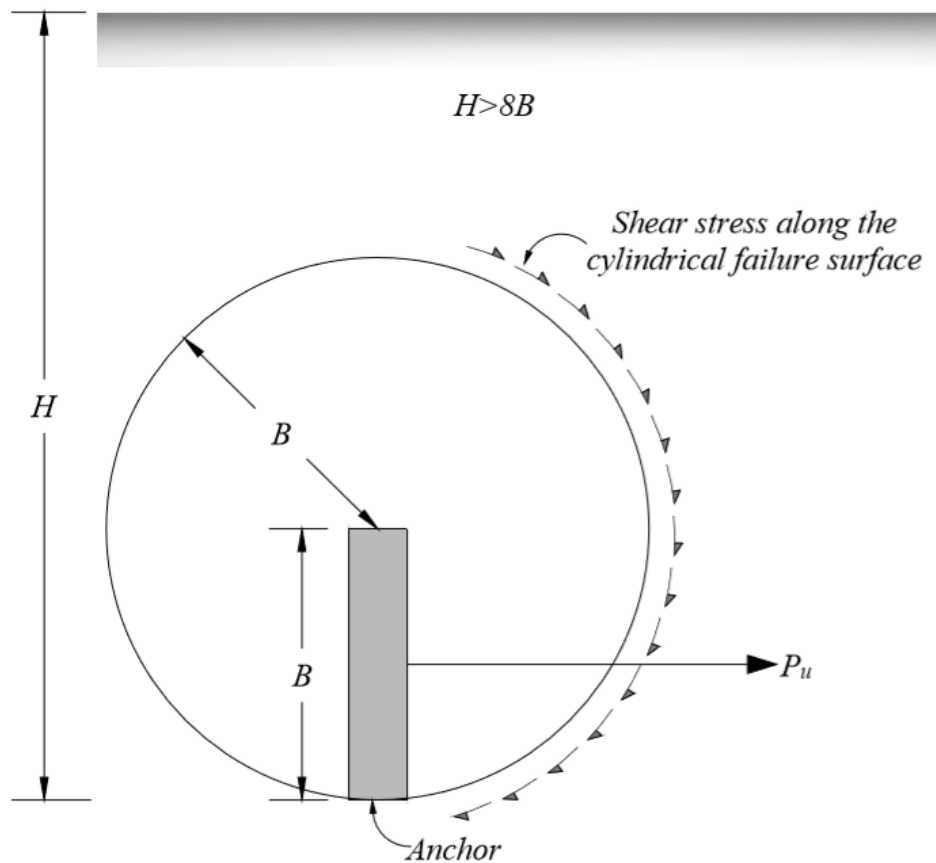


Figure 2.3 Schematic view of a deep anchor

- i) Displacement Finite Element Method (DFEM)
- ii) Upper bound limit analysis
- iii) Lower bound limit analysis
- iv) Limit equilibrium analysis

In addition to the above-mentioned categories, some researchers adopted the method of characteristics. In the next couple of sections some of the available analysis techniques will be discussed in brief.

2.4.1 Displacement Finite Element Method (DFEM)

The displacement finite element technique is now widely used for predicting the load-deformation response, and hence, collapse of geotechnical structures. This technique can deal with complicated loadings, excavation and deposition sequences, geometries of arbitrary shape, anisotropy, layered deposits, and complex stress-strain relationships. Although the ability to incorporate all of these variables can be a distinct advantage when compared to other methods of analysis, it can also be perceived as the greatest disadvantage of the method. In practice, great care must be exercised when finite element

analysis is employed to predict collapse loads. Merifield and Sloan (2006) suggested that such an analysis needs to be performed by qualified and experienced personnel. Even for quite simple problems, experience has indicated that results from the displacement finite element method tend to overestimate the true limit load and, in some instances, fail to provide a clear indication of collapse altogether. The ability of this technique to accurately predict incipient collapse has been studied in Toh and Sloan (1980) and Sloan and Randolph (1982). Researchers who performed DFEM include Sloan (1988), Sloan and Kleeman (1995), Merifield and Sloan (2006).

2.4.2 Upper Bound Analysis

Drucker et al. (1952) developed two limit theorems which are widely used by the geotechnical engineers of the current time. The upper bound limit theorem is one of the two theorems. The upper bound limit theorem is used to bracket the exact ultimate load from above and is based on the notion of a kinematically admissible velocity field. A kinematically admissible velocity field is simply a failure mechanism in which the velocities satisfy both the flow rule and the velocity boundary conditions. To be kinematically admissible, a velocity field must satisfy the set of constraints imposed by compatibility, the velocity boundary conditions, and the flow rule. After prescribing a set of velocities along a specified boundary segment, we can equate the power dissipated internally (caused by plastic yielding within the soil mass and sliding of the velocity discontinuities) to the power dissipated by the external loads to yield a strict upper bound on the true limit load. Upper bound limit analysis was performed by Sloan (1989), Lyamin and Sloan (2002), Kumar and Sahoo (2012) to estimate the ultimate pullout capacity.

Chowdhary and Dash (2016) experimentally observed that in case of shallow anchor, soil undergoes an unrestricted plastic flow, leading to catastrophic failure. Thus, load carrying capacity of shallow anchors can be better estimated by upper bound limit analysis.

2.4.3 Lower Bound Analysis

This is the second theorem developed by Drucker et al. (1952). The lower bound limit theorem is used to bracket the exact ultimate load from below and is based on the notion of a statically admissible stress field. A statically admissible stress field is one where the stresses satisfy equilibrium, the stress boundary conditions, and the yield criterion. The lower bound solution is obtained by modeling a statically admissible stress field using

finite elements where stress discontinuities can occur at the interface between adjacent elements. Application of the stress boundary conditions, equilibrium equations, and yield criterion leads to an expression of the collapse load, which is maximized subject to a set of constraints on the stresses. The lower bound theorem states that if an equilibrium distribution of stress covering the whole body can be found that balances a set of external loads on the stress boundary and nowhere exceeds the yield criterion of the material, the external loads are not higher than the true collapse load. By examining different admissible stress states, the best lower bound value on the external loads can be found. In analyzing pullout capacity, Basudhar and Singh (1994), Smith (1998), Merifield et al. (2006) adopted lower bound limit analysis technique.

In contrast to the observation of Chowdhary and Dash (2016) for shallow anchor, deep anchor follows different pattern. Deep anchor undergoes constrained plastic deformation owing to the overlying surcharge, and complete collapse is inhibited. Thus, it can be understood that load carrying capacity of deep anchors can be better estimated by lower bound limit analysis.

2.4.4 Limit Equilibrium Analysis

The limit equilibrium method is traditionally used to obtain approximate solutions for the stability problems in soil mechanics. The method entails an assumed failure surface of various simple shapes viz. plane, circular, logarithmic spiral. With this assumption, each of the stability problems is reduced to finding one of the most dangerous position of the failure or slip surface of the shape chosen which may not be particularly well founded, but quite often gives acceptable results. In this method, it is also necessary to make certain assumptions regarding the stress distribution along the failure surface such that the overall equation of equilibrium, in terms of stress resultants, may be written for a given problem. Therefore, this simplified method is used to solve various problems by simple statics. Although, the limit equilibrium technique utilizes the basic concept of upper-bound rules of limit analysis, that is, a failure surface is assumed, and a least answer is sought, it does not meet the precise requirements of upper bound rules, so it is not an upper bound. The method basically gives no consideration to soil kinematics, and equilibrium conditions are satisfied in a limited sense. It is clear that a solution obtained using limit equilibrium method is not necessarily upper or lower bound. However, any upper-bound limit analysis solution will obviously be limit equilibrium solution.

2.5 Studies on Anchor Based on Analysis Mode

Based on the mode of analysis, like whether the research was experiment based or theory based, the researches on anchor can be divided into three main segments. These are-

- i) Previous experimental investigations
- ii) Previous analytical investigations
- iii) Previous numerical investigations

A brief description about each of the above-mentioned divisions is provided as under-

2.5.1 Previous Experimental Investigations

Although there are no entirely adequate substitutes for full-scale field testing, tests at the laboratory scale have the advantage of allowing close control of at least some of the variables encountered in practice. In this way, trends and behavior patterns observed in the laboratory can be of value in developing an understanding of performance at larger scales. In addition, observations made in laboratory testing can be used in conjunction with mathematical analyses to develop semi-empirical theories. These theories can then be applied to solve a wider range of problems. The experimental studies on anchor can be classified into two categories which will be discussed in the subsequent paragraphs.

Experimental investigations into plate anchor behavior have generally adopted one of two approaches, namely, conventional methods under *normal gravity* conditions or *centrifuge systems*. Of course, both methods have advantages and disadvantages, and these must be borne in mind when interpreting the results from experimental studies of anchor behavior. Numerous investigators have performed model tests in an attempt to develop semi-empirical relationships that can be used to estimate the capacity of anchors in cohesionless soil. This is evidenced by the number of studies shown in Tables 2.1 and 2.2. More specific details of these studies are provided in later chapters of the thesis when several previous laboratory studies are compared with the new theoretical predictions obtained in the current study.

Prior to 1970, investigations into the field and (or) model testing of horizontal circular anchors or belled piles were conducted by Mors (1959), Giffels et al. (1960), Balla (1961), Turner (1962), Kananyan (1966), Baker and Kondner (1966), and Adams and Hayes (1967). A number of these studies were primarily concerned with testing foundations for transmission towers (Mors, 1959; Balla, 1961; Turner, 1962). In the

majority of these earlier studies, a failure mechanism was assumed, and the pullout capacity was then determined by considering the equilibrium of the soil mass above the anchor and contained by the assumed failure surface. This assumed failure surface ranged within a large variation of pattern.

In contrast to the previous researches on anchor plates, very few experimental studies were found to be reported on anchor blocks (limited L/B). Only three researches (Duncan and Mokwa, 2001; Naser, 2006; and Khan et al., 2017) were found to study the behavior of anchor blocks. Table 2.2 summarizes the experimental studies conducted on anchor blocks. However, observation reveals that only Duncan and Mokwa (2001) conducted field test, whereas the rest two researches focused on laboratory model test. One important observation includes the inability of the present researches to explore the behavior of intermediate and deep anchors. Duncan and Mokwa (2001) investigated the response of anchor blocks placed flush with the ground surface using two backfill materials. Naser (2006) observed the effect of saturation on the pullout capacity. Khan et al. (2017) investigated the response of the anchor blocks when it is placed at different distances from the yielding retaining wall. Nevertheless, the maximum embedment ratio investigated by the researchers is 3.2, which falls under the shallow anchor category. This leaves a lot of space for the present researchers to focus on the anchor block behavior embedded at intermediate and deep depths.

2.5.2 Previous Analytical Investigations

The previous analytical studies post-1970 for vertical anchors, are commonly used by practicing engineers. In general, the analytical methods of calculating pullout capacity of vertical anchor plates are commonly employed for anchor block (Das, 2007). Previous analytical studies of anchors in sand have typically utilized simple approach such as limit equilibrium. In Table 2.3, an attempt was taken to present the number of analytical studies conducted in post-1970 period. It is evident that analytical investigations hardly focused on anchor behavior beyond an embedment depth of 5. In addition, it is apparent that analysis method took place in one of the three forms, such as- empirical, semi-empirical and limit equilibrium. Again, methods proposed by Bowles (1997), Naser (2006), Jadid et al. (2018) were found to be strictly applicable to block anchors.

Table 2.1 Model tests and field tests on vertical anchor plate in frictional soil

Source	Type of testing	Anchor shape	Anchor size (mm)	ϕ' (°)	H/B
Heuckel (1957)	Chamber	Square	75–200	34.0	2
Smith (1962)	Field	Rectangular; $L/B = 1.25, 5$	915	38.5	1–4.5
Neely et al. (1973)	Chamber	Square; rectangular	50.8	38.5	1–5
Das (1975)	Chamber	Square; circular	38–76	34.0	1–5
Das and Seely (1975)	Chamber	Square; rectangular; $L/B = 1, 3, 5$	51	34.0	1–4
Akinmusuru (1978)	Chamber	Strip; rectangular; square; circular; $L/B = 2, 10$	50	24.0 35.0	1–10
Ovesen (1981)	Centrifuge; Field	Square	20	29.5– 37.7	1–3.39
Rowe and Davis (1982)	Sand Chamber	Square; rectangular; $L/B = 1–8.75$	51	32.0	1–8
Dickin and Leung (1983, 1985)	Centrifuge; Chamber	Square; rectangular; strip	25; 50	41.0 ^a	1–8 1–13
Hoshiya and Mandal (1984)	Chamber	Square; rectangular; $L/B = 2, 4, 6$	25.4	29.5	1–6
Murray and Geddes (1989)	Chamber	Square; rectangular; $L/B = 1–10$	50.8	43.6 dense	1–8
Dickin and King (1997)	Centrifuge	Rectangular; $L/B = 7.8$	25	37.3– 46.1	1–12
Chowdhary and Dash (2016)	Chamber	Square	100	32.0– 39.0	1–9

^aMobilized plane strain friction angle, ϕ'_{mp}

Table 2.2 Model tests and field tests on vertical anchor block in frictional soil

Source	Type of testing	Anchor block shape	Anchor block size (mm)	ϕ' (°)	H/B
Duncan and Mokwa (2001)	Field	Rectangular; $L/B = 1.7$	1100×1900×900	50.0	1.0
Naser (2006)	Chamber	Square	150×150×150	43.5	2.0
Khan et al. (2017)	Chamber	Square	150×150×75	37.2– 44.8	3.2

Table 2.3 Analytical studies on vertical anchors in frictional soil

Source	Analysis method	Anchor shape	Anchor roughness	ϕ' ($^\circ$)	H/B
Ovesen and Stromann (1972)	Semi-empirical	Plate	Smooth	25–45	1–3
NAVFAC DM (1986)	Limit equilibrium	Plate	Smooth	Loose; Dense	1–5
BS 8006 (1995)	Semi-empirical	Plate	Smooth	Loose; Dense	1–5
Ghaly (1997)	Empirical	Plate	Rough	34–38.5	1–4
Bowles (1997)	Limit equilibrium	Block	Rough	Loose; Dense	1–5
Naser (2006)	Limit equilibrium	Block	Rough	Loose; Dense	1–5
Jadid et al. (2018)	Limit equilibrium	Block	Rough	0–45	1–3

Thus, formulation of an analytical model applicable to both plate and block anchor deemed necessary. In the subsequent discussions, some of the commonly used analytical methods will be briefly discussed.

Ovesen and Stromann (1972) proposed a semi-empirical method for determining the ultimate resistance of anchors in sand. The ultimate pullout resistance of a continuous anchor as shown in Figure 2.4, per unit length of anchor, P'_u can be calculated from Eq. (2.2).

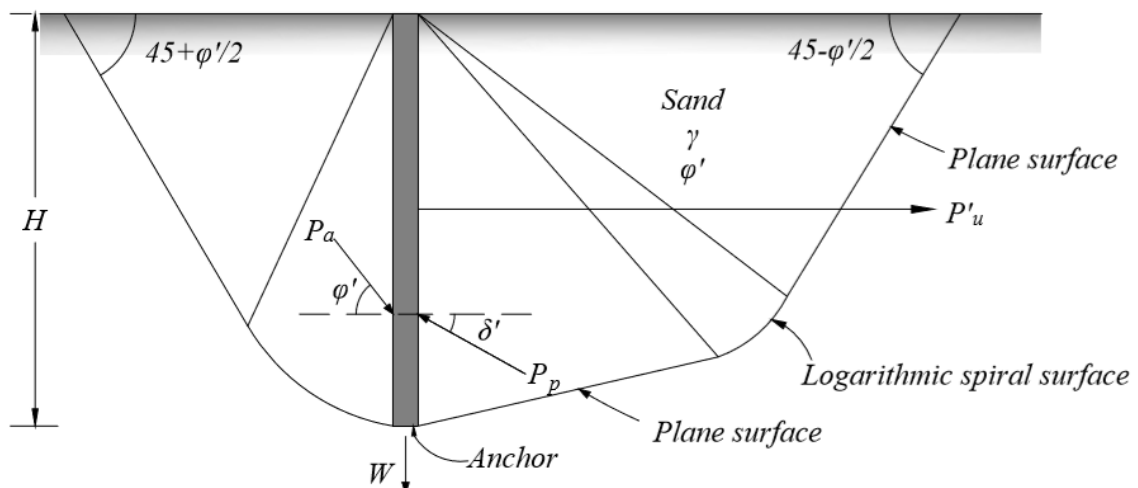


Figure 2.4 Force components assumed by Ovesen and Stromann (1972) for analysis of continuous vertical anchor in frictional soil

$$P'_u = \frac{1}{2} \gamma H^2 (K_p \cos \delta' - K_a \cos \varphi') \quad (2.2)$$

The term $K_p \cos \delta'$ of Eq. (2.2) can be obtained from Figure 2.5 using the value of $K_p \sin \delta' = (W + 0.5\gamma H^2 K_a \sin \varphi') / (0.5\gamma H^2)$ and the angle of internal friction φ' . Here, W is the effective weight per unit length of anchor and coefficient of active and passive earth pressures, K_a, K_p respectively are based on the assumption that $\delta' = \varphi'$ i.e. angle of wall friction=angle of internal friction.

For a continuous strip anchor (Figure 2.6(a)) of height B (which is less than the depth of embedment, H), the ultimate resistance per unit length is corrected as:

$$P'_{us} = \left[\frac{C_{ov} + 1}{C_{ov} + \frac{H}{B}} \right] P'_u \quad (2.3)$$

Where, P'_{us} is the ultimate resistance for strip case, $C_{ov} = 19$ for dense sand and 14 for loose sand.

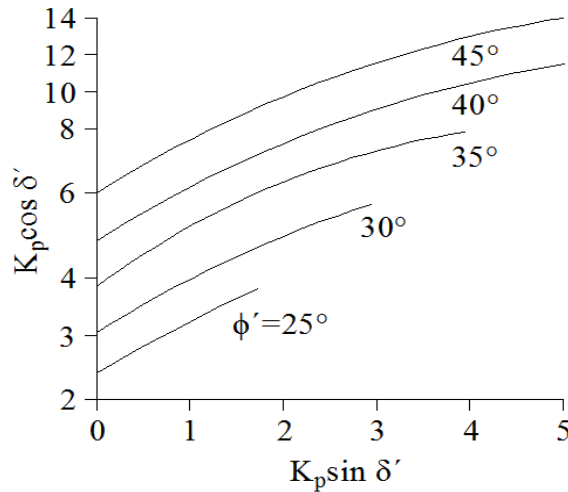


Figure 2.5 Variation of $K_p \cos \delta'$ with $K_p \sin \delta'$ (Ovesen and Stromann, 1972)

In practice, the anchor plates are placed in a row with center-to-center spacing, S' (Figure 2.6(b)). The ultimate resistance of each anchor of length, L is

$$P'_u = P'_{us} B_e \quad (2.4)$$

Where, B_e is the equivalent length and can be obtained from Figure 2.7. It is important to note that the terms dense and loose are subjective in nature. The proponents did not

provide a clear distinction between the two categories. Thus, application of the method requires proper engineering judgement.

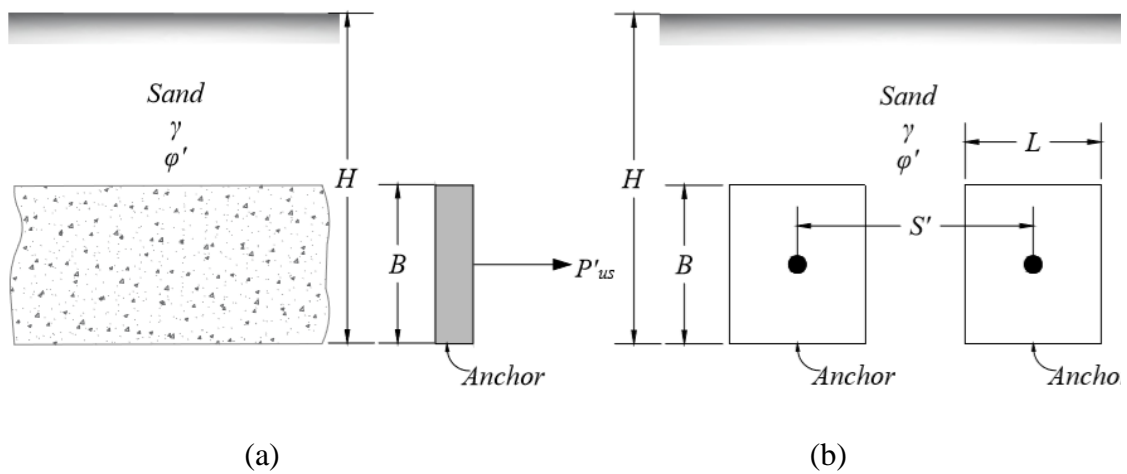


Figure 2.6 Notations adopted by Ovesen and Stromann (1972) for (a) strip anchors, (b) row anchors

According to NAVFAC DM (1986), the anchors should be placed outside the surface making an angle equal to angle of friction of backfill soil, ϕ' with the horizontal as shown in Figure 2.8. To summarize, in Figure 2.8, anchor block left of bc will provide no resistance, again anchor block right of bf will provide full resistance. However, anchor block between bc and bf will provide partial resistance.

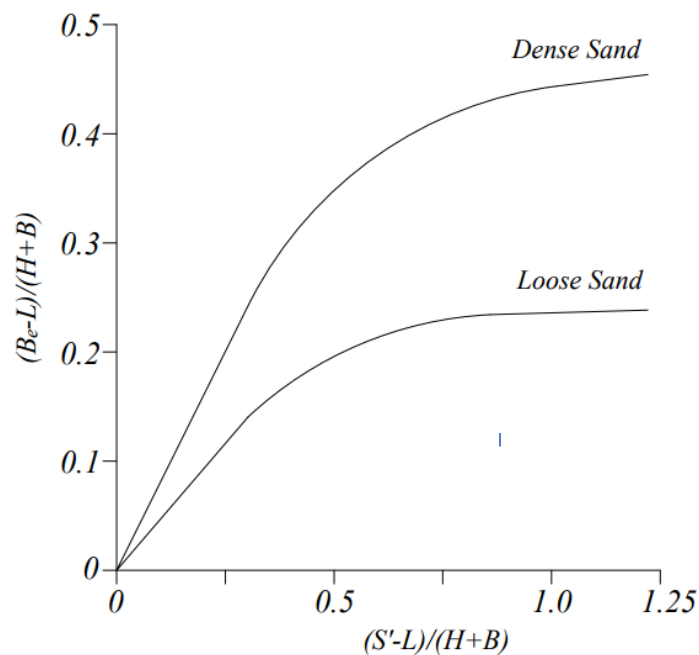


Figure 2.7 Variation of $(B_e - L)/(H + B)$ with $(S' - L)/(H + B)$ for anchors in frictional soil (Ovesen and Stromann, 1972)

Table 2.4 Anchor design methodology as per NAVFAC DM (1986)

Step No.	Methodology
	<p>In Figure 2.9, if anchor is placed right to CC', and in addition, if $h_1 \geq h/2$</p> $P_p = 1/2 K_p \gamma h^2$ $P_a = 1/2 K_a \gamma h^2$ <p>K_p is obtained from AASHTO LRFD Figure 3.11.5.4-2 using $\delta/\phi_f = -0.5$</p>
1	<p>Again, in Figure 2.9, if anchor is placed left to CC', and in addition, if $h_1 = h_2$</p> $P_p = 1/2 K_p \gamma h^2 - (P'_p - P'_a)$ $P_p = 1/2 K_p \gamma h^2 - (1/2 K_p \gamma h_2^2 - 1/2 K_a \gamma h_2^2)$ $P_a = 1/2 K_a \gamma h^2$ <p>K_a is obtained from Figure 3 of Chapter 3 of NAVFAC DM (1986)</p>
	<p>In Figure 2.10, anchorage resistance, if $h_1 \geq h/2$</p> <p>Case I: Continuous wall:</p> <p>Ultimate $P_{uc}/d = P_p - P_a$ where P_{pc}/d is anchor resistance and P_p, P_a taken per linear foot of wall.</p> <p>Case II: Individual anchors:</p> <p>If $d > h + b$, ultimate $P_u = b(P_p - P_a) + 2P_0 \tan \phi'$, where P_0 = resultant force of soil at rest on vertical area cde or $c''de$.</p>
2	<p>If $d = h + b$, P_u/d is 70% of P_u/d for continuous wall</p> <p>L for this condition is L' and $L' = h$.</p> <p>If $d < h + b$, $P_u/d + P_{uc}/d = P_{uc}/d - L'/L (0.3 P_{uc}/d)$, $L' = h$.</p> <p>Again, in Figure 2.10, anchor resistance if $h_1 < h/2$</p> <p>Ultimate P_{uc}/d or P_{uc}/d equals bearing capacity of strip footing of width h_1 and surcharge load $\gamma(h - h_1/2)$, as per Figure 1 of Chapter 4 of NAVFAC DM (1986)</p> <p>In addition, use friction angle ϕ': where $\tan \phi' = 0.6 \tan \phi'$</p>

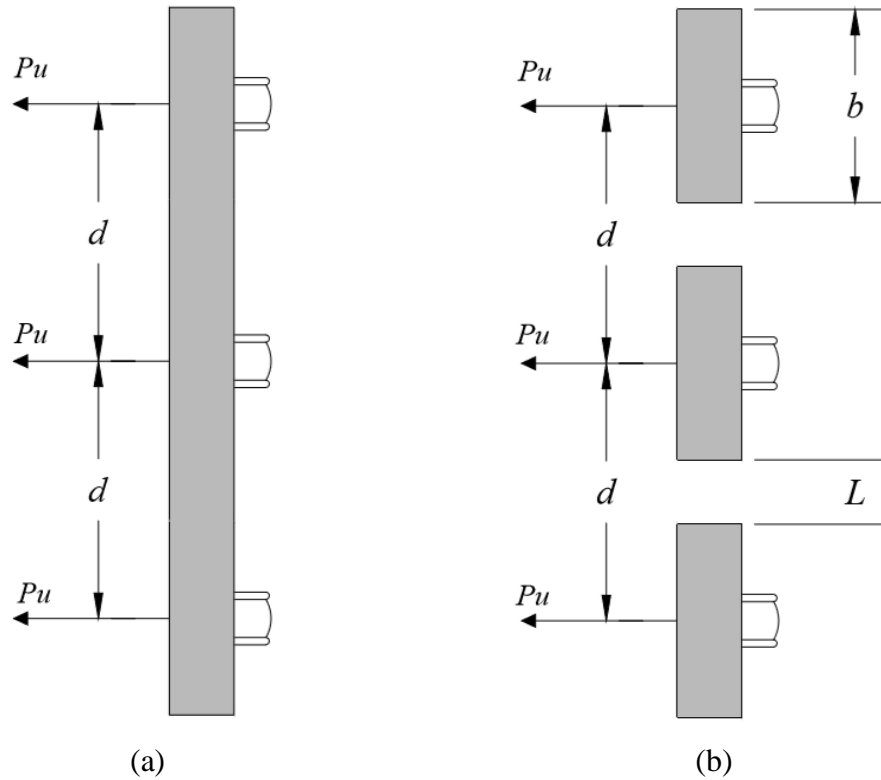


Figure 2.10 Anchor design parameters for (a) continuous wall and (b) individual anchor assumed by NAVFAC DM (1986)

BS 8006 (1995) recommends using passive resistance coefficient while calculating the pullout resistance of an anchor. This is based on the fact that, the conditions at the ends of the structures are quite different from those at the center, which has significant influence on the passive resistance. Ovesen (1964) found that the passive earth pressure against short structures is higher than those predicted by conventional theories (Rankine and Coulomb theories), and the difference can be quite significant. Hansen (1966) developed a method for correcting the results of conventional pressure theories for shape (or 3-D) effects. For short anchors, the ultimate resistance should be multiplied by a coefficient (M) to account for 3-D effects. For a plate anchor passive resistance coefficient (M) is given as:

$$M = 1 + (K_p - K_a)^{0.67} \left[1.1E^4 + \frac{1.6F}{1 + 5\left(\frac{L}{B}\right)} + \frac{0.4(K_p - K_a)E^3F^2}{1 + 0.05\left(\frac{L}{B}\right)} \right] \quad (2.5)$$

Where, $E = 1 - B/H$, $F = 1 - (L/S')^2$, S' is the center-to-center distance between two anchors, L and B are length and height of anchor respectively, and K_p and K_a are coefficient of passive and active earth pressure respectively.

Eq. (2.5) considers both the embedment factor (E) and the shape factor (F). The value of F is zero for long and continuous anchor and is 1.0 for single short anchor. According to the BS 8006 (1995) and Jones (1996), the horizontal pullout resistance of an anchor block is 4 times the passive pressure force acting on anchor block (ignoring the insignificant amount of resistance offered by rebar) i.e. passive resistance coefficient, $M = 4$ is suggested. A factor of safety 2.5 to 3 is used in this method. However, the experimental studies by Khan et al. (2017) indicated that this coefficient is always less than 4.

Ghaly (1997) used the results obtained from 104 laboratory tests, 15 centrifugal tests, and 9 field tests to propose an empirical correlation for the ultimate resistance of single anchors. The soil data he collected had unit weight and internal friction angle ranging from 14 to 16 kN/m³ and 34° to 38.5°, respectively. The embedment depth ratio (H/B) of the anchor plate varied between 1 and 4. This data was incorporated in a generalized form to predict the ultimate horizontal pullout resistance of anchor plates in terms of the influencing parameters. If, $A = BL =$ area of the anchor, then the correlation can be expressed as:

$$P_u = \frac{5.4}{\tan \varphi'} \left(\frac{H^2}{A} \right)^{0.28} \gamma AH \quad (2.6)$$

Where, $\gamma =$ unit weight of soil, $H =$ embedment depth of anchor and $\varphi' =$ angle of internal friction of soil.

Based on horizontal equilibrium analysis of lateral earth pressures and forces acting on an anchor block as depicted in Figure 2.11, Bowles (1997) proposed a general equation to determine the horizontal pullout resistance of anchor as follows:

$$P_u = L(P_p - P_a + F_t + F_b) \quad (2.7)$$

Where, referring to Figure 2.11, if $\gamma_c =$ unit weight of concrete, then,

$$\text{Effective horizontal passive thrust, } P_p = \text{area } abcd$$

$$\text{Effective horizontal active thrust, } P_a = \text{area } a'b'c'd'$$

$$\text{Friction force acting at the top, } F_t = \gamma d_1 \tan \delta$$

$$\text{Friction force acting at the bottom, } F_b = (\gamma d_1 + \gamma_c B) \tan \delta_1$$

The above-mentioned terms can be determined when the angle of friction between soil and concrete (δ and δ_1) acting at the top and bottom of the anchor block as shown in Figure 2.11 are known. For maximum efficiency, Bowles (1997) suggested to locate the anchor block such that the Rankine passive zone in front of the anchor should be completely outside the Rankine active zone behind the retaining wall. A factor of safety 1.2 to 1.5 is suggested for this method.

Naser (2006) analyzed pullout capacity of an anchor using limit equilibrium approach (Figure 2.12). It is important to note that the difference between the analysis of Bowles (1997) and Naser (2006) is that the later assumed the translational movement of the anchor, however, the former considered a rotational movement along the translational movement at limit equilibrium. Nevertheless, both the methods were developed for anchor block analysis only, indicating the applicability of these methods to anchor plate is restricted.

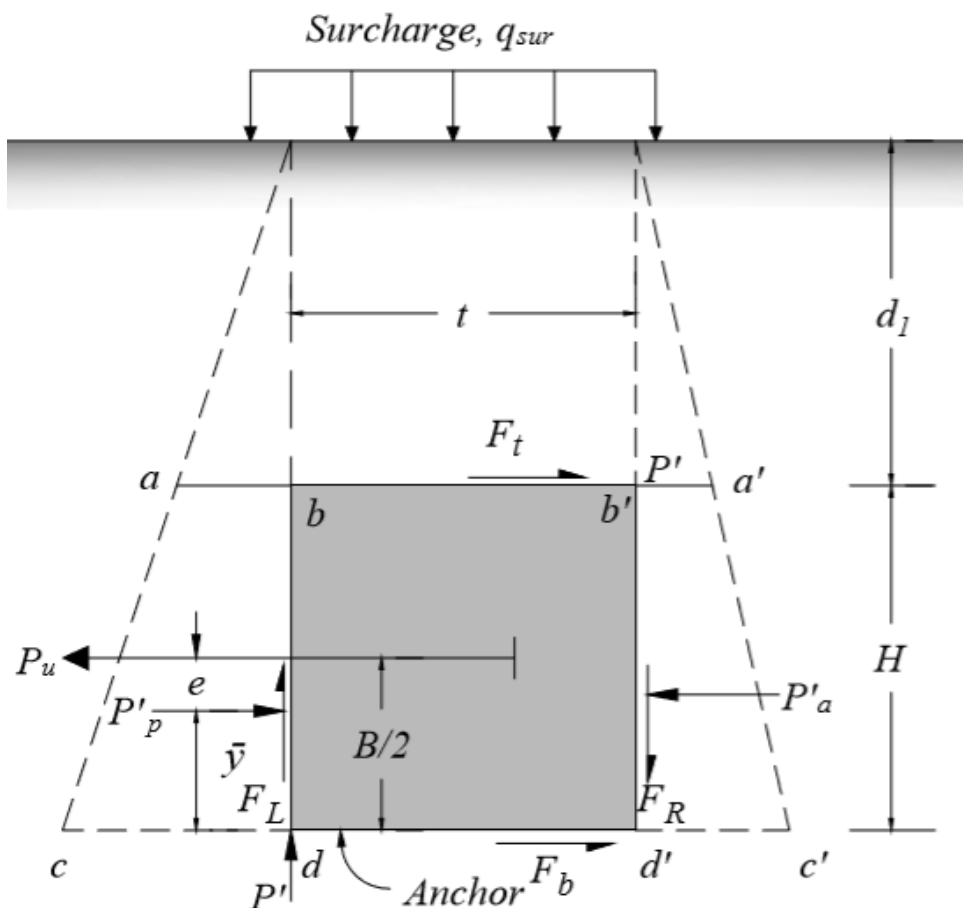


Figure 2.11 Complete set of forces acting on anchor block as per the assumptions of Bowles (1997)

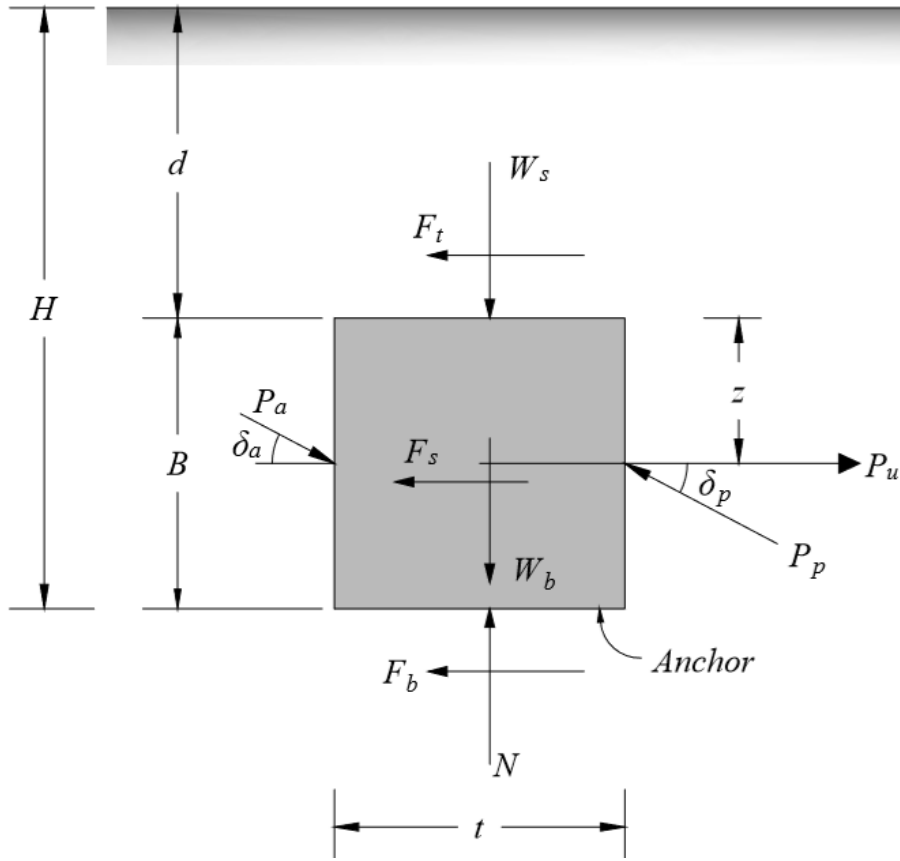


Figure 2.12 Free body diagram of anchor based on the assumptions of Naser (2006)

The ultimate pullout capacity of an anchor (P_u) was obtained from the equilibrium of forces acting on the anchor by summing them along the horizontal direction and multiplying the lateral earth pressures (passive and active) by the 3-D correction factor (M), to yield the Eq. (2.8).

$$P_u = M(P_p - P_a) + F_t + F_s + F_b \quad (2.8)$$

Where, P_p and P_a are the effective horizontal passive and active thrust respectively. The 3-D correction factor (M) may be calculated from Eq. (2.5). Naser (2006) observed that the pullout capacity of block anchor with Rankin theory, corrected for the 3-D effect showed a close agreement with experimental results.

Jadid et al. (2018) derived an expression to calculate the ultimate pullout capacity of the anchor block in cohesionless soil employing a passive wedge model. The ultimate pullout capacity ($P_{ultimate}$) for an anchor block with the dimensions height (B), width (L), thickness (t) and the depth of embedment below soil surface (H) was calculated with the following equation:

$$P_{ultimate} = \frac{W}{\tan(45^\circ - \varphi'/2)} \quad (2.9)$$

Where, W = weight of the soil contained within the failure surface and φ' = angle of internal friction of soil. The failure pattern assumed in the development of Eq. (2.9) is illustrated in Figure 2.13. Explanation of the force components is available in Jadid et al. (2018) and Jadid (2016).

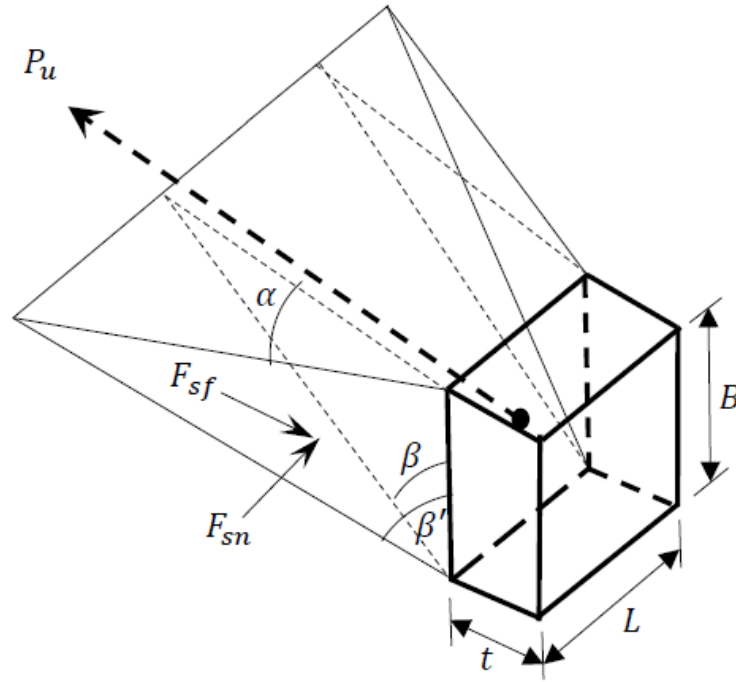


Figure 2.13 Idealized failure pattern in front of single anchor with acting forces in one face of the wedge according to Jadid et al. (2018) (β = angle subtended by central flank with the vertical, β' = angle subtended by side flank with the vertical, F_{sf} = friction force at the side of the wedge, F_{sn} = normal force at the side of the wedge)

Review of literature indicates that the rupture pattern assumed by different investigator is linear, bilinear, logarithmic spiral, composite logarithmic spiral, and circular. Choudhary and Dash (2016) and Zhao et al. (2011) concluded that the rupture pattern depends on some factors of which embedment depth ratio and density of soil are important ones. However, discrepancies continue to exist between predictions and actual measurements. Understandably, choice of failure mechanism played an important role in causing the disparities. Thus, it was also understood that improper choice of failure mechanism might lead to serious discrepancies between experimental result and theoretical predictions.

2.5.3 Previous Numerical Investigations

Although, there are a variety of experimental results in the literature, very few rigorous numerical analyses have been performed to determine the pullout capacity of anchors in sand (Merifield and Sloan, 2006). Most of those numerical analyses were performed for strip anchor. On the other hand, to the knowledge of the author, hardly any effort has been made so far to conduct numerical analysis on anchor block. Although, it is essential to verify theoretical solutions with experimental studies wherever possible, results obtained from laboratory testing alone are typically problem specific. Since, the cost of performing laboratory tests on each and every field problem combination is cost prohibitive, it is necessary to be able to model soil pullout resistance numerically for the purposes of design. A summary of some important previous numerical studies post-1980 on vertical anchors is provided in Table 2.5. However, the researches presented in Table 2.5 is not exhaustive.

Table 2.5 Numerical studies on vertical anchors in frictional soil

Source	Analysis method	Anchor shape	Anchor roughness	ϕ' (°)	H/B
Rowe and Davis (1982)	Elasto–plastic finite element	Strip	Smooth	0–45	1–8
Hanna et al. (1988)	Limit equilibrium	Strip; Inclined	Not Mentioned	Loose; Dense	Shallow; Deep
Murray and Geddes (1989)	Limit analysis–upper bound	Strip; Inclined	Rough; Smooth	43.6	1–8
Basudhar and Singh (1994)	Limit analysis–lower bound	Strip	Rough; Smooth	32; 35; 38	1–5
Merifield and Sloan (2006)	Limit analysis–upper and lower bound	Strip	Rough	20–40	1–10
Bhattacharya and Kumar (2011)	Limit analysis–lower bound	Strip	Rough; Smooth	25–40	1–7
Hanna et al. (2011)	Limit analysis	Strip	Rough	30–45	1–9
Bhattacharya and Kumar (2014)	Limit analysis–lower bound	Strip; Inclined	Rough; Smooth	30–40	3–10
Bhattacharya and Roy (2016)	Limit analysis–lower bound	Strip	Rough; Smooth	30–40	2–7

Observation of Table 2.5 reveals that most of the numerical studies on anchors focused on strip case and no researches were found to report numerical studies on anchor blocks (limited L/B). However, of the numerical studies reported in Table 2.5, most of the researchers investigated both smooth and rough anchors. Merifield and Sloan (2006) observed that though the effect of roughness on the pullout capacity of horizontal anchor is insignificant, the effect is quite prominent for vertical anchors. Another point is that, in contrast to the experimental investigations reported in this paper, behavior of shallow, intermediate and deep anchor is investigated by almost all the numerical researches. Moreover, the inclination of present researchers in the post–2010 period is toward numerical studies.

Most recently, Bhattacharya and Kumar (2011) investigated the effect of vertical spacing of anchor plates and anchor roughness on the pullout capacity of vertical anchors using lower bound finite element analysis. Hanna et al. (2011) using limit analysis showed that the stress-strain condition in a sand mass during and after the installation of an anchor plate, over-consolidation ratio have a significant effect on the pullout capacity. Again, using numerical lower bound limit analysis in combination with linear programming, Bhattacharya and Roy (2016) showed that pullout capacity increases continuously with the decrease in normalized width. Thus, the concepts of anchor plate analyses may provide a significant insight into the understanding the behavior of anchor block failure mechanism as well.

2.6 Summary

Literature reveals that the failure mechanism of anchor plate is explored experimentally and theoretically by many researchers. In contrast, very few researches such as Duncan and Mokwa (2001), Naser (2006), and Khan et al. (2017) conducted experimental studies to investigate the behavior of anchor block. Additionally, Bowles (1997), and Naser (2006) developed analytical approaches for anchor block. However, the analytical methods of calculating pullout capacity of vertical anchor plates are commonly used for anchor blocks in practice. Thus, the key question to the present researchers is that- are these methods focusing on anchor plates can be utilized to simulate the behavior of anchor blocks as well? Author thinks that the difference in the side conditions of anchor plates (plane strain) and anchor blocks (3-D effect) might play a significant role in understanding the actual phenomenon. Nevertheless, rigorous analytical, numerical and

experimental studies might follow to explore the actual answer. As such, developing an analytical model to reliably and accurately predict the pullout capacity for anchor plate and block is the prime objective of the present study. Decisively, during the development of the theory, key importance was given to accuracy and reliability. As it is experimentally evidenced that the failure mechanism of shallow, intermediate and deep anchor differ significantly, only shallow and intermediate anchors are kept as focus in the present study. Thus, applicability of the proposed analysis will be restricted to shallow and intermediate anchors embedded in frictional soils. The predictions of the proposed method will be compared with the laboratory and field test results available in the literature along with other theoretical methods used for anchor design to assess the suitability of the methods.

Chapter 3

THEORY OF THE PROPOSED MODEL

3.1 General

From the present state of art, it is evident that many researches have been conducted on the capacity of vertical anchors especially on anchor plate. However, the inherent assumptions in the available pullout capacity prediction models vary significantly from one another. Recent investigations showed that some assumptions are rather less important than the level of emphasize it was given. In contrast, some important assumptions seemed to be omitted in most models. This understandably explains the discrepancy among the pullout capacity prediction models. Thus, development of an analytical model addressing all relevant assumptions to estimate the capacity of an anchor is deemed necessary. The theory on which the model is developed will be discussed in this chapter.

3.2 Problem Notation

Depending on the orientation of load, an anchor can be positioned horizontally or vertically. Vertical anchor having length L , height B , and width t embedded at a depth H will be considered in the present study. A general layout of the problem is shown in Figure 3.1. An anchor will be considered as shallow if embedment depth ratio (H/B) is less than 3 and will be considered as intermediate if H/B lies within the range of $3 \leq H/B \leq 8$. Here, both the shallow and intermediate anchors are focused which means ultimate pullout capacity of vertical anchors up to an embedment depth ratio of 8 can be determined using the method proposed in the study. This is from the perspective that beyond the limit, failure pattern becomes more localized and the assumptions which will be taken in the process of analysis will not be valid.

3.3 Description of the Proposed Method

The proposed method of present study is applicable for shallow and intermediate anchors. During analyzing, two wedge blocks are assumed to develop due to the anchor pullout. First one is the passive wedge block in front of the anchor and second one is the active

wedge block at the back of the anchor. The basic principle is that whenever pullout force would be exerted by retaining structure via the attachment to a rebar, normal stresses in front of the anchor would increase, causing development of a passive wedge in front of the anchor. However, an active wedge would also develop at the back of the anchor due to frontal movement of itself. The shape of the wedge blocks will be discussed in the subsequent sections. At this point, assuming the system is on the verge of failure, the limit equilibrium condition will be satisfied, using a variable pressure distribution along the failure plane. Then, from the horizontal equilibrium, pullout capacity for the plane strain condition will be determined. In addition to the plane strain situation, side flanks also develop due to the pullout. Subsequently, the contribution of the side flanks is also determined in the present analysis and added to the capacity obtained from the central wedge to obtain the ultimate pullout capacity.

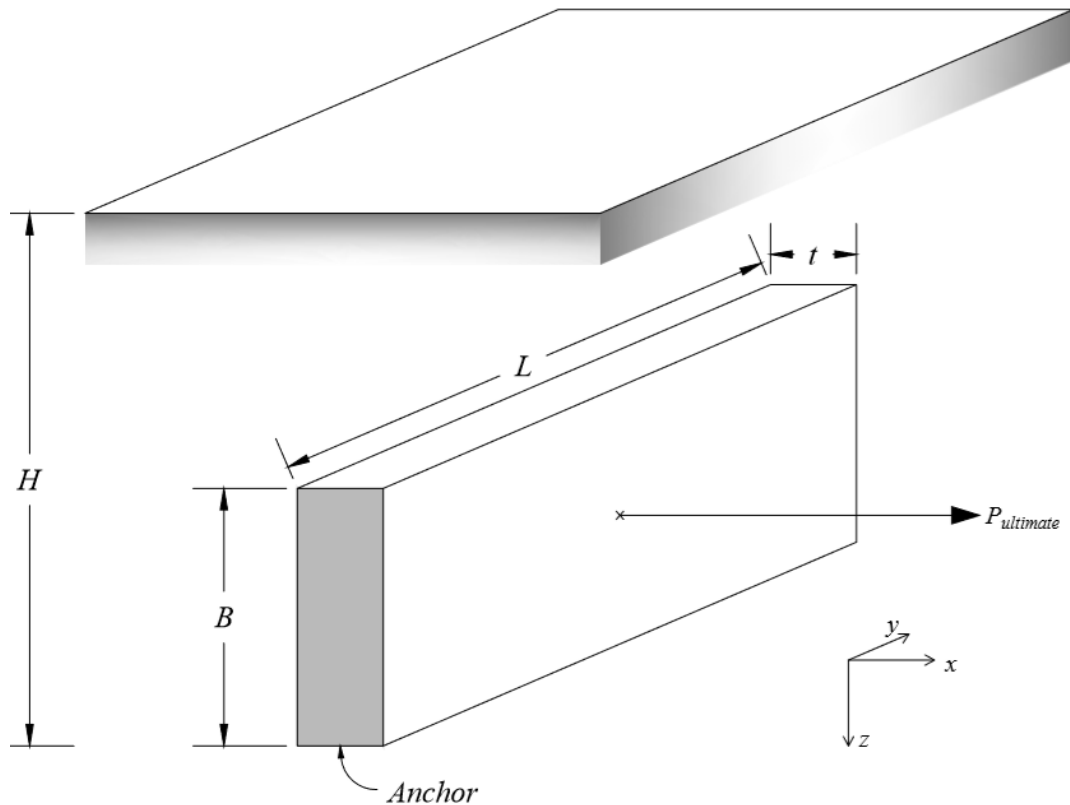


Figure 3.1 Problem notation

3.4 Idealization of the Failure Mechanism

The idealization includes assumptions regarding the shape of failure surface in both the active and the passive sides, pressure distribution on the failure surface, nature of load-

displacement curve, nature of anchor-soil interface and nature of side flanks formed during failure. These topics will be discussed subsequently in the following sections.

3.4.1 Failure Surface in Passive Side

Although the actual failure surface might follow a very irregular pattern, the estimation of pullout resistance requires an idealization of the rupture surface. This failure surface idealization is the first step in problem solving using limit equilibrium technique. Researchers adopted different failure surface starting from the earliest method of analysis proposed by Rankine to estimate the ultimate pullout capacity. The failure surface assumed by Ovesen (1964) entails composite rupture pattern consisting of logarithmic spiral region sandwiched between two straight regions. Figure 3.2 shows the rupture pattern assumed by Ovesen (1964). Dickin and Leung (1985) developed a theoretical model for shallow anchors using planar failure surface considering the inclination of failure surface with the vertical, $\beta = 45^\circ + \phi'/2$.

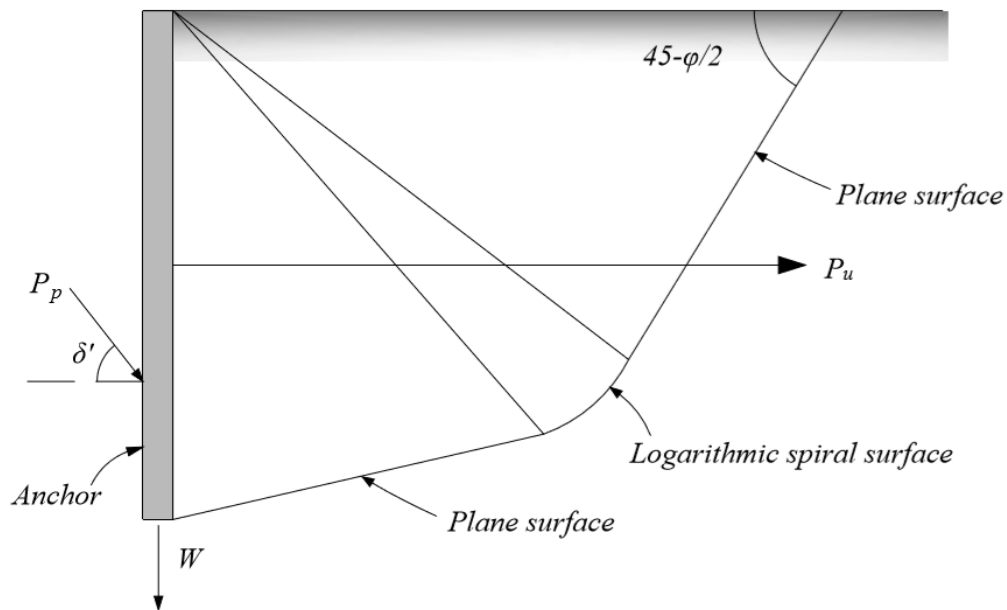
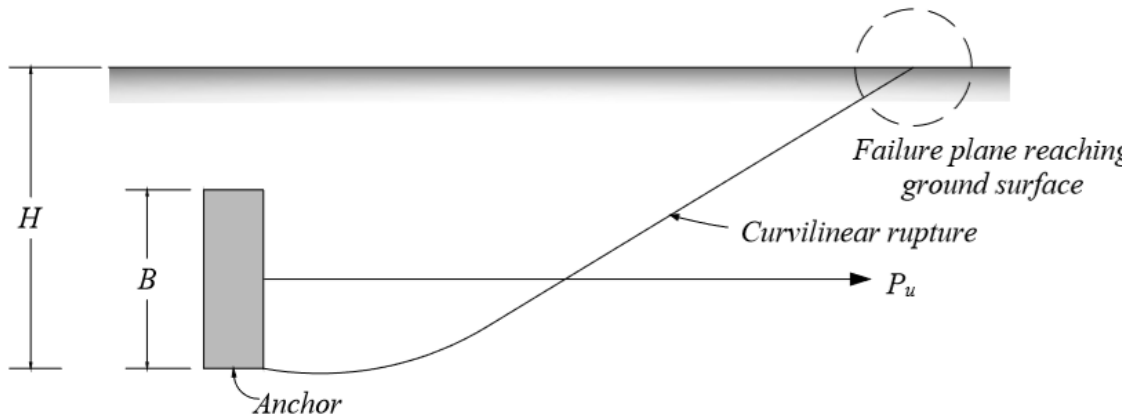


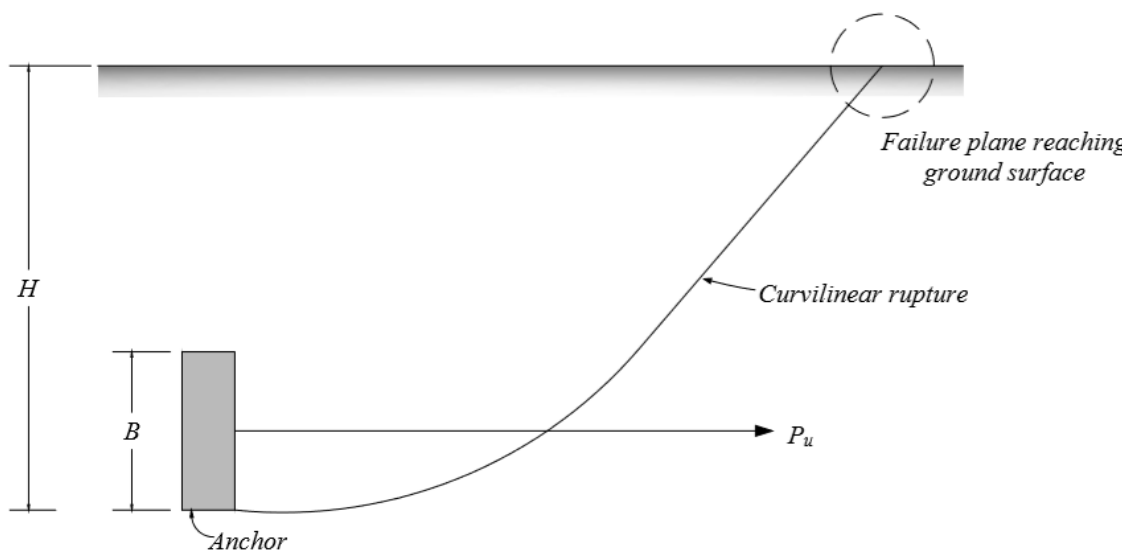
Figure 3.2 Failure surface in the passive side as assumed by Ovesen (1964)

In addition to that, Dickin and Leung (1985) conducted extensive experimental study using centrifugal and conventional model tests. At shallow depth ($H/B < 3$), the failure pattern observed was linear in nature. However, the pattern became complex as the embedment was increased, leading to a curved failure surface. At intermediate depths ($H/B = 5$), the failure observed was curvilinear in nature (Figure 3.3). Beyond an embedment depth ratio of 8, rotational failure occurred. It was suggested in the study that

the minimum depth for which localized shear occurs is 8. They termed this as *critical embedment ratio*. Furthermore, the dependency of critical embedment ratio on the anchor size was criticized.



(a)



(b)

Figure 3.3 Failure surface in the passive side as observed by Dickin and Leung (1985) when (a) $H/B = 3$, (b) $H/B = 5$

NAVFAC DM (1986) suggested adopting β to be similar to the theoretical model of Dickin and Leung (1985) in designing anchor in frictional soil. In Figure 3.4, failure surface assumed by NAVFAC DM (1986) is presented. From the field tests Duncan and Mokwa (2001) observed that the rupture plane could probably be assumed planar if the anchor is placed flush with the existing ground level.

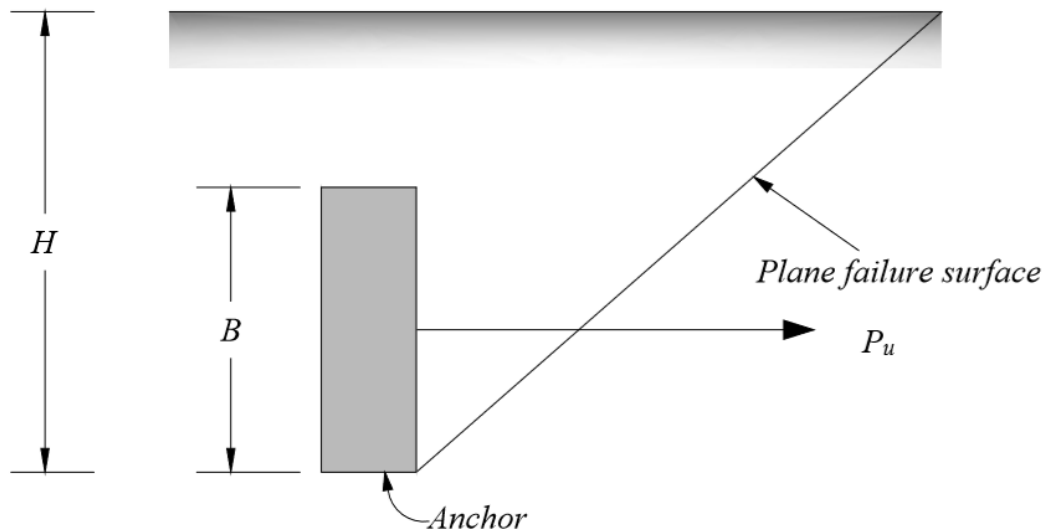


Figure 3.4 Failure surface in the passive side as assumed by NAVFAC DM (1986)

Chowdhary and Dash (2016) through extensive half model test observed the similar phenomenon as observed by Duncan and Mokwa (2001) for surficial anchors. Their experimental investigation confirmed that the soil wedge ruptured as single unit at shallow depth, causing the interface friction between soil and the anchor to be negligible. They further showed that when the anchor is placed flush with ground surface, the failure surface might follow a straight path, however, the failure pattern is observed to be a combination of logarithmic spiral and a straight line, as the embedment depth is increased up to such a limit that local failure occurs. Figure 3.5 shows a schematic sketch of the failure pattern noticed by Chowdhary and Dash (2016). Thus, to predict the pullout capacity, incorporating plane failure surface in the analysis might lead to conservative estimate of the pullout capacity with the increase of embedment depth ratio.

Neely et al. (1973) assumed failure plane consisting of a combination of logarithmic spiral and straight line. Neely et al. (1973), however, proposed two techniques to idealize failure mechanism. Those can be listed as-

- (i) surcharge method, and
- (ii) equivalent free surface method.

Surcharge method is completely based on the theory of plasticity. Here, it is assumed that the soil located above the top level of the anchor can be considered as a simple surcharge. The failure surface in the soil consist of an arc of logarithmic spiral and a straight line.

Figure 3.6 demonstrate typical failure mechanism using Neely's (1973) surcharge method.

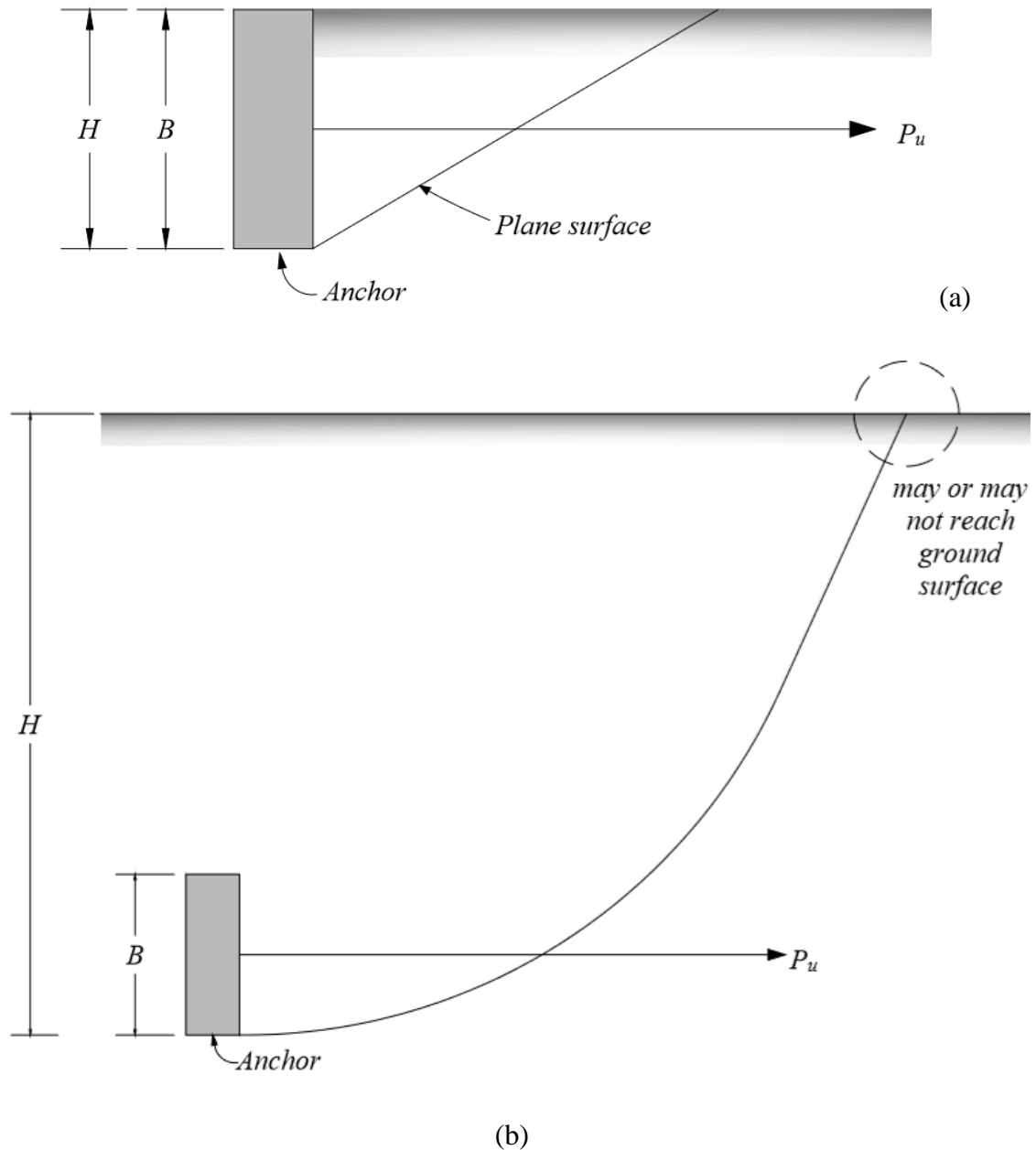


Figure 3.5 Failure surface in the passive side as observed by Choudhury and Dash (2016) when (a) $H/B = 1$, (b) $H/B = 5$

In *equivalent free surface* method, the assumed failure surface in soil, ACD (Figure 3.7), is an arc of a logarithmic spiral with the center at O . OD is a straight line which is the *equivalent free surface*. The concept of the equivalent free surface is analogical to the method developed by Meyerhof (1951) to predict the ultimate bearing capacity of foundations. It is to be noted that along the equivalent free surface, OD , the shear stress τ can be expressed in the form of Eq. (3.1).

$$\tau = m \sigma \tan \varphi' \quad (3.1)$$

Where, σ = effective normal stress, m = mobilization factor and φ' = angle of internal friction of soil. The magnitude of m may vary between zero and one. Neely et al. (1973) developed design charts expressed in non-dimensional form, as force coefficients. To summarize, this method also considers that the failure plane is a combination of logarithmic spiral and a straight line; however, considerations regarding the shear stress above the top level of the anchor are duly accounted for.

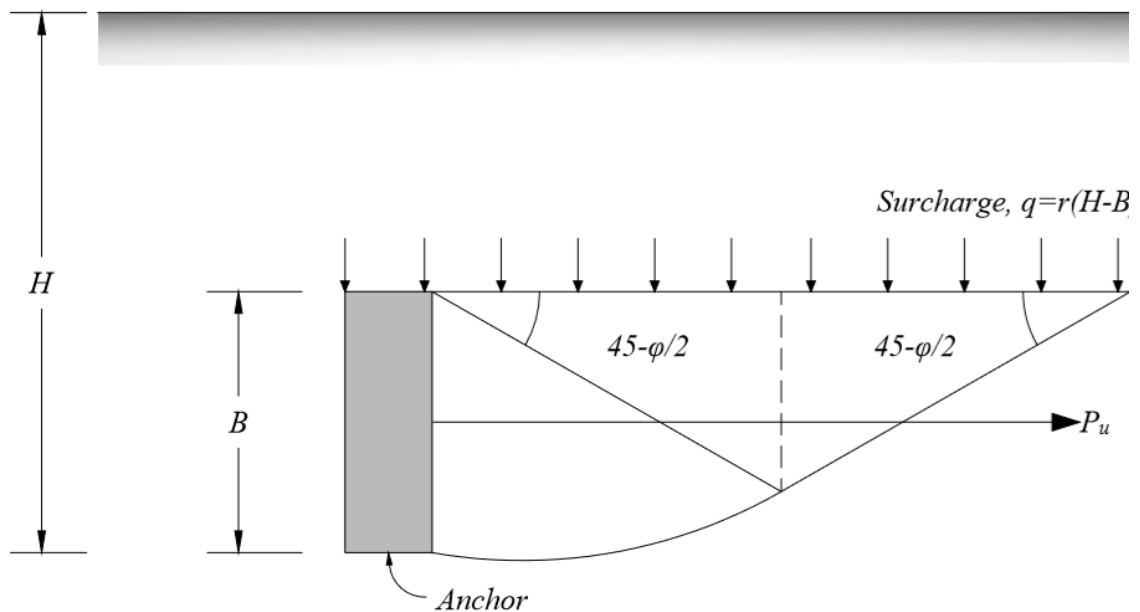


Figure 3.6 Failure mechanism idealization by Neely's (1973) surcharge method

In summary, author has two options to idealize the failure mechanism. First one suggests neglecting the shear resistance above the top of anchor and the second one suggest considering the shear resistance by using the principle of equivalent free surface. Although the first option neglects the shearing resistance of soil above the top surface of the anchor, but the effect of soil weight above the base is considered in both the options.

Terzaghi (1948) neglected soil resistance above footing level for the analysis of bearing capacity of the soil. Dickin and Leung (1985) conducted laboratory tests and observed that solution using Neely's (1973) surcharge method provide compatible values in most of the cases. In contrast, free surface provided greatest deviations from their experimental results.

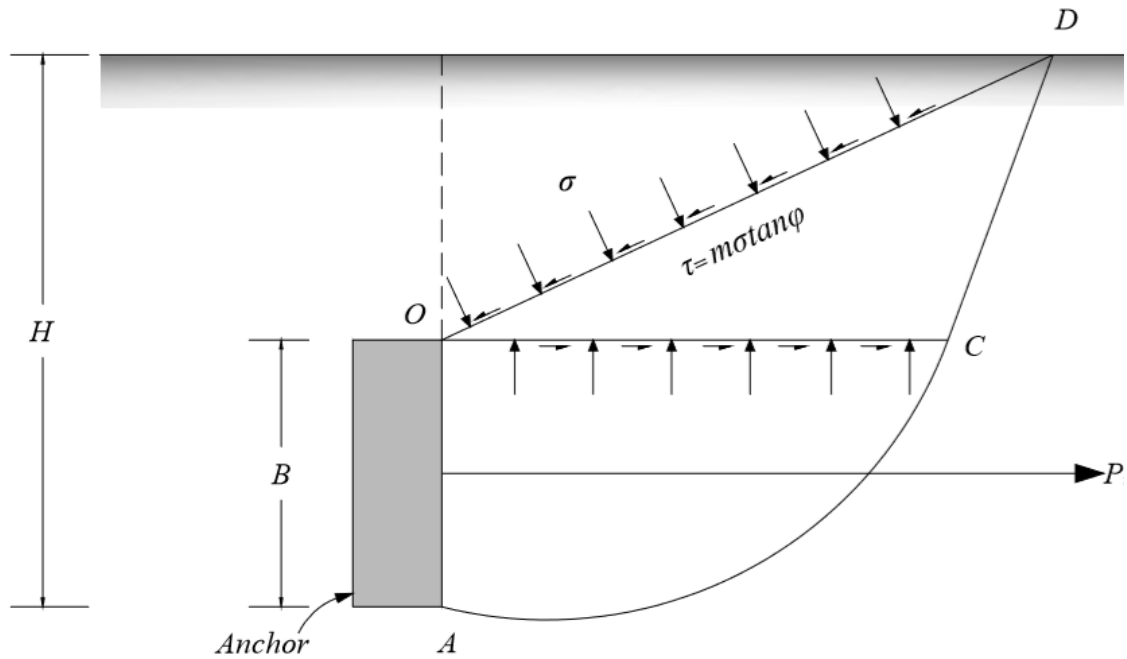
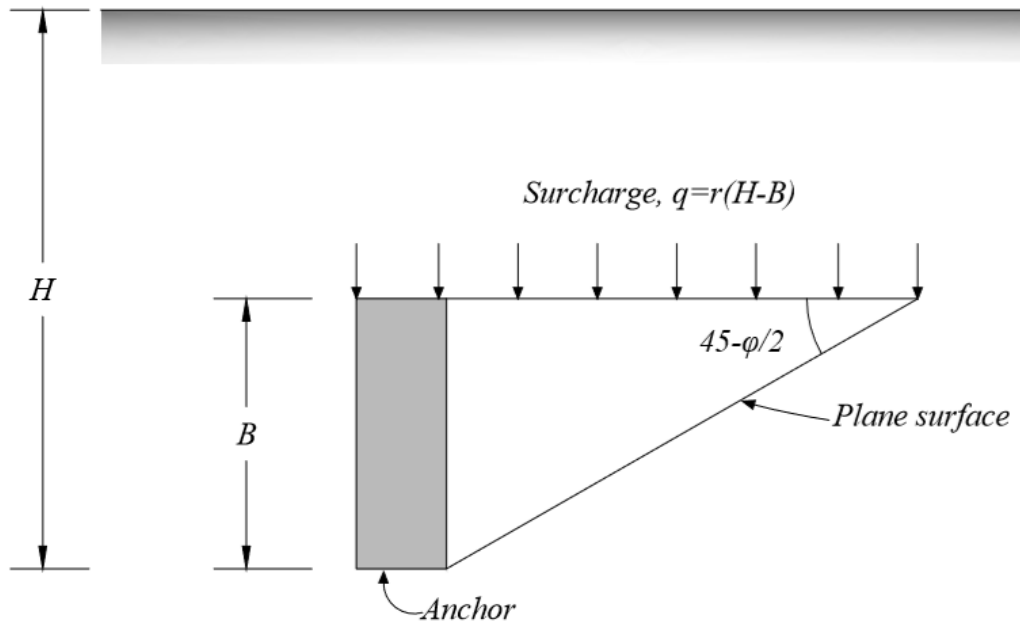


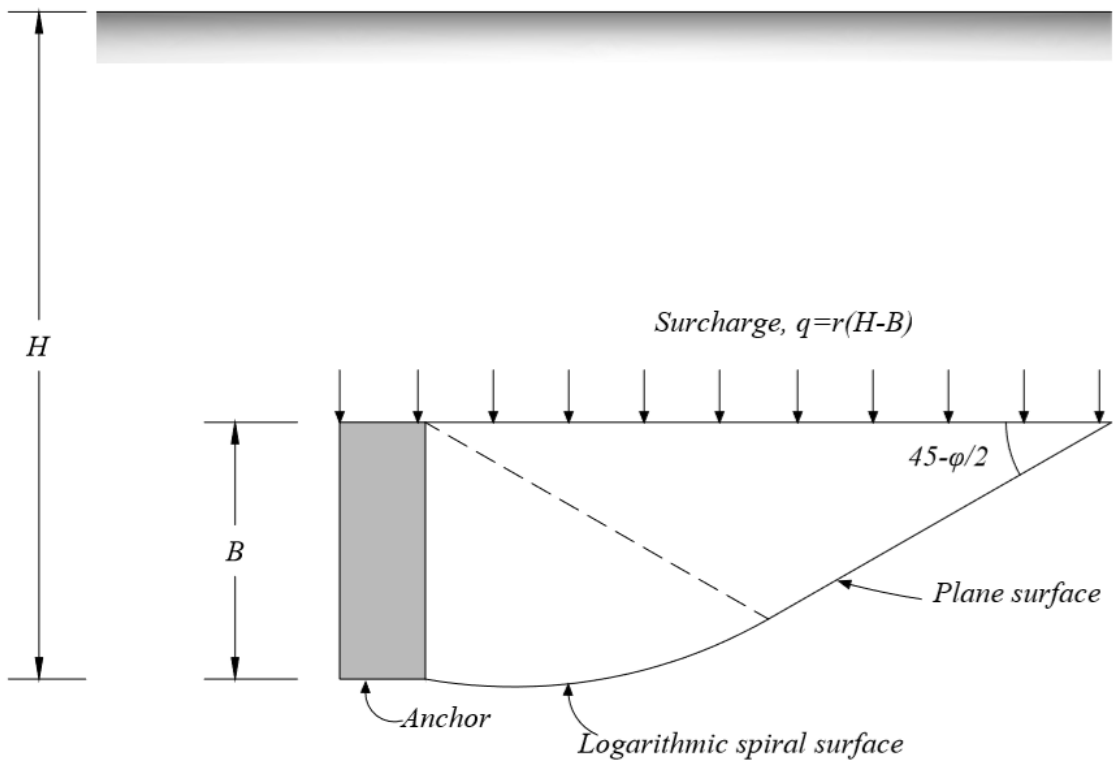
Figure 3.7 Failure mechanism idealization by Neely's (1973) equivalent free surface method

The experimental results of Choudhary and Dash (2016) suggested that for intermediate anchor, the failure surface might not reach the existing ground level depending on the soil properties. Furthermore, neglecting the shearing resistance above the top level of anchor would provide a conservative estimate, which is important from the reliability perspective. Thus, to achieve a conservative and reliable estimate, first option seems more accurate in such situation and the second option should not be opted as experimental evidences suggest that the later one might provide unreliable estimate of pullout capacity. Additionally, it was noted that the failure plane changes its nature with the change of embedment depth.

Subsequently, considering all the possibilities, at shallow depth, the failure plane would be considered as planar as presented in Figure 3.8(a). The inclination of the failure plane can be estimated from the Rankine theory. At intermediate depth, the failure plane would be considered to contain logarithmic spiral surface followed by a plane surface. In Figure 3.8(b), a schematic sketch of the assumed failure plane in the passive side for intermediate anchors is shown. For both shallow and intermediate anchors, the soil above the top level of anchor is shown. For both shallow and intermediate anchors, the soil above the top level of anchor is considered to provide a simple surcharge over the hypothetical plane flush with the top of the anchor.



(a)



(b)

Figure 3.8 Geometry of the passive failure wedge developed in front of (a) a shallow anchor, and (b) an intermediate anchor as assumed in the present study

3.4.2 Failure Surface in Active Side

Similar to the case of assuming a predetermined failure surface in the passive side, failure pattern in the active side needs to be ascertained. Merifield and Sloan (2006), through limit analysis, observed the formation of active wedge behind the anchor, concluding that failure in anchored soil is characterized by active failure zone immediately behind the anchor, and an extensive passive failure zone in front of the anchor. Choudhary and Dash (2016) reported that the failure pattern behind the anchor consists of a column of soil collapsing into the gap formed due to the forward movement of the anchor, contributing to the active pressure. However, Merifield and Sloan (2006) suggested that although the effect of active thrust could be neglected for greater depths, the effect is significant at shallow depth. It was also observed that the size of active failure zone behind the anchor decreases with an increase in the φ' and the effect is maximized at $H/B < 2$, and in loose sands. Bowles (1997), and Naser (2006) also suggested consideration of active thrust on the back face of anchor. Thus, overlooking active failure wedge might lead to erroneous result for anchors laid at surficial layers.

Teng (1962) adopted planar failure surface in the active side of anchor to estimate the pullout capacity. Ovesen (1964), however, adopted failure surface consisting of an arc of logarithmic spiral followed by a straight line, in the active side of anchor (Figure 3.9). Numerical investigation by Merifield and Sloan (2006) reveals failure pattern in the active side is almost linear and its inclination could simply be estimated from the angle suggested by Rankine (Figure 3.10). Merifield and Sloan (2006) observed that the failure plane reached ground surface in the active side of the anchor. Very recently, in the development of an analytical model to estimate active thrust, Kame et al. (2012a) assumed a failure surface consisting of an arc of logarithmic spiral followed by a straight line. Nevertheless, the arc seemed to be too small and can be considered planar. As the present study covers a wider range of embedment depth, it will be assumed that active failure wedge forms at the back of anchor. The failure plane will be assumed to be inclined at $45^\circ + \varphi'/2$ with the horizontal in the active side of the anchor. Figure 3.11 shows the geometry of active failure wedge assumed in the present study.

Thus, the present analysis considers both the passive and active forces as they form in the front and at the back of the anchor respectively.

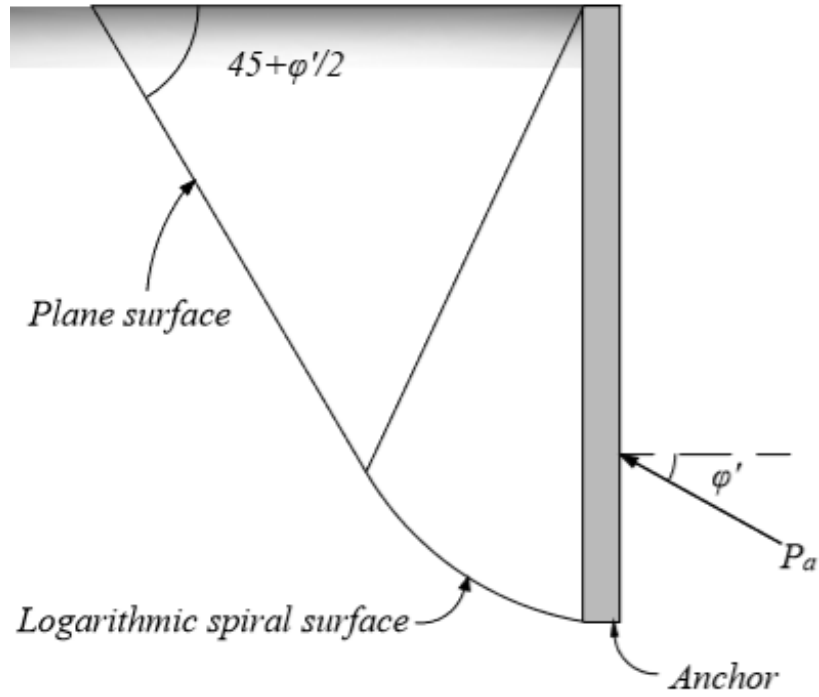


Figure 3.9 Failure surface in the active side as per the assumption of Ovesen (1964) and Kame et al. (2012a, b)

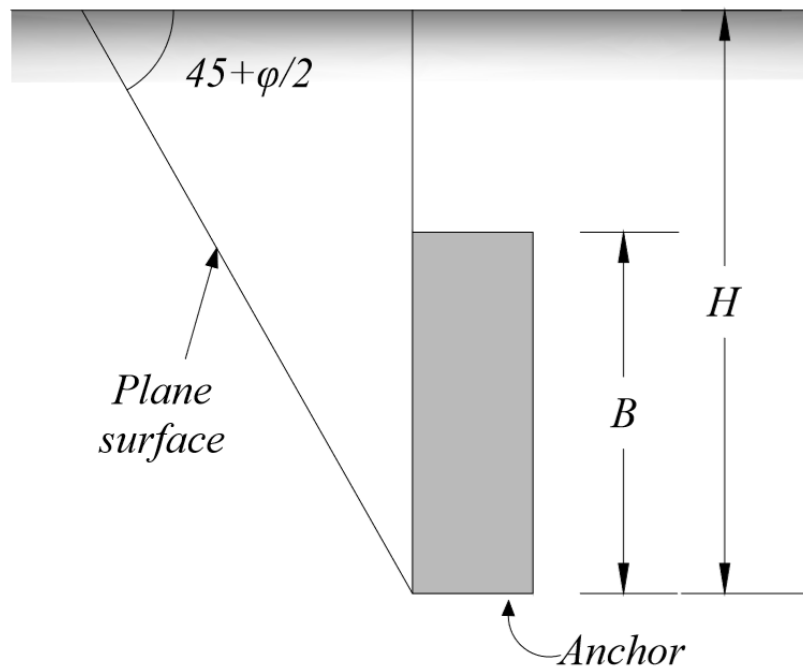


Figure 3.10 Failure surface in the active side as per the assumption of Merifield and Sloan (2006)

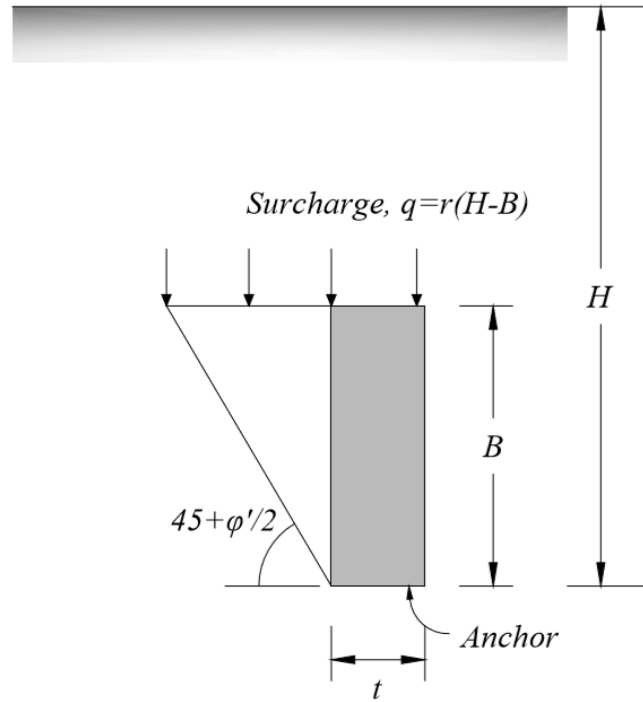


Figure 3.11 Geometry of the active failure wedge developed at the back of anchor as assumed in the present study

3.4.3 Pressure Distribution on the Failure Surface

One of the important steps in solving problem utilizing limit equilibrium theory is to assume a pressure distribution along the failure plane. As failure commences along the failure surface which is assumed as a combination of an arc of logarithmic spiral and a straight line, reactive pressure generates over that surface. One of the most common similarities among different models in the available literature (Dickin and Leung, 1985; Jadid et al., 2018) is to assume a uniform pressure distribution along the failure surface. However, such idealization resulted in extremely optimistic pullout capacities. Although, reliability is ensured in such case, the accuracy is highly sacrificed. It is understandable that the generated pressure will not be the same at all the points along the failure surface. Thus, to address non-uniform pressure distribution along the failure surface, Kötter (1903) equation will be utilized. In cohesionless soil medium, under plane strain condition, in passive state of equilibrium, Kötter (1903) equation can be expressed as-

$$\frac{dp}{ds} + 2p \tan\phi' \frac{d\alpha}{ds} = \gamma \sin(\alpha + \phi') \quad (3.2)$$

Similarly, in cohesionless soil medium, under plane strain condition, in active state of equilibrium, Kötter (1903) equation can be expressed as-

$$\frac{dp}{ds} - 2p \tan\phi' \frac{d\alpha}{ds} = \gamma \sin(\alpha - \phi') \quad (3.3)$$

Notations used are presented in Figure 3.12 and addressed in detail in the Chapter 4. It is to be noted that Kötter's equation is valid for plane strain cases. Patki et al. (2017), Patki et al. (2015) showed successful application of the equation in observing retaining wall behavior. Dewaiker and Mohapatro (2003), Patki et al. (2017) utilized Kötter (1903) equation to estimate the bearing capacity factor, N . Kame et al. (2012a), Patki et al. (2015) showed the successful application of Kötter's equation to estimate the passive earth pressure coefficient. However, in this analysis Kötter's equation will be used in conjunction with limit equilibrium approach. Such conjunctive use was successfully adopted by Kame et al. (2012b) and Patki et al. (2015). The pressure obtained from Eq. (3.2) and Eq. (3.3) can be integrated over the surface area to obtain the magnitude of resultant soil reaction in both horizontal and vertical direction. A typical pressure distribution along the failure surface in both the active and passive side is illustrated in Figure 3.12.

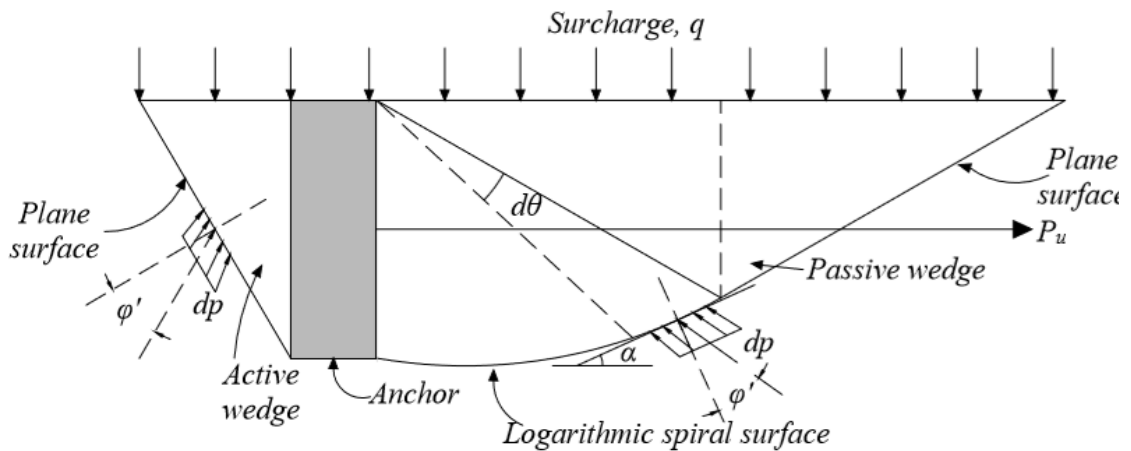


Figure 3.12 Pressure distribution on the failure surface assumed in the present study

However, author wants to clarify that the proposed analysis is focused to solve the pullout capacity of an anchor when the embedment depth ratio is less than 8. Beyond this embedment depth ratio, circular failure pattern occurs as evidenced in the works of Das (1990) and Biarez et al. (1965) and such local failure pattern cannot be addressed by the proposed technique.

3.4.4 Load Displacement Curve

The prime objective in this study is to determine the ultimate pullout capacity. But, what does it mean by *ultimate pullout capacity*? Neely et al. (1973), observed three different load-displacement relationships from their laboratory model test (Figure 3.13). These are-

- i) Case I: $L/B > 2$ and $H/B < 2$

For anchors with such geometric condition, load increases up to a point where displacement reaches a maximum value and remains constant thereafter. The constant value reached is considered as the ultimate pullout force.

- ii) Case II: $L/B < 2$ and $H/B > 2$

For anchors with such geometric condition, load increases up to a maximum value, after which the load-displacement diagram becomes practically linear. The ultimate pullout capacity can be obtained by extending the slope of the linear portion up to a distance when it intersects load axis.

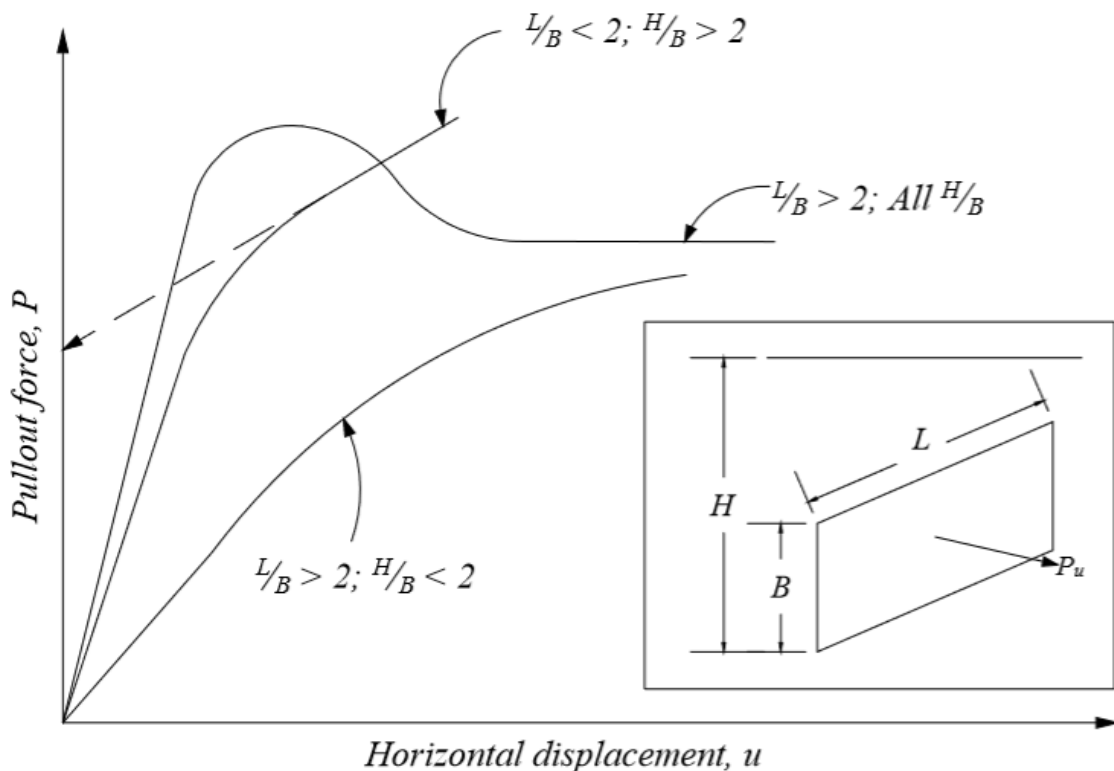


Figure 3.13 Typical load-deflection curves depicting anchor failure criteria

iii) Case III: $L/B > 2$ and all H/B

For anchors with such geometric condition, load increases up to a peak value and decreases thereafter with the increase in displacement.

As the limit equilibrium technique is adopted in the present study, it inherently suggests assumption of a predetermined failure surface and also the pressure distribution in that surface. This pressure in the prescribed failure plane will develop only when the bonding between the soil particles is lost. Thus, any pressure developed beyond the failure of soil, will initiate plastic deformation, resulting in increase of displacement. To ascertain the deformation at failure, a chart developed by Neely et al. (1973) can be used, which is based on laboratory model test and presented in Figure 3.14. However, in some circumstances design layout does not allow significant horizontal displacement. Therefore, maximum pullout capacity may not be attained in some specific field situation. Using the technique of the present study, one can only obtain the ultimate pullout capacity.

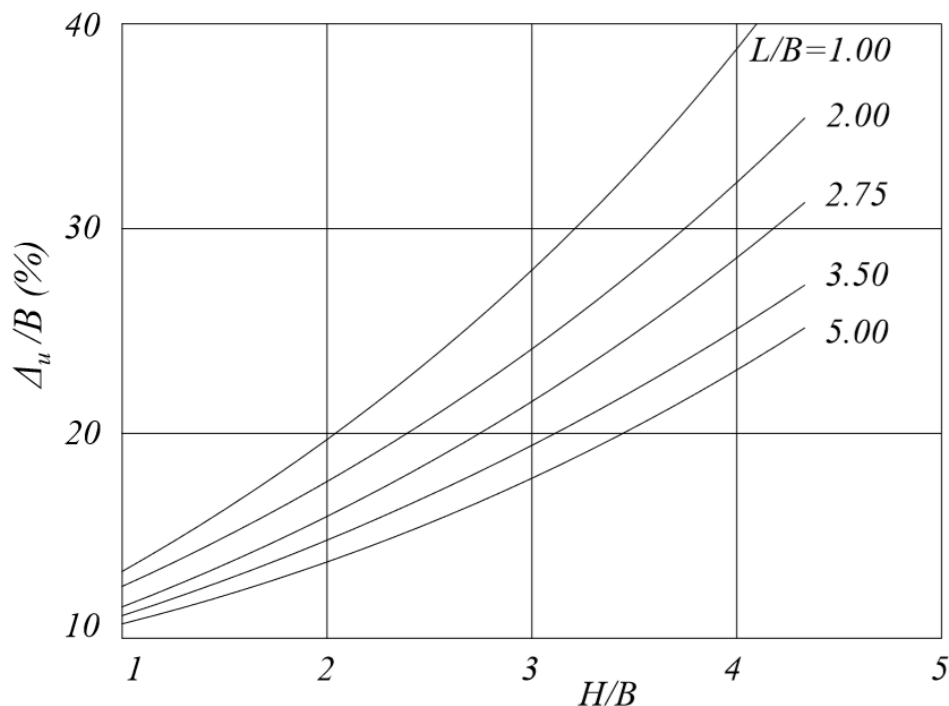


Figure 3.14 Design chart to estimate deformation at failure, developed by Neely et al. (1973)

Ghaly (1997), however, from the experimental results of Das and Seely (1975) proposed a relation between pullout capacity at any instance with allowable anchor deflection, which can be expressed as-

$$\frac{P_i}{P_u} = 2.2 \left(\frac{u}{H} \right)^{0.3} \quad (3.4)$$

Using this equation, inserting the allowable anchor deflection, the pullout capacity corresponding to an allowable anchor deflection can be obtained.

3.4.5 Anchor-soil Interface

Earlier studies on vertical anchors in sand by Rowe and Davis (1982) have revealed that anchor interface roughness significantly affects the ultimate anchor capacity. Merifield and Sloan (2006), however found no significant effect of anchor roughness on the pullout capacity for horizontal anchors in sand. But, for vertical anchors, the effect was substantial, and it requires necessary consideration in design. They observed that for vertical anchors, changing the interface roughness from perfectly rough to perfectly smooth can lead to a reduction in the anchor capacity by as much as 67%. The effect of anchor roughness was found to decrease with an increase in embedment depth for all friction angles considered by Merifield and Sloan (2006). The greatest rate of change in the roughness correction factor occurs between embedment ratios of 1 and 4. Merifield and Sloan (2006) incorporated a term to demonstrate the effect of anchor roughness. The term can be expressed as-

$$F_\delta = \frac{q_{u(rough)}}{q_{u(smooth)}} \quad (3.5)$$

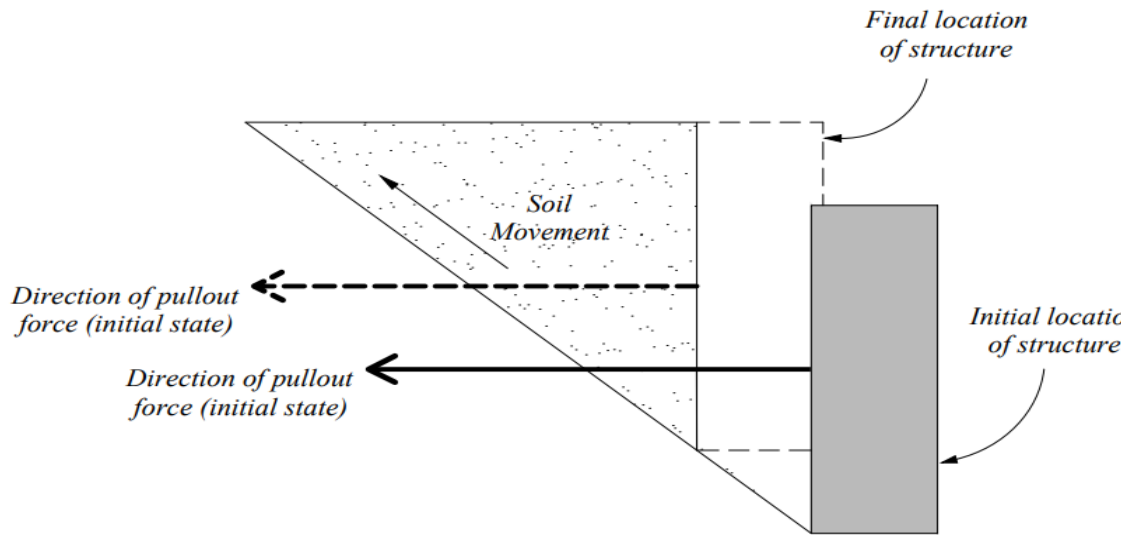
Where, $q_{u(rough)}$ = ultimate pullout capacity for rough anchor, and $q_{u(smooth)}$ = ultimate pullout capacity for smooth anchor. For $\phi' = 30^\circ$, for example, the anchor correction factor F_δ increases from approximately 1.15 for $H/B = 10$ to around 1.90 for $H/B = 1$. Two thirds of the total variation in fact occurs between $H/B = 4$ and 1.

In the case of a rough anchor, significant shear stresses will develop at the anchor interface in response to this upward movement. These shear stresses are resisted by the interface and contribute to the anchor capacity. The rupture surface pattern of passive soil wedge depends on many factors, including but not limited to the embedment depth of anchor, interface friction between soil and anchor, the density of soil. Duncan and Mokwa (2001) suggested that a certain magnitude of relative shear displacement across the interface is required to mobilize interface friction. They indicated that the amount of relative shear displacement required to mobilize the full strength of the interface is

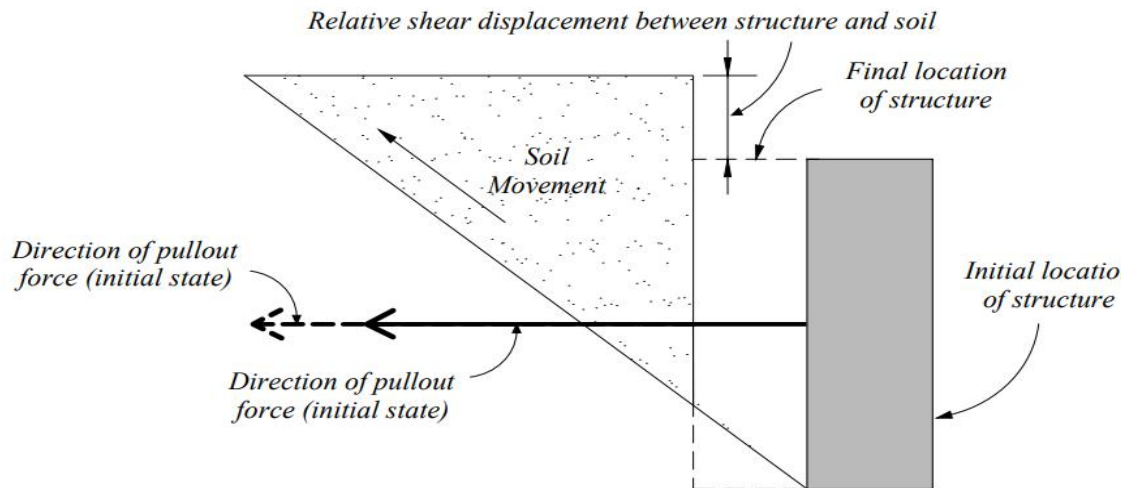
typically less than 2.5–6 mm. They further recommended that smaller relative displacements across the interface will result in only partial mobilization of the interface friction. It is to be noted that the occurrence of relative shear displacement will depend on whether the structure is heavy or light. Thus, analysis method largely depends on the assumption regarding the consideration of the structure to be heavy or light.

In case of light structures, the upward component of the passive resistance is so large as to cause upward movement of the anchor (Duncan and Mokwa, 2001). Thus, both the soil and structure move together like a single unit as illustrated in Figure 3.15(a). As a result, the shear forces across the interface cannot get mobilized. Duncan and Mokwa (2001) conducted a field test on reinforced concrete anchor block of size $1.1 \times 1.9 \times 0.9$ m using two different backfill materials. They observed that as the load was increased, both the anchor and the passive failure wedge moved together in lateral and upward direction and concluded that the interface friction for shallow anchor is controlled by the weight of anchor itself for vertical equilibrium rather than the relative displacement across the interface.

However, the scenario is completely different for heavy structures. Duncan and Mokwa (2001) indicated that if the vertical component of passive force is smaller than the weight of the structure, a slip will occur across the interface. In such situation, the soil moves in horizontal and upward direction, whereas the structure moves only in horizontal direction. As the soil moves upward with respect to the structure, there is a downward shear force on the soil and an upward shear force on the structure. Thus, in response to this upward movement, significant shear stresses develop at the anchor interface. This relative shear displacement will in turn mobilize the interface friction providing additional shear stresses to the system. These shear stresses contribute significantly to the pullout capacity (Duncan and Mokwa, 2001; Merifield and Sloan, 2006; and Kame et al., 2012a). From the extensive numerical analysis, Merifield and Sloan (2006), Kumar and Sahoo (2012), and Bhattacharyya and Kumar (2014) showed that the interface roughness has a significant influence on pullout capacity of a strip anchor. The shear stress developed along a rough interface tends to force the rupture surface downwards below the bottom of the anchor (Merifield and Sloan, 2006). Therefore, the rupture surface of the soil wedge becomes curvilinear.



(a)



(b)

Figure 3.15 Movement of the anchor-soil system due to pullout in (a) a light structure, (b) a heavy structure

The technique to determine δ for light and heavy structure is significantly different as suggested by Duncan and Mokwa (2001). For light structure, the interface friction angle completely depends on the weight of the anchor itself, but, for large structures several factors interact with each other to affect δ . For light structure, δ can be calculated using the expression $\delta = \tan^{-1} \left(\frac{W_b}{P_u} \right)$ and for heavy structure, force equilibrium of three forces, viz. the weight of the soil within the failure wedge, reactive force on the failure surface and the passive pressure on the wedge block is satisfied to obtain δ . It was reported by

Duncan and Mokwa (2001) that δ remains in the range of 4° – 6° when the anchor top is kept flush with the top of the existing ground level. However, with the increase of embedment depth, δ is also expected to increase.

Frictional resistance between soil and structure will obviously develop in the horizontal direction, since the pullout force from retaining structure causes horizontal shear displacement between soil and anchor. But, the key concern is the assumption of mobilization of vertical shear stresses. However, irrespective of the consideration of the weight of the structure, mobilization of interface frictional stress is observed by all the researchers discussed above, which leads no scope to omit the effect.

In the present analysis, the interface friction will be considered along all the faces of the anchor, as the soil-structure interface is assumed to be rough, and the structure can either be light or heavy. Existing studies suggest that for plate anchor (not strip ones), the mobilization of horizontal frictional forces although may be neglected due to the fact that surface area is smaller, for anchor block, the magnitude should not be ignored. Thus, author found it more logical to consider the interface friction to simulate the actual failure scenario. In the pullout capacity prediction models of the existing literature, δ is assumed preliminarily based on the anchor material. Some standard guidelines for estimating δ can be found in Potyondy (1961), Gireesha and Muthukkumaran (2011), Tiwari and Al-Adhadh (2014). In contrast, in the present analysis, as the failure surface is predetermined, owing to the equilibrium condition to be satisfied by the horizontal and vertical component of the passive earth pressures, δ will be obtained.

3.4.6 Formation of Side Flanks

The next consideration is based on the dilatancy property of soil. Soils, depending on their relative denseness undergo dilation during plastic deformation. Soil dilatancy is found to have a significant effect on the response of a vertical anchor. Merifield and Sloan (2006) observed that in the extreme case of an anchor in a dense non-dilatant soil ($\varphi' = 40^\circ, \psi' = 0^\circ$), the ultimate capacity was estimated to be approximately half of that for the same anchor in an associated soil ($\varphi' = 40^\circ, \psi' = 40^\circ$). They also suggested that because of localization, these results need to be treated with caution.

Zhao et al. (2011), Giampa et al. (2016) also suggested that dilatancy of soil mass needs to be considered as it plays a significant role in the pullout capacity of an anchor.

Dilatancy during plastic deformation tends to cause the soil in front of the anchor to lock up, and it is necessary for an extensive plastic region to develop before there is sufficient freedom for the collapse to occur (Rowe and Davis, 1982). Laboratory test results and numerical analysis also confirmed the formation of side wedges caused by dilation of soil (Rowe and Davis, 1982; Dickin and Leung, 1983; Kouzer and Kumar, 2009; Giampa et al., 2016). As an approximation, Reese et al. (1974) and Lin et al. (2014) suggested using $\alpha' = \varphi'/2$. This formation of side wedges inhibits the plane strain condition (2-Dimensional problem) and causes 3-Dimensional problem for the anchor. The conventional lateral earth pressure theory (Rankine, Coulomb) was developed for 2-Dimensional situation, which can be directly utilized for long/continuous anchor (e.g. strip anchor). For an anchor with limited aspect ratio, however, the different side conditions due to the formation of side flanks must be taken into consideration while utilizing the conventional lateral earth pressure theory to account the 3-Dimensional situation. The proposed method utilizes Kötter (1903) equation which also has the applicability in the plane strain problems. Thus, author made an effort to estimate the pullout capacity contributed from the side flanks as formed during the commencement of failure. The additional contribution will then be added to the pullout capacity obtained from the central region of the failure wedge, obtained from limit equilibrium analysis coupled with the assumption of pressure distribution using Kötter equation considering plane strain condition.

Rowe (1978) derived approximate values of dilatancy angle, ψ' for a particular value of φ_{ps} and φ_{cp} from the stress-dilatancy relationship. The relationship can be expressed as Eq. (3.6) and will be adopted in the present analysis to estimate α' .

$$\tan\left(45 + \frac{\psi'}{2}\right) = \frac{\tan\left(45 + \frac{\varphi_{ps}}{2}\right)}{\tan\left(45 + \frac{\varphi_{cp}}{2}\right)} \quad (3.6)$$

Where, φ_{ps} = peak plane strain friction angle, and φ_{cp} = critical state friction angle. In this study, from force equilibrium, the contributions from the side flanks will be estimated assuming $\psi' = \alpha'$. Dickin and Leung (1985), Lin et al. (2014) suggested that the passive failure angle at the side flank of the wedge can be reasonably approximated to be equal to $45^\circ + \varphi'/2$. On the contrary, author has different perspective to contradict the concept. Through extensive experimental investigation, it is established that as the embedment

depth increases, the failure path becomes curvilinear in nature. The curvilinear surface can better be approximated as logarithmic spiral surface. At an embedment depth ratio greater than 8, the failure pattern becomes circular. The failure wedge entails both central region and side flanks. However, in the junction region of the boundary of central region and side flank, a sudden jump from logarithmic spiral curve to a straight curve can hardly occur, as the total failure wedge works as a single unit. Thus, author thinks it would be more reasonable to consider a logarithmic spiral failure surface in the side flanks as well.

During the idealization of the failure mechanism of the side flanks, however, three approaches can be followed. The theory behind each of these methods is discussed herein.

In contrast to Neely's (1973) surcharge method, the first approach would consider the shear resistance of the soil above the top level of the anchor. This approach may generate over-optimistic results since both the weight and the shear resistance above the top level of anchor is being considered. However, in this approach, the shear resistance developed along the failure plane will be assumed to be uniform.

The second approach considers Neely's (1973) surcharge method and frictional force developed at the bottom of the wedge is uniform. However, as mentioned earlier in this chapter, this method does not consider the shear resistance obtained from the soil above the top level of the anchor.

Figure 3.16 shows a schematic sketch of the side flanks developed. From the illustration, it can be observed that the flank has a known width and height if the dilatancy angle is known in advance. Superimposing the two side flanks, an equivalent rectangular wedge having a width equal to the width of a single triangular wedge can be obtained. The width of wedge while development of the pullout capacity assuming plane strain condition, was B . Now, it is assumed that plane strain condition exists in the rectangular wedge also, then the thickness of the modified wedge can be taken as $(B + 2btan\alpha')$. This is the third approach. However, it is worth mentioning that such approach will omit the resistance obtained from the vertical face of the side flanks.

During the development of the theory for contribution from side flanks using first and second approaches, active force component, side friction component of anchor and bottom friction component of anchor is not considered, as these items are already considered during equilibrium condition of the failure wedge while considering plane

strain condition. Consideration of the above-mentioned terms might lead to double consideration of the force components.

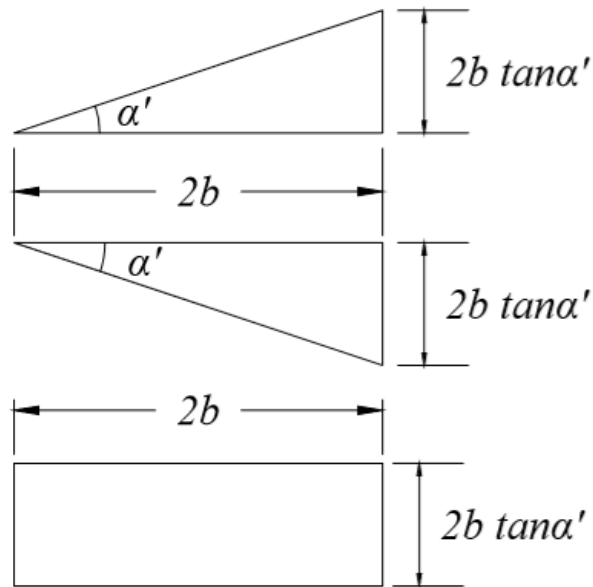


Figure 3.16 Plan view of the side flank formation during anchor pullout and consideration of equivalent rectangle to replace two triangles

3.5 Summary

In this chapter the assumptions associated with the analytical model to predict the pullout capacity of a vertical anchor is elaborately explained. The idealization includes assumptions regarding the shape of failure surface in both the active and the passive sides, pressure distribution on the failure surface, nature of load-displacement curve, nature of anchor-soil interface and nature of side flanks formed during failure. Applicability of the theory is also identified. The next chapter will focus on the mathematical basis of the assumption.

Chapter 4

DEVELOPMENT OF THE MATHEMATICAL MODEL

4.1 General

The theory on which the model is based is explained in the previous chapter. This chapter will elaborately show the mathematical formulation of the assumptions taken. Firstly, the analysis technique will be discussed. Thereafter, the breakdown of the techniques will be presented.

4.2 Analysis Technique

The total analysis technique has been broken down into two segments. In the first segment, the plane strain condition would be considered to determine the pullout capacity. Thereafter, in second segment the contribution from the side flanks formed during pullout will be considered.

4.3 Passive Pressure Calculation

The assumed failure surface in the passive side consists of an arc of logarithmic spiral and a straight line during most of the range of embedment depth ratio considered. The total passive pressure is the sum of the contributing resistances generating from the surcharge above the top level of anchor and the self-weight of the soil within the failure wedge along the assumed failure surface. Thus, owing to the equilibrium condition to be satisfied, total passive resistance acting in horizontal and vertical direction will be obtained.

4.3.1 Passive Pressure in Logarithmic Spiral Surface

As discussed in the previous chapter, failure surface entails a combination of logarithmic spiral curve and a tangent section following that curve for intermediate anchors. For shallow anchors, the failure surface is planar in nature. The passive pressure along the vertical anchor-soil interface can be estimated from the resistance developed along the failure plane due to surcharge and self-weight of soil. A schematic diagram of the assumed failure surface in the passive side is provided in Figure 4.1.

$$90 + \theta + 180 - \alpha + 90 - \varphi' = 360 \quad (4.3)$$

$$\text{or, } \theta - \alpha - \varphi' = 0 \quad (4.4)$$

$$\text{or, } \theta = \alpha + \varphi' \quad (4.5)$$

$$\therefore d\theta = d\alpha \quad (4.6)$$

The maximum spiral angle can be obtained from the geometry of $\angle IBD$ as

$$\theta_m = 90 - \left(45 - \frac{\varphi'}{2}\right) = 45 + \frac{\varphi'}{2} \quad (4.7)$$

From the theory of logarithmic spiral, a relationship between the differential surface and differential angle can be established, which can be expressed as-

$$ds = r \sec \varphi' d\theta \quad (4.8)$$

Putting the basic theory of logarithmic spiral surface from Eq. (4.8) in Eq. (4.2),

$$\frac{dp}{r \sec \varphi' d\theta} + 2p \tan \varphi' \frac{d\alpha}{r \sec \varphi' d\theta} = r \sin(\alpha + \varphi') \quad (4.9)$$

$$\text{or, } \frac{1}{r} \cos \varphi' \frac{dp}{d\theta} + \frac{2p \tan \varphi' d\alpha}{r \sec \varphi' d\theta} = \gamma \sin(\alpha + \varphi') \quad (4.10)$$

As obtained previously from the geometry of quadrilateral $BD'GG'$ in Figure 4.1,

$$\theta = \alpha + \varphi'$$

$$\therefore \alpha = \theta - \varphi'$$

Putting the value of α in Eq. (4.10),

$$\frac{1}{r} \cos \varphi' \frac{dp}{d\theta} + \frac{2p}{r} \sin \varphi' = \gamma \sin(\theta - \varphi' + \varphi') \quad (4.11)$$

$$\text{or, } \frac{1}{r} \cos \varphi' \frac{dp}{d\theta} + \frac{2p}{r} \sin \varphi' = \gamma \sin \theta \quad (4.12)$$

$$\text{or, } \frac{1}{r} \cos \varphi' \frac{dp}{d\theta} = \gamma \sin \theta - \frac{2p}{r} \sin \varphi' \quad (4.13)$$

$$or, \frac{dp}{d\theta} = \left(\gamma \sin \theta - \frac{2p}{r} \sin \varphi' \right) \frac{r}{\cos \varphi'} \quad (4.14)$$

$$or, \frac{dp}{d\theta} = \left(\gamma \sin \theta - \frac{2p}{r} \sin \varphi' \right) \frac{r_0 e^{\theta \tan \varphi'}}{\cos \varphi'} \quad (4.15)$$

$$or, \frac{dp}{d\theta} = \frac{\gamma r_0}{\cos \varphi'} e^{\theta \tan \varphi'} \sin \theta - \frac{2p}{\cos \varphi'} \sin \varphi' \quad (4.16)$$

$$or, \frac{dp}{d\theta} = \frac{\gamma r_0}{\cos \varphi'} e^{\theta \tan \varphi'} \sin \theta - 2p \tan \varphi' \quad (4.17)$$

Now, giving the complex constant terms a simple form,

$$a = \frac{\gamma r_0}{\cos \varphi'} \quad (4.18)$$

$$b = 2 \tan \varphi' \quad (4.19)$$

$$m = \tan \varphi' \quad (4.20)$$

Putting in Eq. (4.59),

$$\frac{dp}{d\theta} = a e^{m\theta} \sin \theta - bp \quad (4.21)$$

Considering, $\frac{d}{d\theta} = D$,

$$Dp + bp = a e^{m\theta} \sin \theta \quad (4.22)$$

$$or, (D + b)p = a e^{m\theta} \sin \theta \quad (4.23)$$

Such type of differential equation has two solution functions, viz. complementary function and particular integral. The complementary function can be obtained as-

The complementary function:

$$P = e^{m\theta} \quad (4.24)$$

Differentiating both sides,

$$Dp = m e^{m\theta} = mp \quad (4.25)$$

$$(D + b)p = 0 \quad (4.26)$$

Putting the value of P ,

$$m e^{m\theta} + b e^{m\theta} = 0 \quad (4.27)$$

$$\text{or, } e^{m\theta} (m + b) = 0 \quad (4.28)$$

$$\therefore m = -b \quad (4.29)$$

Thus, the complementary function (C.F) is-

$$C.F = c e^{-b\theta} \quad (4.30)$$

Where, c is a constant.

The particular integral:

$$P.I = a \frac{1}{D + b} e^{m\theta} \sin \theta \quad (4.31)$$

$$= a e^{m\theta} \frac{1}{(D + m) + b} \sin \theta \quad (4.32)$$

$$= a e^{m\theta} \frac{1}{D + b + m} \sin \theta \quad (4.33)$$

$$= a e^{m\theta} \frac{D - (b + m)}{\{D + (b + m)\}\{D - (b + m)\}} \sin \theta \quad (4.34)$$

$$= a e^{m\theta} \frac{D - (b + m)}{D^2 - (b + m)^2} \sin \theta \quad (4.35)$$

$$= a e^{m\theta} \frac{D - (b + m)}{-1 - b^2 - 2bm - m^2} \sin \theta \quad (4.36)$$

$$= -a e^{m\theta} \frac{D - (b + m)}{1 + b^2 + 2bm + m^2} \sin \theta \quad (4.37)$$

The particular integral (P.I) can be obtained as-

$$P.I = \frac{-a e^{m\theta}}{b^2 + 2bm + m^2 + 1} [\cos \theta - (b + m) \sin \theta] \quad (4.38)$$

Thus, the solution can be found by summing up both the complementary function and the particular integral.

$$\therefore P = \frac{-a e^{m\theta}}{b^2 + 2bm + m^2 + 1} [\cos \theta - (b + m) \sin \theta] + c e^{-b\theta} \quad (4.39)$$

Boundary condition; at $\theta = \theta_m ; P = P_E$

Putting values of a, b, m in Eq. (4.39),

$$P = - \frac{\frac{\gamma r_0}{\cos \varphi'} e^{m\theta}}{4 (\tan \varphi')^2 + 4 (\tan \varphi')^2 + (\tan \varphi')^2 + 1} (\cos \theta + 3 \tan \varphi' \sin \theta) + ce^{-2\theta \tan \varphi'} \quad (4.40)$$

$$\text{or, } P = - \frac{\frac{\gamma r_0}{\cos \varphi'} e^{\theta \tan \varphi'}}{9 (\tan \varphi')^2 + 1} (\cos \theta + 3 \tan \varphi' \sin \theta) + ce^{-2\theta \tan \varphi'} \quad (4.41)$$

Considering,

$$K = - \frac{\frac{\gamma r_0}{\cos \varphi'} e^{\theta \tan \varphi'}}{9 (\tan \varphi')^2 + 1} \quad (4.42)$$

Eq. (4.70) stands-

$$P = Ke^{\theta \tan \varphi'} (\cos \theta + 3 \tan \varphi' \sin \theta) + ce^{-2\theta \tan \varphi'} \quad (4.43)$$

Putting the value of boundary condition,

$$P_E = Ke^{\theta_m \tan \varphi'} (\cos \theta_m + 3 \tan \varphi' \sin \theta_m) + ce^{-2*\theta_m*\tan \varphi'} \quad (4.44)$$

$$\text{or, } ce^{-2*\theta_m*\tan \varphi'} = P_E - Ke^{\theta_m \tan \varphi'} (\cos \theta_m + 3 \tan \varphi' \sin \theta_m) \quad (4.45)$$

$$\text{or, } c = \frac{P_E - Ke^{\theta_m \tan \varphi'} (\cos \theta_m + 3 \tan \varphi' \sin \theta_m)}{e^{-2\theta_m \tan \varphi'}} \quad (4.46)$$

$$\text{or, } c = P_E e^{2\theta_m \tan \varphi'} - Ke^{3\theta_m \tan \varphi'} (\cos \theta_m + 3 \tan \varphi' \sin \theta_m)$$

$$\text{or, } c = P_E e^{2\theta_m \tan \varphi'} - K'$$

Where,

$$K' = Ke^{3\theta_m \tan \varphi'} (\cos \theta_m + 3 \tan \varphi' \sin \theta_m) \quad (4.47)$$

Now, to obtain the total reactive force, a surface integral needs to be performed over logarithmic spiral surface DE of Figure 4.1.

$$\therefore R_{PL} = \int_0^s p ds \quad (4.48)$$

However, the components of the reaction in horizontal and vertical direction need to be found. This needs the inclination of the force to be ascertained. Thus, the inclination of the force with horizontal can be obtained as below.

$$\begin{aligned}
\angle IBG &= \angle IBE + \angle EBD - \angle GBD \\
&= 45 - \frac{\varphi'}{2} + \theta_m - \theta \\
&= 45 - \frac{\varphi'}{2} + 45 + \frac{\varphi'}{2} - \theta \\
&= 90 - \theta
\end{aligned}$$

Thus, putting the value of inclination,

$$R_{PLV} = \int_0^{\theta_m} p \sin(90 - \varphi' - \alpha) ds \quad (4.49)$$

Again, as established earlier that $\theta = \alpha + \varphi'$,

$$\therefore 90 - (\alpha + \varphi') = (90 - \theta)$$

Thus,

$$\therefore R_{PLV} = \int_0^{\theta_m} p \sin(90 - \theta) ds \quad (4.50)$$

$$= \int_0^{\theta_m} p \cos \theta ds \quad (4.51)$$

Similarly,

$$R_{PLH} = \int_0^{\theta_m} p \sin \theta ds \quad (4.52)$$

From the theory of logarithmic spiral, it is already established that $ds = r \sec \varphi' d\theta$.

Therefore,

$$R_{Y_1PH} = \int_0^{\theta_m} p \sin \theta r \sec \varphi' d\theta \quad (4.53)$$

$$= \int_0^{\theta_m} p \sin \theta r_0 e^{\theta \tan \varphi'} \sec \varphi' d\theta \quad (4.54)$$

$$= r_0 \sec \varphi' \int_0^{\theta_m} p e^{\theta \tan \varphi'} \sin \theta d\theta \quad (4.55)$$

Putting value of P from Eq. (4.43),

$$= r_0 \sec \varphi' \int_0^{\theta_m} (K e^{\theta \tan \varphi'} \cos \theta e^{\theta \tan \varphi'} \sin \theta + K e^{\theta \tan \varphi'} 3 \tan \varphi' \sin \theta e^{\theta \tan \varphi'} \sin \theta + (P_E e^{2\theta_m \tan \varphi'} - K') e^{-2\theta \tan \varphi'} e^{\theta \tan \varphi'} \sin \theta) d\theta \quad (4.56)$$

$$= r_0 \sec \varphi' \int_0^{\theta_m} (K e^{2\theta \tan \varphi'} \cos \theta \sin \theta + K e^{2\theta \tan \varphi'} 3 \tan \varphi' (\sin \theta)^2 + (P_E e^{2\theta_m \tan \varphi'} - K') e^{-\theta \tan \varphi'} \sin \theta) d\theta \quad (4.57)$$

$$= r_0 \sec \varphi' \int_0^{\theta_m} \left(\frac{K}{2} e^{2\theta \tan \varphi'} \sin 2\theta + 3 \tan \varphi' K e^{2\theta \tan \varphi'} (\sin \theta)^2 + (P_E e^{2\theta_m \tan \varphi'} e^{-\theta \tan \varphi'} \sin \theta - K' e^{-\theta \tan \varphi'} \sin \theta) \right) d\theta \quad (4.58)$$

From trigonometry, it is known that $2 (\sin \theta)^2 = 1 - \cos 2\theta$.

$$\therefore R_{PLH} = r_0 \sec \varphi' \int_0^{\theta_m} \left\{ \frac{K}{2} e^{2\theta \tan \varphi'} \sin 2\theta + 3 \tan \varphi' \frac{K}{2} e^{2\theta \tan \varphi'} (1 - \cos 2\theta) + (P_E e^{2\theta_m \tan \varphi'} e^{-\theta \tan \varphi'} \sin \theta - K' e^{-\theta \tan \varphi'} \sin \theta) \right\} d\theta \quad (4.59)$$

$$\begin{aligned} \text{or, } R_{PLH} &= r_0 \sec \varphi' \frac{K}{2} \int_0^{\theta_m} e^{2\theta \tan \varphi'} \sin 2\theta d\theta \\ &+ r_0 \sec \varphi' 3 \tan \varphi' \frac{K}{2} \int_0^{\theta_m} e^{2\theta \tan \varphi'} d\theta \\ &- r_0 \sec \varphi' \frac{3}{2} \tan \varphi' K \int_0^{\theta_m} e^{2\theta \tan \varphi'} \cos 2\theta d\theta \\ &+ r_0 \sec \varphi' P_E e^{2\theta_m \tan \varphi'} \int_0^{\theta_m} e^{-\theta \tan \varphi'} \sin \theta d\theta \\ &- r_0 \sec \varphi' K' \int_0^{\theta_m} e^{-\theta \tan \varphi'} \sin \theta d\theta \end{aligned} \quad (4.60)$$

Now, performing simple integration (Refer to Appendix A for more details),

$$\begin{aligned}
R_{PLH} &= r_0 \sec \varphi' \frac{K}{2} 2I_1 + r_0 \sec \varphi' P_E e^{2\theta_m \tan \varphi'} .I_2 - r_0 \sec \varphi' K' I_2 \\
&\quad + r_0 \sec \varphi' 3 \tan \varphi' \frac{K}{2} \frac{(e^{2\theta_m \tan \varphi'} - 1)}{2 \tan \varphi'} \\
&\quad - r_0 \sec \varphi' 3 \tan \varphi' \frac{K}{2} 2J_1
\end{aligned} \tag{4.61}$$

$$\begin{aligned}
or, R_{PLH} &= r_0 \sec \varphi' K I_1 + r_0 \sec \varphi' P_E e^{2\theta_m \tan \varphi'} .I_2 - r_0 \sec \varphi' K' I_2 \\
&\quad - r_0 \sec \varphi' 3 \tan \varphi' K J_2 + r_0 \sec \varphi' \frac{3K}{4} (e^{2\theta_m \tan \varphi'} - 1)
\end{aligned} \tag{4.62}$$

$$\begin{aligned}
or, R_{PLH} &= r_0 \sec \varphi' [K I_1 + P_E e^{2\theta_m \tan \varphi'} I_2 - K' I_2 + 3 \tan \varphi' K J_2 \\
&\quad + \frac{3K}{4} (e^{2\theta_m \tan \varphi'} - 1)]
\end{aligned} \tag{4.63}$$

Similarly, the vertical component can be obtained as-

$$R_{PLV} = \int_0^{\theta_m} P \cos \theta ds \tag{4.64}$$

$$= \int_0^{\theta_m} P \cos \theta r \sec \varphi' d\theta \tag{4.65}$$

$$= \int_0^{\theta_m} P \cos \theta r_0 e^{\theta \tan \varphi'} \sec \varphi' d\theta \tag{4.66}$$

$$= r_0 \sec \varphi' \int_0^{\theta_m} P e^{\theta \tan \varphi'} \cos \theta d\theta \tag{4.67}$$

Putting value of P from Eq. (4.72),

$$\begin{aligned}
&= r_0 \sec \varphi' \int_0^{\theta_m} \{K e^{\theta \tan \varphi'} \cos \theta e^{\theta \tan \varphi'} \cos \theta \\
&\quad + K e^{\theta \tan \varphi'} 3 \tan \varphi' \sin \theta e^{\theta \tan \varphi'} \cos \theta + (P_E e^{2\theta_m \tan \varphi'} \\
&\quad - K') e^{-\theta 2 \tan \varphi'} e^{\theta \tan \varphi'} \cos \theta \} d\theta
\end{aligned} \tag{4.68}$$

$$\begin{aligned}
&= r_0 \sec \varphi' \int_0^{\theta_m} (K e^{2\theta \tan \varphi'} (\cos \theta)^2) d\theta \\
&\quad + r_0 \sec \varphi' K \frac{3}{2} \tan \varphi' \int_0^{\theta_m} e^{2\theta \tan \varphi'} \sin \theta \cos \theta d\theta \\
&\quad + r_0 \sec \varphi' P_E e^{2\theta_m \tan \varphi'} \int e^{-\theta \tan \varphi'} \cos \theta d\theta \\
&\quad - r_0 \sec \varphi' K' \int e^{-\theta \tan \varphi'} \cos \theta d\theta
\end{aligned} \tag{4.69}$$

From trigonometry, it is known that $2 (\cos \theta)^2 = 1 + \cos 2\theta$

$$\begin{aligned}
\therefore R_{PLV} &= r_0 \sec \varphi' \int_0^{\theta_m} K e^{2\theta \tan \varphi'} (1 + \cos 2\theta) d\theta \\
&\quad + r_0 \sec \varphi' K \frac{3}{2} \tan \varphi' \int_0^{\theta_m} e^{2\theta \tan \varphi'} \sin 2\theta d\theta \\
&\quad + r_0 \sec \varphi' P_E e^{2\theta_m \tan \varphi'} \int_0^{\theta_m} e^{-\theta \tan \varphi'} \cos \theta d\theta \\
&\quad - r_0 \sec \varphi' K' \int_0^{\theta_m} e^{-\theta \tan \varphi'} \cos \theta d\theta
\end{aligned} \tag{4.70}$$

$$\begin{aligned}
\text{or, } R_{PLV} &= r_0 \sec \varphi' \frac{K}{2} \int_0^{\theta_m} e^{2\theta \tan \varphi'} d\theta \\
&\quad + r_0 \sec \varphi' \frac{K}{2} \int_0^{\theta_m} e^{2\theta \tan \varphi'} \cos 2\theta d\theta \\
&\quad + r_0 \sec \varphi' K \frac{3}{2} \tan \varphi' \int_0^{\theta_m} e^{2\theta \tan \varphi'} \sin 2\theta d\theta \\
&\quad + r_0 \sec \varphi' P_E e^{2\theta_m \tan \varphi'} \int_0^{\theta_m} e^{-\theta \tan \varphi'} \cos \theta d\theta \\
&\quad - r_0 \sec \varphi' K' \int_0^{\theta_m} e^{-\theta \tan \varphi'} \cos \theta d\theta
\end{aligned} \tag{4.71}$$

Now, performing simple integration the horizontal component of the reaction force developed can be obtained as the form of Eq. (4.72). Detailed calculation is provided in Appendix A.

$$\begin{aligned}
R_{PLV} = r_0 \sec \varphi' \frac{K (e^{2\theta_m \tan \varphi'} - 1)}{2 \tan \varphi'} + r_0 \sec \varphi' \frac{K}{2} 2J_1 \\
+ r_0 \sec \varphi' K \frac{3}{2} \tan \varphi' 2I_1 + r_0 \sec \varphi' P_E e^{2\theta_m \tan \varphi'} J_2 \\
- r_0 \sec \varphi' K' J_2
\end{aligned} \tag{4.72}$$

$$\begin{aligned}
\text{or, } R_{PLV} = r_0 \sec \varphi' \left[\frac{K (e^{2\theta_m \tan \varphi'} - 1)}{4 \tan \varphi'} + KJ_1 + 3KI_1 \tan \varphi' \right. \\
\left. + P_E e^{2\theta_m \tan \varphi'} J_2 - K' J_2 \right]
\end{aligned} \tag{4.73}$$

4.3.2 Passive Pressure in Plane Surface

Figure 4.2 shows the free body diagram depicting the forces generated from surcharge and self-weight on the plane failure surface. From the geometry of the wedge block IEF (Figure 4.2), as the EF surface considered here is plane, it can be understood that-

$$\frac{d\alpha}{ds} = 0 \tag{4.74}$$

In passive side, $\alpha = 45 - \frac{\varphi'}{2}$

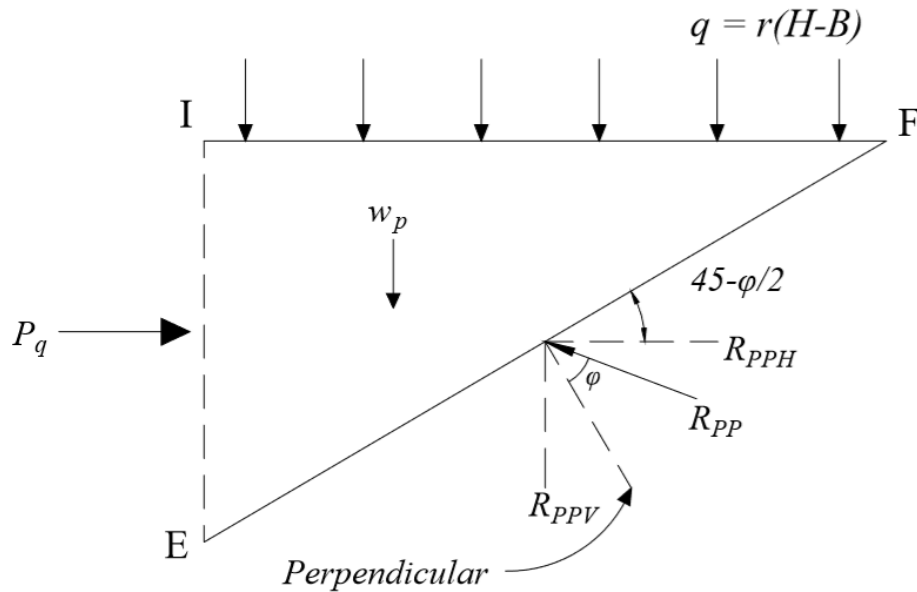


Figure 4.2 Free body diagram showing the forces acting in planar zone

Eq. (4.2) stands,

$$\frac{dp}{ds} = \gamma \sin(\alpha + \varphi') \quad (4.75)$$

$$\text{or, } \frac{dp}{ds} = \gamma \sin(45 - \frac{\varphi'}{2} + \varphi') \quad (4.76)$$

$$\text{or, } \frac{dp}{ds} = \gamma \sin(45 + \frac{\varphi'}{2}) \quad (4.77)$$

$$\text{or, } dp = \gamma \sin(45 + \frac{\varphi'}{2}) ds \quad (4.78)$$

Integrating within the limits,

$$\int_{P_F}^{P_E} dp = \gamma \sin(45 + \frac{\varphi'}{2}) \int_0^{l_{EF}} ds \quad (4.79)$$

$$\text{or, } P_E - P_F = \gamma \sin(45 + \frac{\varphi'}{2}) l_{EF} \quad (4.80)$$

$$\text{or, } P_E = \gamma \sin(45 + \frac{\varphi'}{2}) l_{EF} + P_F \quad (4.81)$$

The vertical pressure acting on point F of the failure wedge IEF is equal to $\gamma(H - B)$. The corresponding horizontal pressure can be determined as $K_p\gamma(H - B)$. Thus, the component of the pressure along a plane subtending an angle equal to φ' can be determined as

$$P_F = K_p\gamma(H - B) \cos(45 - \frac{\varphi'}{2}) \quad (4.82)$$

Thus, Eq. (4.81) stands

$$P_E = \gamma \sin(45 + \frac{\varphi'}{2}) l_{EF} + K_p\gamma(H - B) \cos(45 - \frac{\varphi'}{2}) \quad (4.83)$$

Thus, the total force working on the plane failure surface EF can be estimated as $\frac{1}{2}l_{EF}(P_E + P_F)$.

$$R_{PP} = \frac{1}{2}l_{EF} \left\{ \gamma \sin(45 + \frac{\varphi'}{2}) l_{EF} + 2K_p\gamma(H - B) \cos(45 - \frac{\varphi'}{2}) \right\} \quad (4.84)$$

As the inclination of the reaction is $45 - \varphi'/2$ with the horizontal, the component of force in horizontal and vertical direction can be obtained as follows.

$$R_{PPH} = \frac{1}{2} l_{EF} \left\{ \gamma \sin\left(45 + \frac{\phi'}{2}\right) l_{EF} + 2K_p \gamma (H - B) \cos\left(45 - \frac{\phi'}{2}\right) \right\} \quad (4.85)$$

$$* \cos\left(45 - \frac{\phi'}{2}\right)$$

$$R_{PPV} = \frac{1}{2} l_{EF} \left\{ \gamma \sin\left(45 + \frac{\phi'}{2}\right) l_{EF} + 2K_p \gamma (H - B) \cos\left(45 - \frac{\phi'}{2}\right) \right\} \quad (4.86)$$

$$* \sin\left(45 - \frac{\phi'}{2}\right)$$

In Figure 4.3, passive resistance forces acting on the failure surface is shown. Therefore, the horizontal component of passive force on vertical surface can be obtained from horizontal equilibrium of the forces shown in Figure 4.3 as,

$$P_{PH} = R_{PLH} + R_{PPH} \quad (4.87)$$

Similarly, the vertical component of passive force acting on the vertical surface can be obtained from vertical equilibrium of the forces shown in Figure 4.3.

$$P_{PV} = R_{PLV} + R_{PPV} - W_l - W_p - q \quad (4.88)$$

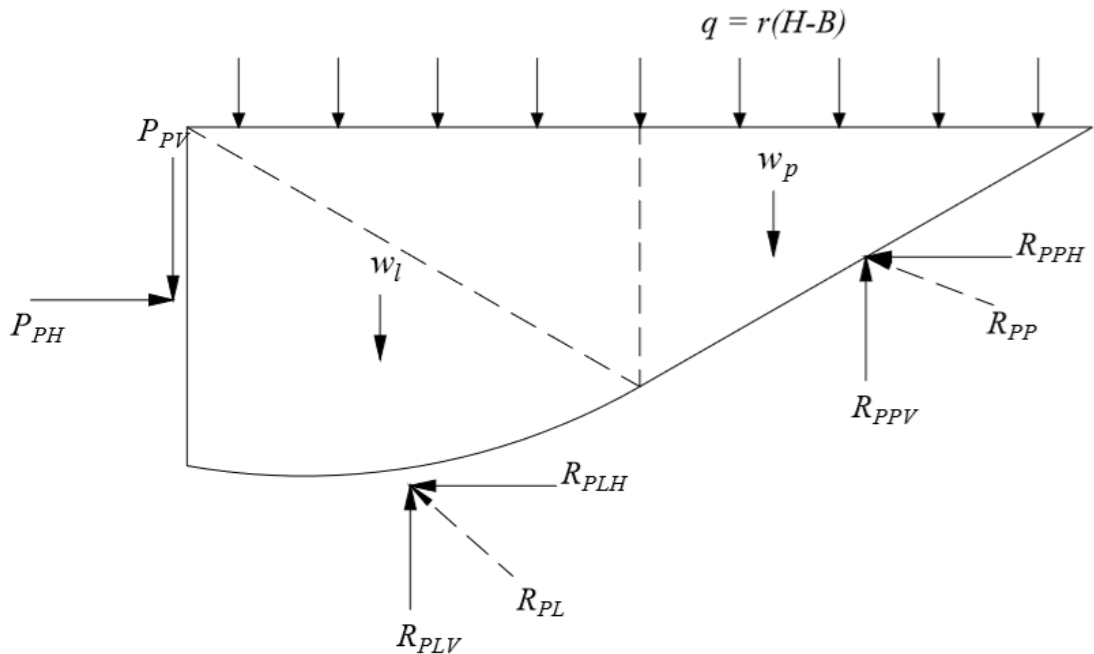


Figure 4.3 Free body diagram showing passive resistance forces acting on the failure surface

4.4 Active Pressure Calculation

A similar approach adopted for estimation of total passive resistance will be used to estimate the total active resistance from the back of anchor. However, the only difference is that only planar failure surface is assumed in active side, in contrast to the combination of logarithmic spiral arc and straight line in the passive side. In Figure 4.4, the wedge block in active side along with the forces acting is presented.

In cohesionless soil medium, under plane strain condition, in active state of equilibrium, Kötter equation can be expressed as-

$$\frac{dp}{ds} - 2p \tan\phi' \frac{d\alpha}{ds} = \gamma \sin(\alpha - \phi') \quad (4.89)$$

Figure 4.4 shows the failure plane due to the stress generated across the failure plane. As the surface being considered here is plane-

$$\frac{d\alpha}{ds} = 0 \quad (4.90)$$

Thus, the Kötter equation stands-

$$\frac{dp}{ds} = \gamma \sin(\alpha - \phi') \quad (4.91)$$

Since, in active side, $\alpha = 45 + \frac{\phi'}{2}$

$$dp = \gamma \sin\left(45 + \frac{\phi'}{2} - \phi'\right) ds \quad (4.92)$$

$$\text{or, } dp = \gamma \sin\left(45 - \frac{\phi'}{2}\right) ds \quad (4.93)$$

Integrating,

$$\int_{P_P}^{P_R} dp = \gamma \sin\left(45 - \frac{\phi'}{2}\right) \int_0^{l_{PR}} ds \quad (4.94)$$

$$P_R - P_P = \gamma \sin\left(45 - \frac{\phi'}{2}\right) l_{PR} \quad (4.95)$$

$$P_R = \gamma \sin\left(45 - \frac{\phi'}{2}\right) l_{PR} + P_P \quad (4.96)$$

The vertical pressure acting on point F of the failure wedge IEF is equal to $\gamma(H - B)$. The corresponding horizontal pressure can be determined as $K_a\gamma(H - B)$. Thus, the component of the pressure along a plane subtending an angle equal to φ' can be determined as

$$P_P = K_a\gamma(H - B) \cos\left(45 + \frac{\varphi'}{2}\right) \quad (4.97)$$

Thus, Eq. (4.96) stands

$$P_R = \gamma \sin\left(45 - \frac{\varphi'}{2}\right) l_{PR} + K_a\gamma(H - B) \cos\left(45 + \frac{\varphi'}{2}\right) \quad (4.98)$$

Total force acting on the failure surface due to self-weight is $= \frac{1}{2}(P_P + P_R) \cdot l_{PR}$

$$R_{AP} = \frac{1}{2} l_{PR} \left\{ \gamma \sin\left(45 - \frac{\varphi'}{2}\right) l_{PR} + 2K_a\gamma(H - B) \cos\left(45 + \frac{\varphi'}{2}\right) \right\} \quad (4.99)$$

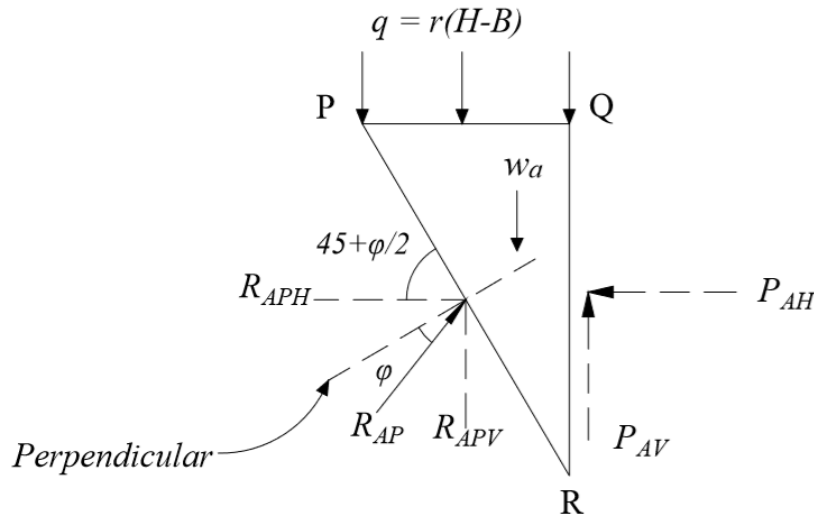


Figure 4.4 Free body diagram showing the wedge block in active side

As the inclination of the reaction is $45 + \varphi'/2$ with the horizontal, the component of force in horizontal and vertical direction can be obtained as the form of Eq. (4.100) and Eq. (4.101).

$$R_{APH} = \frac{1}{2} l_{PR} \left\{ \gamma \sin\left(45 - \frac{\varphi'}{2}\right) l_{PR} + 2K_a\gamma(H - B) \cos\left(45 + \frac{\varphi'}{2}\right) \right\} \cos\left(45 + \frac{\varphi'}{2}\right) \quad (4.100)$$

$$R_{APV} = \frac{1}{2} l_{PR} \left\{ \gamma \sin\left(45 - \frac{\varphi'}{2}\right) l_{PR} + 2K_a \gamma (H - B) \cos\left(45 + \frac{\varphi'}{2}\right) \right\} \sin\left(45 + \frac{\varphi'}{2}\right) \quad (4.101)$$

4.5 Friction Forces around the Anchor

It is to be noted that whenever pullout force is exerted via the attachment to a rebar, side friction would be developed along the outer surfaces of the anchor. However, the magnitude of the force would depend on the roughness of the interface. This is elaborately discussed in the previous chapter. Thus, friction components can be determined as-

$$F_b = \gamma H \tan \delta_b L t \quad (4.104)$$

$$F_t = W_s \tan \delta_t = \gamma (H - B) \tan \delta_t L t \quad (4.105)$$

$$F_s = \gamma \left(H - \frac{B}{2} \right) \tan \delta_s B t \quad (4.106)$$

4.6 Equilibrium of the Anchor

As all the force components are known, horizontal equilibrium needs to be maintained to obtain the pullout capacity. Figure 4.5 shows the forces acting on the free body of anchor.

Thus, from horizontal equilibrium,

$$P_{AH} L + P_u - P_{PH} L - 2F_s - F_b - F_t = 0 \quad (4.107)$$

$$\text{or, } P_u = (P_{PH} - P_{AH}) L + 2F_s + F_b + F_t \quad (4.108)$$

Thus, putting the values from Eq. (4.87), Eq. (4.102), Eq. (4.104), Eq. (4.105), and Eq. (4.106) the ultimate pullout capacity can be obtained. As discussed in the previous chapter, the pullout capacity obtained from Eq. (4.108) considers the contribution from central flank only.

4.7 Contribution from the Side Flanks

In the last chapter, the theory of the approach is explained. As mentioned there, three approaches can be followed to estimate the contribution from the side flanks to ultimate pullout capacity. Thus, at first, the mathematics of first approach will be presented.

Subsequently, other approaches will be addressed. Figure 4.6 depicts the failure mechanism assumed.

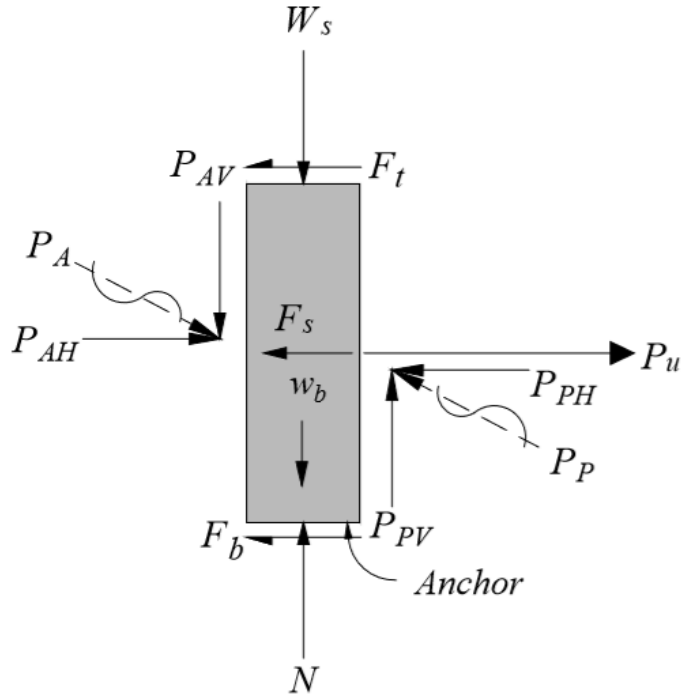


Figure 4.5 Free body diagram showing the forces acting on anchor

From vertical equilibrium, $\sum F_v = 0$;

$$W + 2F_{sf} \cos \beta + F_{bf} \cos \beta - F_{bn} \sin \beta = 0 \quad (4.109)$$

The relationship between the forces in horizontal and vertical face of the failure surface in soil can be given by the expression of Eq. (4.110) from the theory of soil mechanics as-

$$F_{bf} = F_{bn} \tan \varphi \quad (4.110)$$

Putting the value in Eq. (4.109),

$$W + 2F_{sf} \cos \beta + F_{bn} \tan \varphi' \cos \beta - F_{bn} \sin \beta = 0 \quad (4.111)$$

$$\text{or, } F_{bn} (\tan \varphi' \cos \beta - \sin \beta) = -W - 2F_{sf} \cos \beta \quad (4.112)$$

$$\text{or, } F_{bn} = \frac{W + 2F_{sf} \cos \beta}{(\sin \beta - \tan \varphi' \cos \beta)} \quad (4.113)$$

From horizontal equilibrium, $\sum F_h = 0$;

$$P_{u_{side}} - 2F_{sf} \sin \beta \cos \alpha' + 2F_{sn} \sin \alpha' - F_{bf} \sin \beta - F_{bn} \cos \beta = 0 \quad (4.114)$$

Putting Eq. (4.110) into Eq. (4.114),

$$P_{u_{side}} - 2F_{sf} \sin \beta \cos \alpha + 2F_{sn} \sin \alpha' - F_{bn} \tan \varphi' \sin \beta - F_{bn} \cos \beta = 0 \quad (4.115)$$

$$\text{or, } P_{u_{side}} - 2F_{sf} \sin \beta \cos \alpha' + 2F_{sn} \sin \alpha' - F_{bn} (\tan \varphi' \sin \beta + \cos \beta) = 0 \quad (4.116)$$

$$\text{or, } P_{u_{side}} = 2F_{sf} \sin \beta \cos \alpha' - 2F_{sn} \sin \alpha + F_{bn} (\tan \varphi' \sin \beta + \cos \beta) \quad (4.117)$$

Putting Eq. (4.113) in Eq. (4.117),

$$P_{u_{side}} = 2F_{sf} \sin \beta \cos \alpha' - 2F_{sn} \sin \alpha' + \frac{W + 2F_{sf} \cos \beta}{(\sin \beta - \tan \varphi' \cos \beta)} (\tan \varphi' \sin \beta + \cos \beta) \quad (4.118)$$

From trigonometric transformation,

$$\frac{(\tan \varphi' \sin \beta + \cos \beta)}{(\sin \beta - \tan \varphi' \cos \beta)} = \frac{1 + \tan \varphi' \tan \beta}{\tan \beta - \tan \varphi'} = \frac{1}{\tan(\beta - \varphi')} \quad (4.119)$$

Putting it in Eq. (4.118), the expression becomes-

$$P_{u_{side}} = 2F_{sf} \sin \beta \cos \alpha' - 2F_{sn} \sin \alpha' + \frac{W + 2F_{sf} \cos \beta}{\tan(\beta - \varphi')} \quad (4.120)$$

Determination of the parameters F_{sf} , and F_{sn} requires estimation of the area within the failure surface.

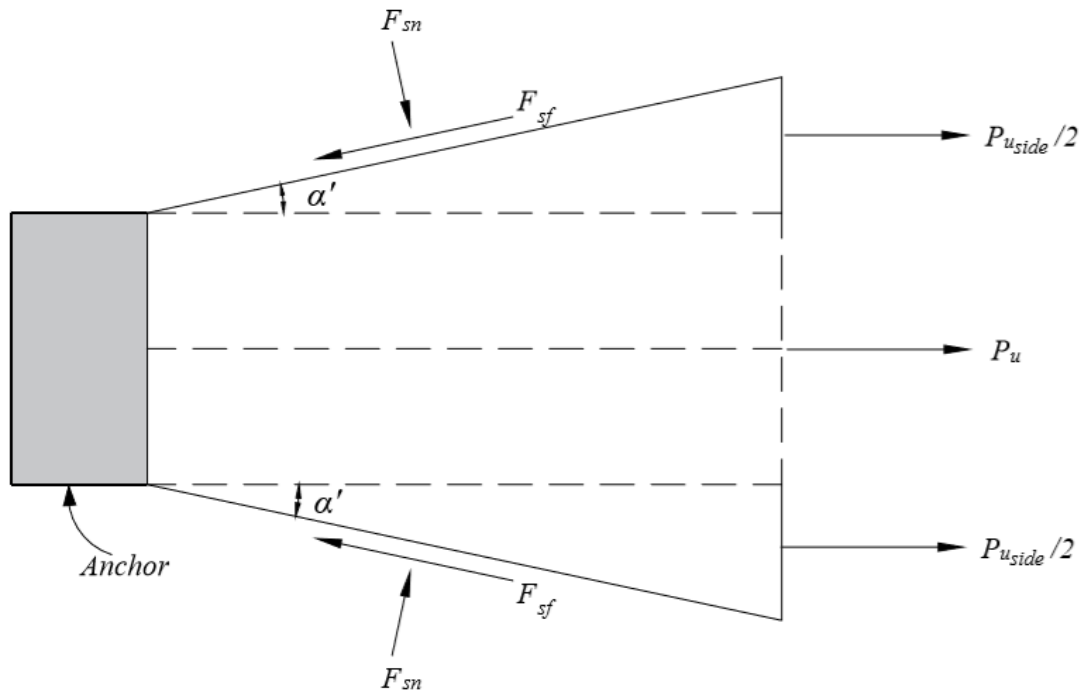
Area within zone *ODE*:

Zone *ODE* is schematized in Figure 4.7.

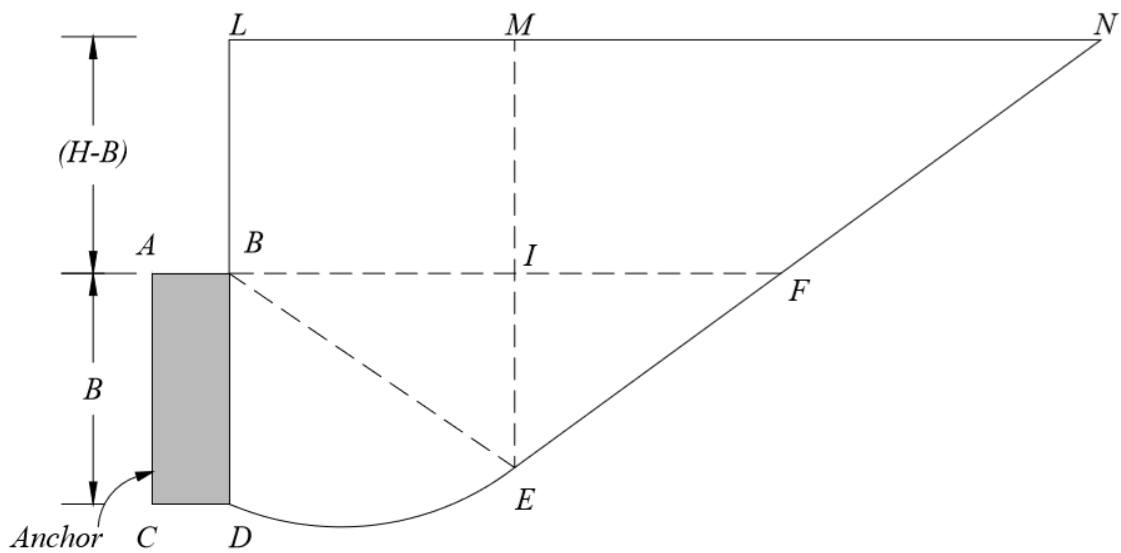
$$A = \int_0^{\theta_m} \frac{1}{2} r (r d\theta) \quad (4.121)$$

Using simple integration, (Refer to Appendix A for more detail)

$$A = \frac{r_1^2 - r_0^2}{4 \tan \varphi'} \quad (4.122)$$



(a)



(b)

Figure 4.6 Formation of side flanks due to pullout force exerted from the tie rod (a) plan view, (b) sectional view

From Figure 4.8, using simple geometry,

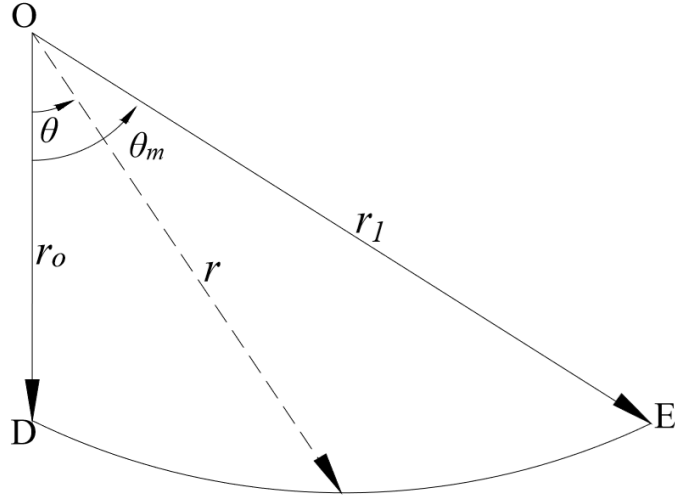


Figure 4.7 Schematic view of Zone ODE to estimate the enclosed area

$$\frac{b}{r_1} = \cos\left(45 - \frac{\varphi'}{2}\right) \text{ or, } b = r_1 \cos\left(45 - \frac{\varphi'}{2}\right) \quad (4.123)$$

It is known that-

$$r_1 = r_0 e^{\theta_m \tan \varphi'}; \text{ or, } r_1 = r_0 e^{\left(\frac{\pi}{4} + \frac{\varphi'}{2}\right) \tan \varphi'}; \text{ or, } r_1 = k r_0; \text{ or, } r_1 = k B \text{ [Where, } k = f(\varphi)] \quad (4.124)$$

$$\therefore b = k B \cos\left(45 - \frac{\varphi'}{2}\right) = BI = IF = k' B \quad (4.125)$$

Where,

$$k' = k \cos\left(45 - \frac{\varphi'}{2}\right) \quad (4.126)$$

Again, from $\triangle BIE$ in Figure 4.8,

$$\begin{aligned} \frac{h}{r_1} &= \sin\left(45 - \frac{\varphi'}{2}\right); \text{ or, } h = r_1 \sin\left(45 - \frac{\varphi'}{2}\right) \\ &= k B \sin\left(45 - \frac{\varphi'}{2}\right) = k'' B = IE \end{aligned} \quad (4.127)$$

Where,

$$k'' = k \sin\left(45 - \frac{\phi'}{2}\right) \quad (4.128)$$

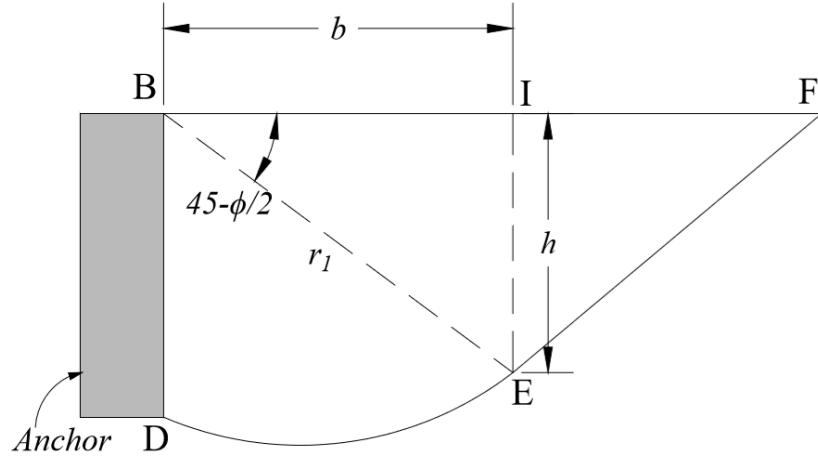


Figure 4.8 Geometry of the failure surface in passive side to estimate some anchor parameters

The distance EM (Figure 4.6(b)) can be determined as-

$$EM = (H - B) + IE = (H - B) + k''B \quad (4.129)$$

Total area can be obtained as-

$$\sum A = \Delta BDE + \Delta BIE + \square BILM + \Delta EMN \quad (4.130)$$

$$\text{Area of } \Delta BIE = \frac{1}{2} \cdot b \cdot k'' \cdot B = \frac{1}{2} k''B \cdot k'' \cdot B = \frac{1}{2} k''^2 B^2 \quad (4.131)$$

$$\text{Area of } \square BILM = b(H - B) = k''B(H - B) \quad (4.132)$$

$$\text{Area of } \Delta EMN = \frac{1}{2} MN * ME = \frac{1}{2} b \left(1 + \frac{H - B}{k''B}\right) * (k''B + H - B) \quad (4.133)$$

$$\text{Area of } \Delta BDE = \frac{r_1^2 - B^2}{4 \tan \phi'} \quad (4.134)$$

Thus, F_{sn} and F_{sf} can be estimated as-

$$F_{sn} = \sum_{i=1}^4 A_i * \frac{1}{\cos \alpha'} \cdot K_a \gamma h_c \quad (4.135)$$

$$F_{sf} = F_{sn} \cdot \tan \varphi' \quad (4.136)$$

Determination of h_c :

Locating h_c requires proper estimation of the centroid of the area within the failure surface.

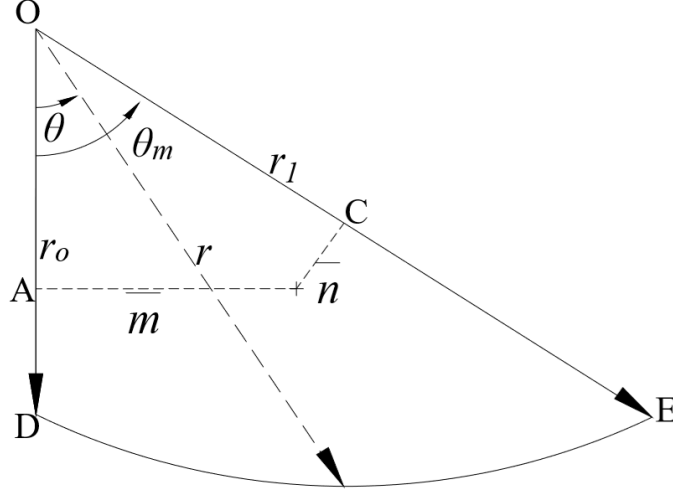


Figure 4.9 Estimation of the centroid of Zone *ODE*

In, Zone *ODE* of Figure 4.9, Hijab (1956) suggested that the centroid can be estimated if the two parameters \bar{m} and \bar{n} are known.

$$\bar{m} = \frac{4}{3} * \frac{r_0 \tan \varphi'}{1 + 9 (\tan \varphi')^2} \left[\frac{\left(\frac{r_0}{r_1}\right)^3 (3 \tan \varphi' \sin \theta - \cos \theta) + 1}{\left(\frac{r_1}{r_0}\right)^2 - 1} \right] \quad (4.137)$$

$$\bar{n} = \frac{4}{3} * \frac{r_0 \tan \varphi'}{1 + 9 (\tan \varphi')^2} \left[\frac{\left(\frac{r_0}{r_1}\right)^3 - 3 \tan \varphi' \sin \theta - \cos \theta}{\left(\frac{r_1}{r_0}\right)^2 - 1} \right] \quad (4.138)$$

Using the principle of Pythagoras, iteration can be performed to locate distance *OA*.

$$\bar{m}^2 + OA^2 = \bar{n}^2 + OC^2 \quad (4.139)$$

Applying simple geometry, the centroid can be located.

$$\tan \alpha = \frac{\bar{m}}{OA}; \text{ or, } OA = \frac{\bar{m}}{\tan \alpha'} \left[\theta_m = 45 - \frac{\varphi}{2} \right] \quad (4.140)$$

Again,

$$\tan(\theta_m - \alpha') = \frac{\bar{n}}{OC}; \text{ or, } OC = \frac{\bar{n}}{\tan(\theta_m - \alpha')} \quad (4.141)$$

From $\triangle OAB$ and $\triangle OCB$

$$\alpha = \tan^{-1} \left[\frac{\sin \theta_m}{\frac{\bar{n}}{\bar{m}} + \cos \theta_m} \right] \quad (4.142)$$

Detailed calculation is provided in Appendix A. Putting the obtained value, OA can be determined.

$$\tan \alpha = \frac{\bar{m}}{OA} \quad (4.143)$$

$$\text{or, } OA = \frac{\bar{m}}{\tan \alpha'} \quad (4.144)$$

$$\text{Distance from the surface} = BL + h_1 = H - B + OA \quad (4.145)$$

In $\triangle BIE$;

$$\text{center} = \frac{IE}{3} = \frac{k''B}{3} \quad (4.146)$$

$$\text{Distance from the surface} = MI + \frac{k''B}{3} = H - B + \frac{k''B}{3} \quad (4.147)$$

In $\triangle EMN$;

$$\text{center} = \frac{ME}{3} = \frac{MI + IE}{3} = \frac{H - B + k''B}{3} \quad (4.148)$$

In $\square BIML$;

$$\text{center} = \frac{H - B}{2} \quad (4.149)$$

$$\therefore \sum_{i=1}^4 A_i h_i = \sum_{i=1}^4 A_i * h_c \quad (4.150)$$

$$\text{Actual area} = \frac{A_i}{\cos \alpha'} \quad (4.151)$$

$\cos \alpha'$ cancels out from both sides. Thus, the effect was not considered in either side.

Weight components:

$$V = \oint A dy \quad (4.152)$$

Figure 4.10 shows the volume to be integrated to obtain the weight of the system in side flank.

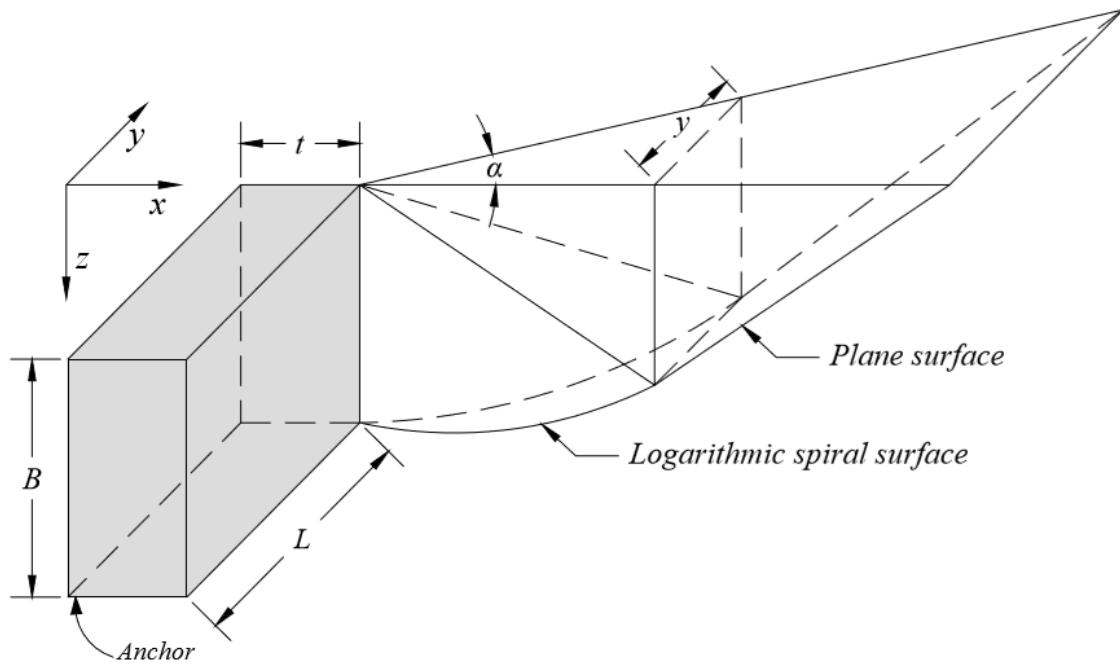


Figure 4.10 Integration volume to obtain the weight enclosed within the failure surface in side flanks

From geometry of the side flank as depicted in Figure 4.10,

$$\tan \alpha' = \frac{y}{x}; \text{ or, } y = x \tan \alpha' \quad (4.153)$$

Differentiating both sides,

$$dy = \tan \alpha' dx \quad (4.154)$$

at $x = 0; y = 0$ and at $x = x_m; y = y_m$

From the principle of similar triangle, from ΔEIF and ΔEMN in Figure 4.6(b) the limit of the volume to be integrated can be obtained as follows-

$$\begin{aligned} \frac{MN}{EM} &= \frac{IF}{IE} \text{ or, } MN = \frac{IF}{IE} * EM \text{ or, } MN = \frac{b}{IE} * (IE + IM) \text{ or, } MN \\ &= b \left(1 + \frac{IM}{IE} \right) \end{aligned} \quad (4.155)$$

$$\text{or, } MN = b \left(1 + \frac{H - B}{IE} \right) \text{ or, } MN = b \left(1 + \frac{H - B}{k''B} \right) \quad (4.156)$$

$$\begin{aligned} LN &= LM + MN \text{ or, } LN = b + b \left(1 + \frac{H - B}{k''B} \right) \text{ or, } LN \\ &= b + b + b \cdot \frac{1}{k''} \left(\frac{H}{B} - \frac{B}{B} \right) \end{aligned} \quad (4.157)$$

$$\text{or, } LN = 2b + b \cdot \frac{1}{k''} \left(\frac{H}{B} - 1 \right) \text{ or, } LN = b \left[2 + \frac{1}{k''} \left(\frac{H}{B} - 1 \right) \right] \quad (4.158)$$

From Figure 4.10, the limit of volume integration can be set from 0 to y_m .

$$x_m = LN \quad (4.159)$$

$$\begin{aligned} V &= \int_0^{y_m} A \, dy \\ &= \int_0^{x_m} A \tan \alpha' \, dx \\ &= A \tan \alpha' \int_0^{x_m} dx = A \tan \alpha' [x]_0^{x_m} \end{aligned} \quad (4.160)$$

$$\text{Volume, } V = A \tan \alpha' b \left[2 + \frac{1}{k''} \left(\frac{H}{B} - 1 \right) \right] \quad (4.161)$$

Where,

$$A = \sum_{i=1}^4 A_i \quad (4.162)$$

Thus, total weight of soil within the failure wedge in passive side can be estimated as-

$$W = \gamma * \sum V \quad (4.163)$$

As already mentioned in the previous chapter, active force and both the bottom and side friction forces are not considered here, as these items are already considered in plane strain capacity determination.

Now, the second approach will be illustrated. The difference between the two approaches is that the later one neglects the shear resistance above the top surface of the anchor which means the weight component will not be considered above that level. Thus, it will affect the centroid determination only.

Determination of h_c :

Locating h_c requires proper estimation of the centroid of the area within the failure surface.

In, Zone *ODE* of Figure 4.9, *OA* can be determined from Eq. (4.144).

From ΔBEF in Figure 4.8,

$$\text{center} = \frac{IE}{3} = \frac{k''B}{3} \quad (4.164)$$

$$\text{Distance from the surface} = \frac{k'B}{3} \quad (4.165)$$

$$\therefore \sum_{i=1}^2 A_i h_i = \sum_{i=1}^2 A_i * h_c \quad (4.166)$$

However, area in the inclined surface can be determined using Eq. (4.130).

As side flanks having similar geometry develop from both the edges of the anchor, an equivalent rectangle (from plan view) can be considered for the simplicity of analysis instead of two triangular wedges independently. The third approach uses Kötter equation; however, the width of the wedge is $(B + 2btan\alpha')$. Thus, the contribution from the side flanks using the present approach can be determined by replacing B with $(B + 2btan\alpha')$. It is to be noted that in this approach, the friction developed along the vertical face of the triangular wedges is not considered, leading to a conservative result. It eventually suggests that application of the third approach considers a plane strain condition. However, application of the first two approaches considers a 3-D analysis.

Finally, putting the values of F_{sn} , F_{sf} , and W from Eq. (4.135), Eq. (4.136) and Eq. (4.163) in Eq. (4.120), the expression of contribution from side flanks stands as-

$$\begin{aligned}
& P_{u_{side}} \\
& = 2 \sum_{i=1}^n A_i \cdot K_a \gamma h_c \cdot \tan \varphi' \sin(45 + \varphi'/2) - 2 \sum_{i=1}^n A_i \cdot K_a \gamma h_c \tan \alpha' \\
& + \frac{\gamma \sum_{i=1}^n A_i \tan \alpha' b \left[2 + \frac{1}{k''} \left(\frac{H}{B} - 1 \right) \right] + 2 \sum_{i=1}^n A_i * \frac{1}{\cos \alpha'} \cdot K_a \gamma h_c \cdot \tan \varphi'}{\sec(45 + \varphi'/2) * \tan(45 - \varphi'/2)}
\end{aligned} \tag{4.167}$$

Thus, the pullout capacity of anchor considering the three-dimensional effect can be obtained by adding the pullout capacity obtained from plane strain condition to the pullout capacity that can be obtained from the sides of the wedge block. Therefore,

$$P_{ultimate} = P_u + P_{u_{side}} \tag{4.168}$$

Finally, putting the values from Eq. (4.108) and Eq. (4.167), the ultimate pullout capacity can be obtained. However, this obtained pullout capacity will be compared to the pullout prediction models in the available literature and the suitability will be assessed for any particular situation. The next chapter contains the validation of the model.

4.8 Summary

In this chapter an elaborate mathematical insight into the determination of pullout capacity for both shallow and intermediate anchor is presented. At first pullout capacity is obtained assuming a plane strain condition and then the contribution of the side flank is taken into consideration.

Chapter 5

RESULTS AND DISCUSSIONS

5.1 General

The results obtained from a selection of existing theoretical and experimental studies are reported in this section. The results are then compared with the predictions from the present study and a brief discussion is presented.

For convenience, the comparison with the existing techniques will be presented in the analogous form presented in the literature of interest. Two commonly used parameters will thus be used to compare the predictions from different models. These are-

- i) Anchor breakout factor
- ii) Force coefficient

Anchor breakout factor will be denoted as, N_γ and will be expressed as-

$$N_\gamma = \frac{P_{ultimate}}{\gamma HBL} \quad (5.1)$$

Force coefficient will be denoted as, $M_{\gamma q}$ and will be expressed as-

$$M_{\gamma q} = \frac{P_{ultimate}}{\gamma B^2 L} \quad (5.2)$$

The comparison can take one of the two forms, such as (i) comparison with experimental studies, and (ii) comparison with theoretical studies.

5.2 Comparison with Experimental Studies

Although numerical studies have caught the attention of present researchers there are no better alternative to full scale field tests. However, field scale experimental techniques are generally cost restrictive. Thus, researchers also focused on prototype chamber model tests and centrifuge tests. The results obtained from several experimental studies will now be compared with the predictions from the present method.

Experimental investigation on the behavior of vertical anchor has been studied by Neely et al. (1973). Both the square and rectangular anchors having an embedment depth ratio

up to 5 were tested. Three aspect ratios such as 1, 2 and 5, with a friction angle of 38.5° were investigated. The reported breakout factors corresponding to an aspect ratio of 5 are presented in Figure 5.1. It can be observed that for embedment depth ratio within the range of 1 to 4, the predicted breakout factor from the present study is in good agreement with the reported breakout factor in Neely et al. (1973). Beyond the aforementioned range, Neely's (1973) experimental scheme seems to overestimate the breakout factor. It was also reported in Neely et al. (1973) that for an embedment depth ratio greater than 2, very large displacements were observed, implying load-displacement curves were still increasing when the test was terminated. Thus, the ultimate pullout capacity would vary from the reported one. This might have caused the discrepancy of breakout factors between the predicted pullout capacity from the present study with the Neely et al. (1973) reported capacities beyond an embedment depth ratio of 4.

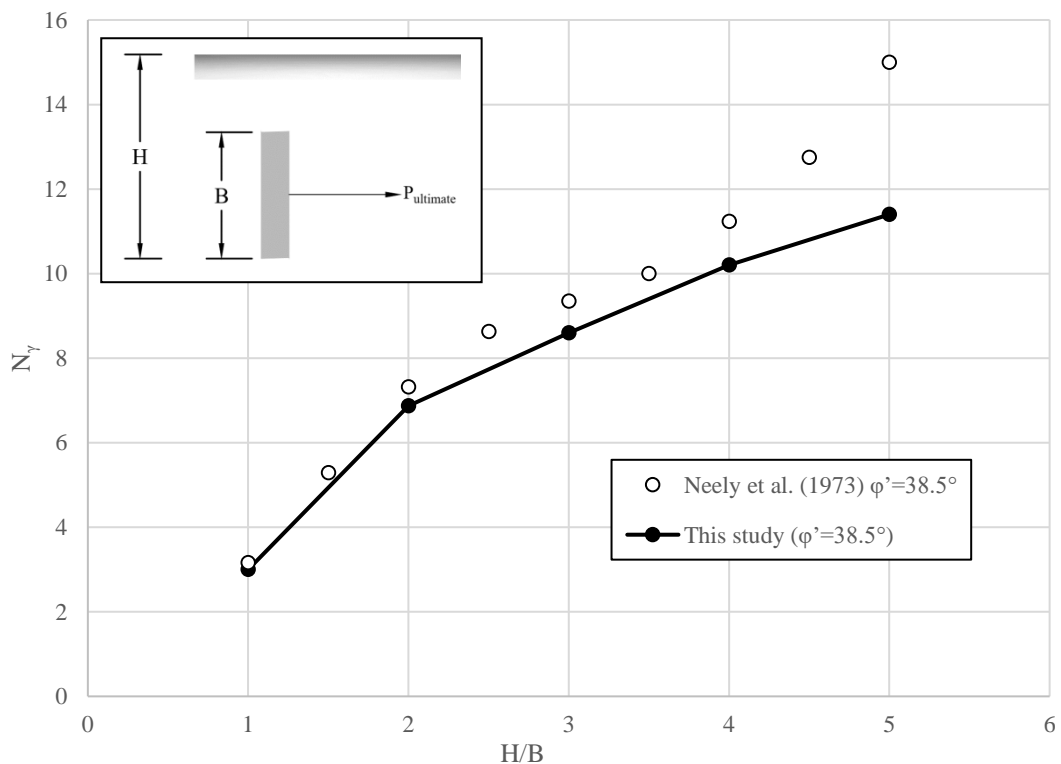


Figure 5.1 Comparison of breakout factors with Neely et al. (1973)

The capacity of vertical plate anchors has also been studied by Akinmusuru (1978) and Hoshiya and Mandal (1984). Akinmusuru (1978) investigated square, rectangular and circular anchors with an embedment depth ratio ranging from 1 to 10. Hoshiya and Mandal (1984) conducted tests on small scale anchors in a 300 mm \times 400 mm sand chamber. The results are presented in Figure 5.2. Based on the rigorous numerical

investigations of Merifield and Sloan (2006), Hanna et al. (2011), it can be said that the chamber considered by them was insufficient to contain the whole collapse mechanism, which eventually caused the overprediction of the methods. Throughout the embedment depth ratio considered both the methods predicted pullout capacity significantly higher than the prediction from the present study. The overprediction was as much as 145% at an embedment depth ratio of 7. Thus, boundary condition might have contributed to the observed breakout factor.

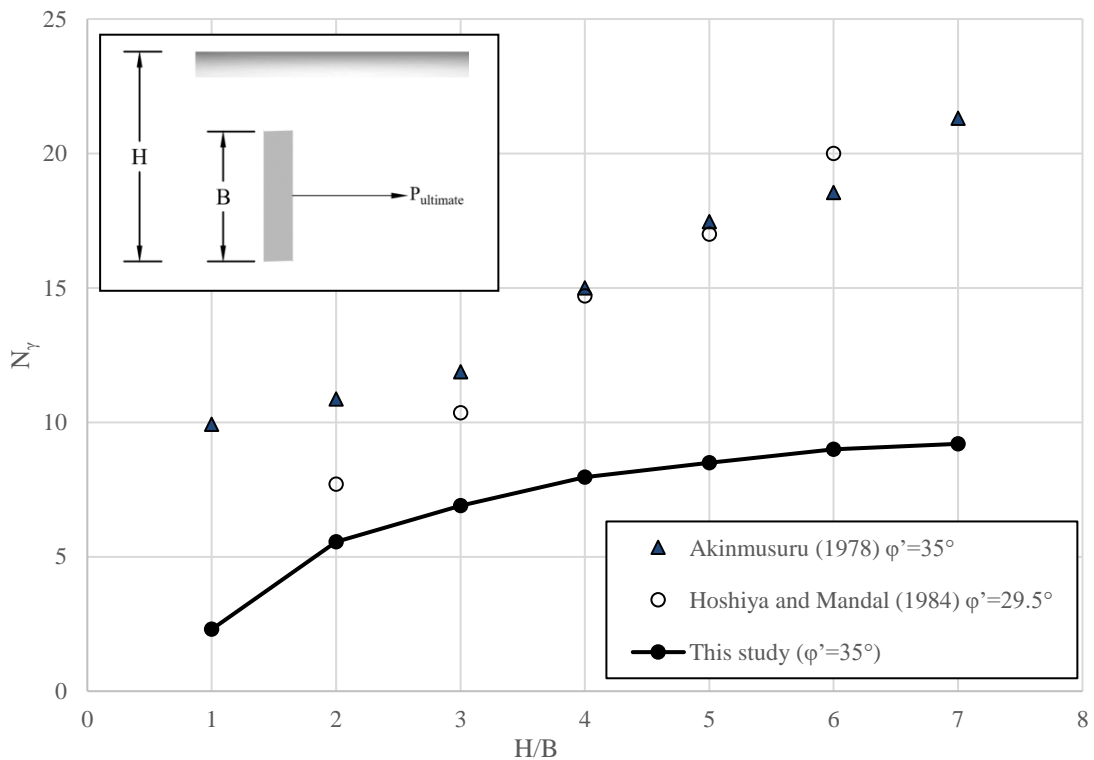


Figure 5.2 Comparison of breakout factors with Akinmusuru (1978) and Hoshiya and Mandal (1984)

Dickin and Leung (1983) conducted small-scale conventional model tests and also centrifuge tests on vertical anchors placed in sand. Some of the results are presented in Figure 5.3. It can be observed that for the embedment depth ratio considered, the predictions from the current method provided higher breakout factors compared to the 50 mm model tests and centrifuge test results of Dickin and Leung (1983) in most of the cases. The maximum overprediction was 12.1% compared to the centrifuge test, and it was 2.6% compared to the 50 mm model test. However, Dickin and Leung (1983), while comparing the experimental results with the existing theoretical method observed the optimistic output of their experimental program. Only Biarez et al. (1965) method

predicted lower than Dickin and Leung (1983). It is also to be noted that both the 50 mm model test result and centrifuge test results didn't match, and the discrepancy was as much as 17%, owing to the scale errors incurred in the model and centrifuge tests. Although, Dickin and Leung (1983) concluded that the results obtained from centrifuge model tests provide a more reliable basis for full scale anchor design, such assumption is debatable at the current state-of-the-art, since both the small-scale model tests and centrifuge tests are subjected to significant scale errors while extrapolating to field conditions.

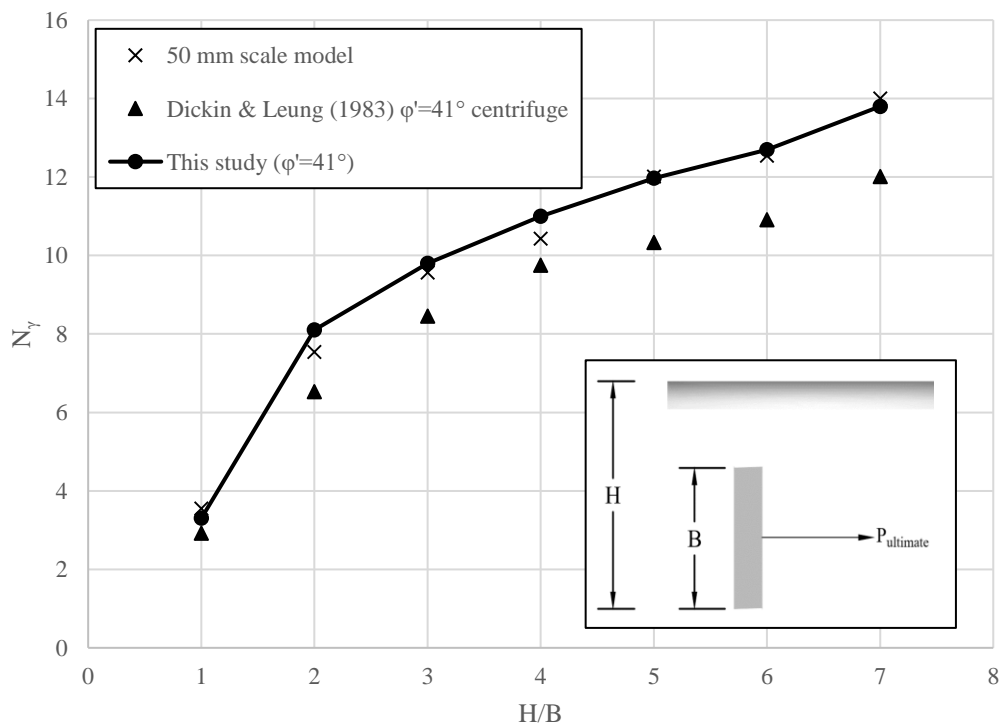


Figure 5.3 Comparison of breakout factors with Dickin and Leung (1983)

Dickin and Leung (1985) conducted prototype tests using two different size anchors. Their test program included tests on both continuous and single anchors with width/height ratios of 1, 2 and 5 at embedment ratios up to 8. Some of the test results are presented in Figure 5.4, expressed in terms of dimensionless force coefficient, $M_{\gamma q}$. The agreement of the prediction of the present analysis with that of square anchor is highly encouraging, indicated by exact matches within the embedment depth ratios of 2 to 8. For rectangular anchors, the present analysis provides a close estimate with the observation of Dickin and Leung (1985) as well. For all the aspect ratios considered, at an embedment depth ratio of 1, the present analysis seems to underpredict the force coefficient and for the other embedment depth considered, the prediction from present model provides an almost

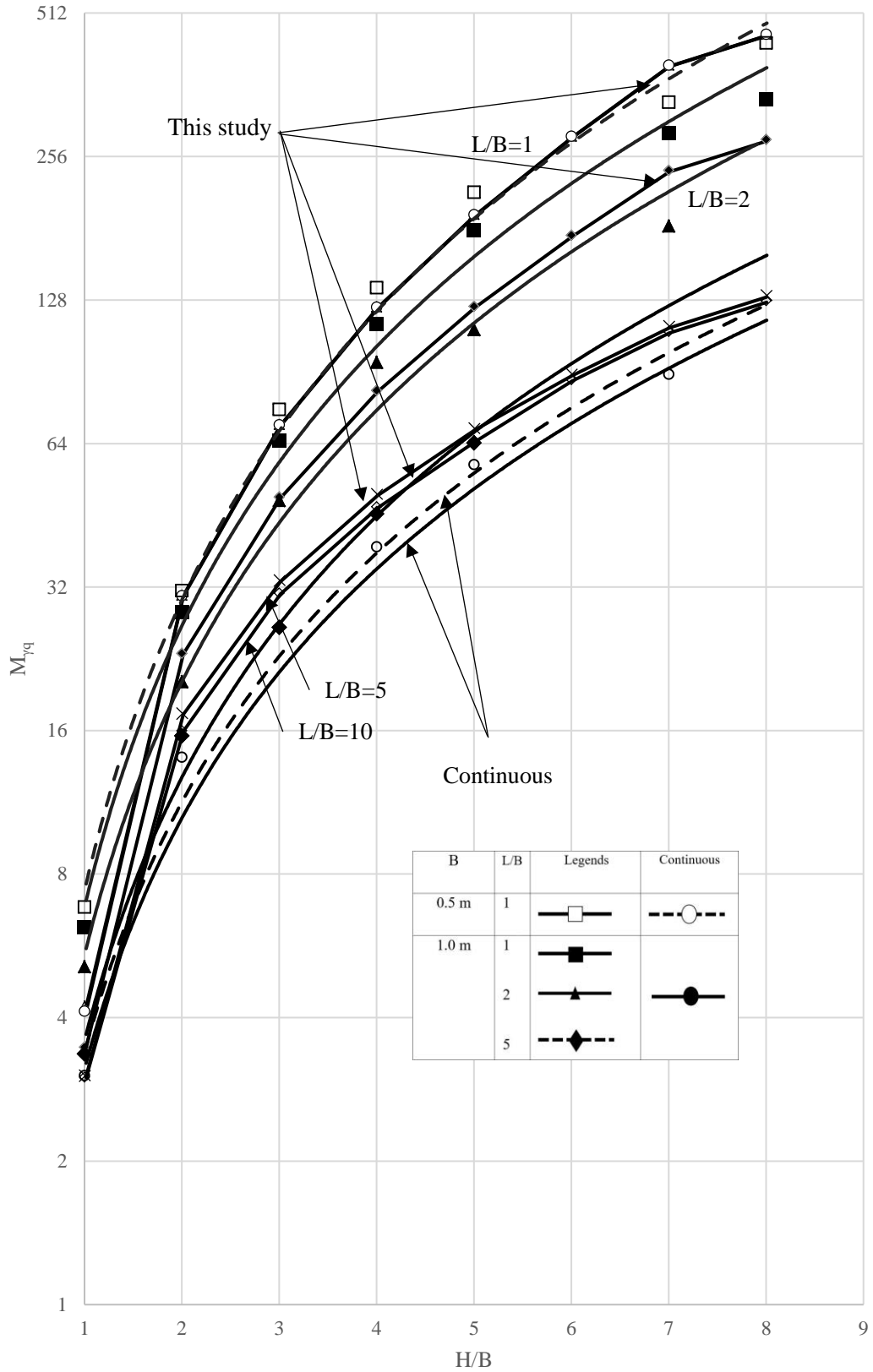


Figure 5.4 Comparison of breakout factors with Dickin and Leung (1985)

exact match with the experimental observations. In addition, at any particular embedment depth ratio, the effect of anchor geometry is apparent from Figure 5.4. It seems that with the increase of aspect ratio, the force coefficient decreases. It can also be observed that the decrease of force coefficient is negligible with the increase of aspect ratio from 5 to 10, and experimental results corresponding to continuous anchor almost matches the curve corresponding to an aspect ratio of 5 or 10.

In Figure 5.5, the available theoretical prediction methods such as, Biarez et al. (1965), Ovesen and Stromann (1972), Meyerhof (1973), Neely et al. (1973) are compared with the model test results using 50 mm high continuous anchors of Dickin and Leung (1985). The prediction of the present analysis is also presented in the same plot. It seems that in general all the theoretical prediction techniques yielded a higher estimation of force coefficient compared to the same reported by Dickin and Leung (1985). Compared to the other theoretical methods, the prediction from the present analysis seems to provide the best results. The maximum discrepancy (underprediction) of the present method is about 12% at an embedment depth ratio of 1.

However, among other theoretical methods, only Biarez et al. (1965) provided the lowest overprediction, which is 55.7%, indicating the better accuracy of the present method. It is important to note that throughout the embedment depth ratio considered, the prediction from the present model provide a lower force coefficient compared to the experimental results of Dickin and Leung (1985). From the reliability point of view, such underprediction is highly encouraging. It should be noted that at shallow depth, the present analysis assumes a planar failure surface, however, in actual field conditions, a non-linear failure surface may occur, which might increase the weight contained within the failure surface. This might be considered as an explanation of maximum underprediction of force coefficient at shallow depth using the present analysis technique.

In Figure 5.6, a comparison among the theoretical predictions available in the existing literature, the estimate from the present study and the experimental force coefficient reported for a 25 mm prototype centrifuge model test by Dickin and Leung (1985) are presented. It seems that the prediction from Biarez et al. (1965) and the prediction from the present model is in close agreement with the experimental results reported by Dickin and Leung (1985). It is important to note that the failure mechanism assumed by Biarez et al. (1965) is rotational in nature, which is the general occurrence for deep anchors.

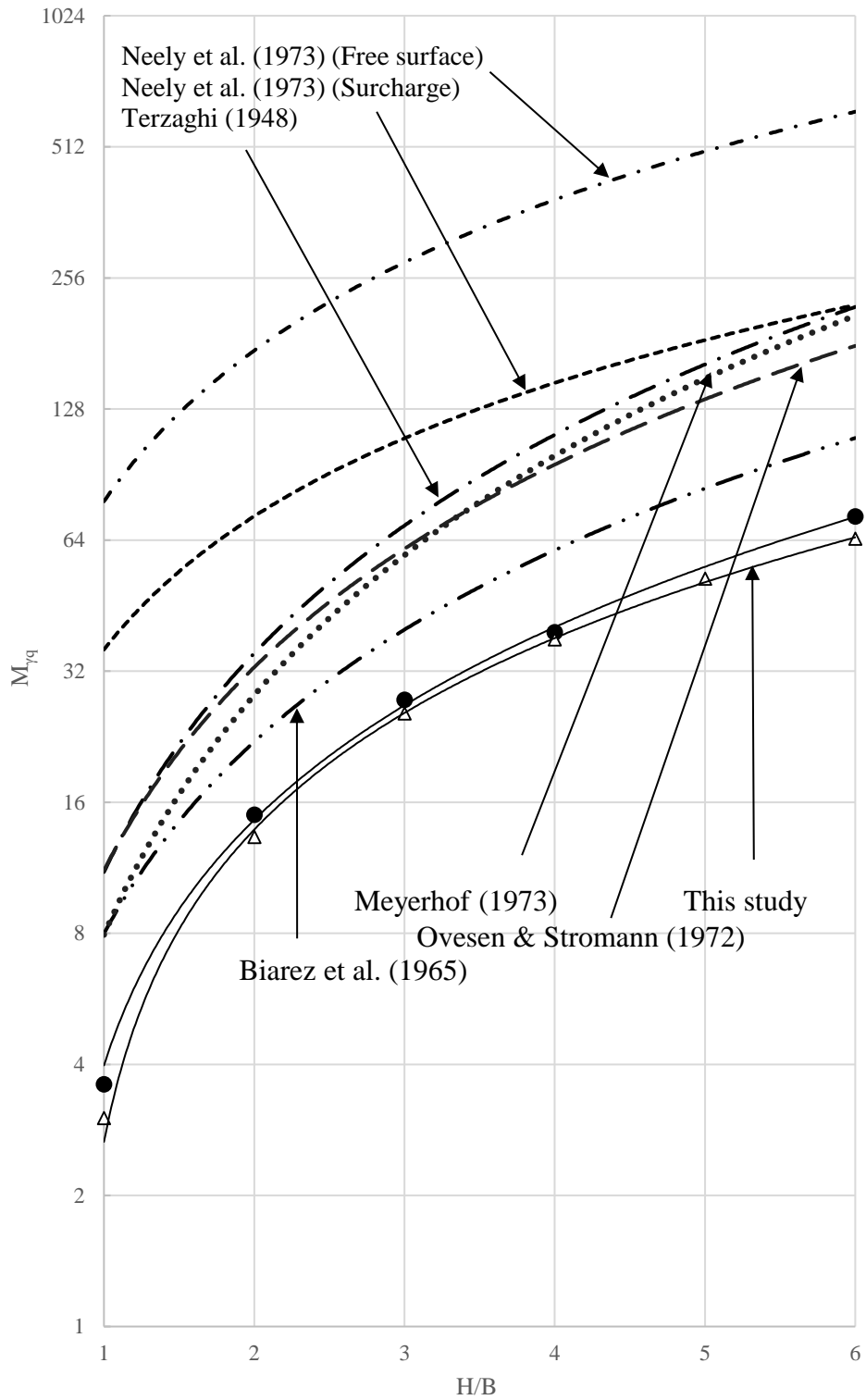


Figure 5.5 Comparison of force coefficients obtained from existing theoretical prediction techniques with the experimental force coefficients reported in Dickin and Leung (1985) corresponding to 50 mm high anchor

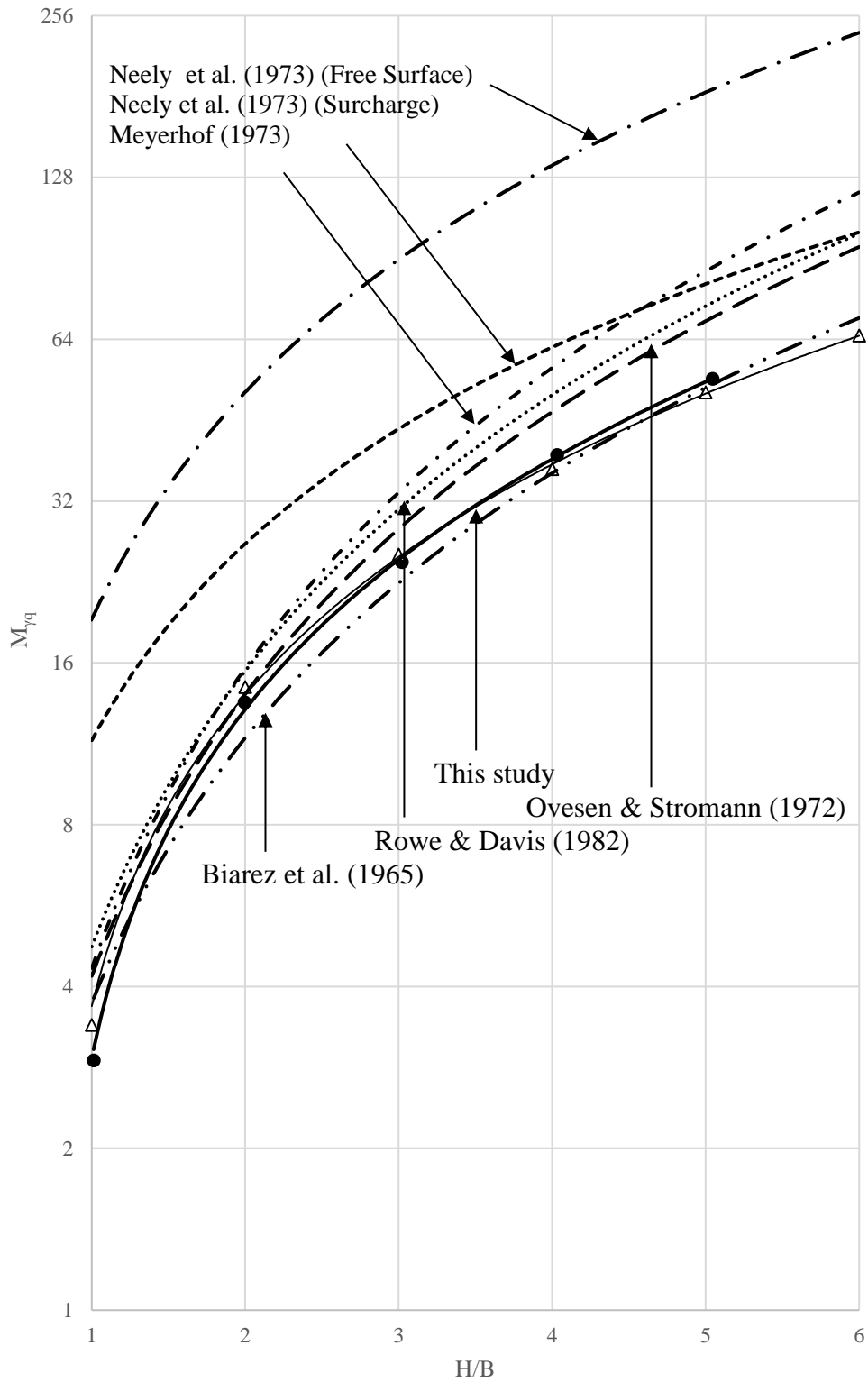


Figure 5.6 Comparison of force coefficient obtained from existing theoretical prediction techniques with the experimental force coefficients reported in Dickin and Leung (1985) corresponding to 25 mm high anchor

For the anchor size considered in the study of Dickin and Leung (1985), it is possible that the failure mechanism followed the hypothesis proposed by the same. It means that the failure might have been localized and the soil located in front of the anchor might have taken the place behind the anchor due to the frontal movement of itself causing a rotational failure. This might be considered as a possible explanation of good agreement between the prediction of Biarez et al. (1965) and the experimental observation.

However, the overprediction of the existing pullout capacity prediction models are evident from Figure 5.6. From Figure 5.5 and Figure 5.6 it can be seen that in both the cases, the prediction from Neely's (1973) surcharge method and equivalent free surface method provide a significant overestimation of the force coefficient, suggesting a cautious use of the model. Methods proposed by Ovesen and Stromann (1972), Meyerhof (1973), Rowe and Davis (1982) also provided a substantial overprediction throughout the embedment depth considered. From reliability perspective such overprediction is highly discouraging. The maximum overestimation from the present model was observed to be 3.3% at an embedment depth ratio of 2 and the maximum underprediction was observed to be 2.6% at an embedment depth ratio of 5. Nevertheless, the prediction from the present model was within a band of $\pm 3.5\%$ of the experimental observation. Thus, considering the agreement with the experimental results, present model and Biarez et al. (1965) model are better to capture the failure scenario.

5.3 Comparison with Theoretical Studies

While comparing with the results of the surcharge method of Neely et al. (1973), it was observed that the predictions from the present analysis are in close agreement when the embedment depth ratio is in the range of 2-5 for both the friction angle considered (Figure 5.7). Neely's equivalent free surface method provided an overestimate of the breakout factor for most of the embedment depths considered. For the cases when anchors are placed flush with the surface, Neely's surcharge method and equivalent free surface method seems to overpredict the breakout factors. It is important to note that during the development of theory of the present study it was shown that the failure mechanism at shallow depth follows a linear rupture pattern, however, Neely's study assumed that the failure to be in a logarithmic spiral plane. Thus, the additional weight contained within the logarithmic spiral failure surface might have caused the higher estimations of Neely's methods at an embedment depth ratio less than 2 at a friction angle of 40° . It can also be

observed that with the increase of friction angle the prediction range of different methods increases, which means the disparity among the predictions of different methods increases. For instance, at an embedment depth ratio of 3, and a ϕ' of 30° , the breakout factor is within the range of 3.55-5.95, whereas for a ϕ' of 40° , the breakout factor varies in the range of 9.88-13.20.

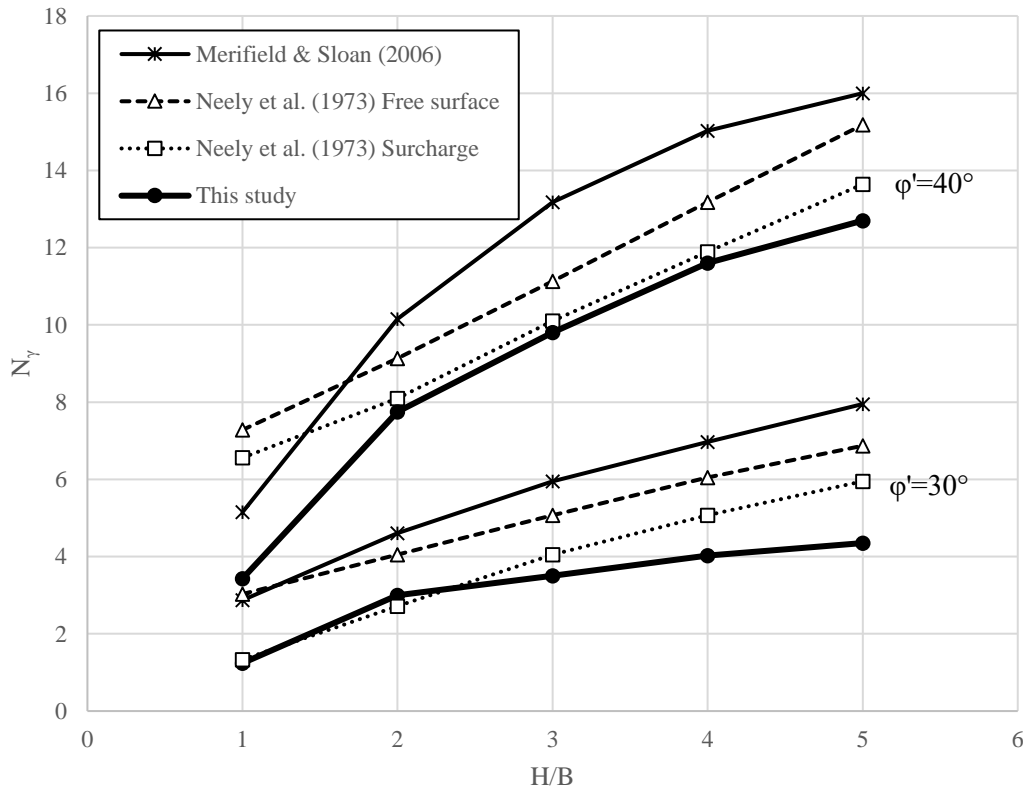


Figure 5.7 Comparison of breakout factors with Merifield and Sloan (2006), and Neely et al. (1973)

While observing the predictions from Merifield and Sloan (2006), it can be found that for most of the embedment depth ratio considered, it provided an overestimation of breakout factor. The overestimation increases as the friction angle increases. However, with the increase of friction angle, the increase of breakout factor at an embedment depth ratio of 1 was found to be negligible. It suggests that for surficial anchors, the effect of friction angle on breakout factor is marginal. This observation is coherent with the predictions from the current model, where the breakout factor increased from 1.15 to 3.25 with the increase of friction angle from 30° to 40° . Whereas, using Neely's surcharge method and

equivalent free surface method, the breakout factor was found to increase from 1.31 to 6.7 and 2.95 to 7.2 respectively.

Meyerhof (1973) presented a semi-empirical theory to predict the pullout capacity of anchors. In the method proposed, Meyerhof (1973) didn't explain the interface roughness and incorporation of it in the method. In addition, it was not explicitly mentioned whether the method was for smooth or rough anchors. From the comparison presented in Figure 5.8 it can be observed that Meyerhof (1973) method provided a lower estimate of breakout factor for most of the embedment ratio considered, especially at a friction angle of 40°. However, from the observation of breakout factor estimate at a friction angle of 30°, it is hard to comment on the interface roughness assumed by Meyerhof (1973) during his analysis.

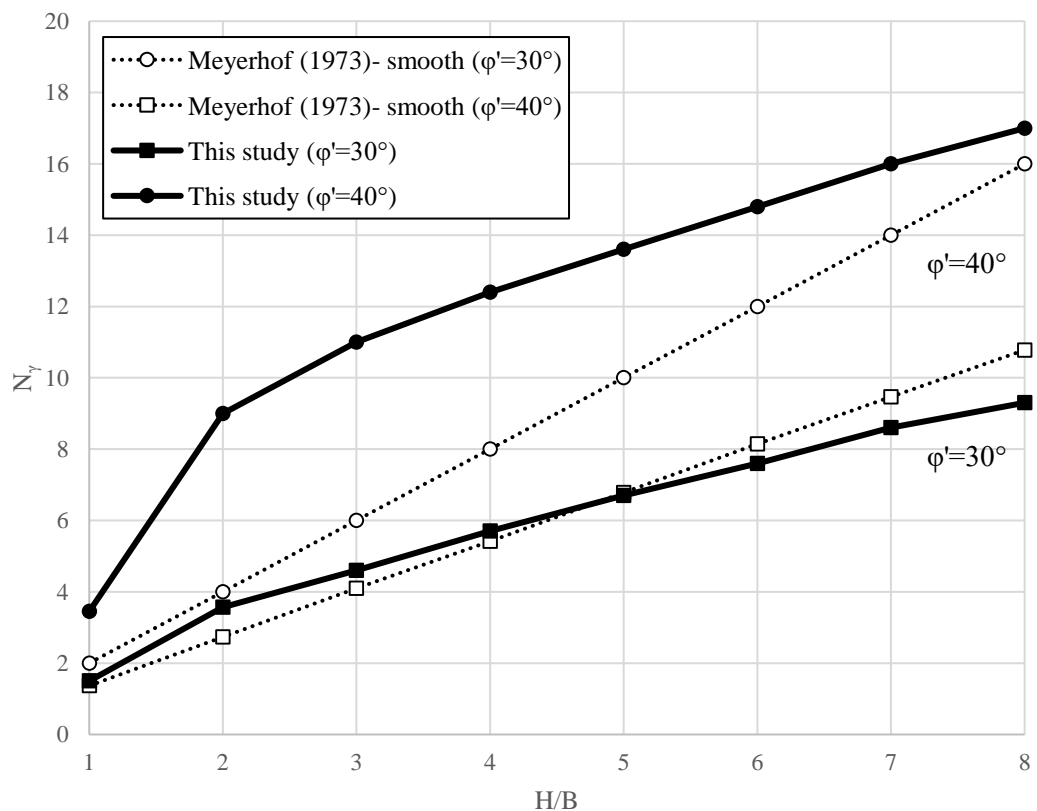


Figure 5.8 Comparison of breakout factors with Meyerhof (1973)

In addition, it can be observed that with the increase of friction angle from 30° to 40°, the discrepancy seems to be magnified, indicating that the method of Meyerhof (1973) might have been proposed for smooth anchors. It can also be observed that for denser soil, the

prediction of Meyerhof (1973) is highly conservative. This observation is in agreement with Merifield and Sloan (2006), who also noticed the conservatism of Meyerhof (1973) method. For instance, the breakout factor corresponding to an embedment depth ratio of 4 and a ϕ' of 40° , are 8 in Meyerhof (1973) method and 12.4 in the present method, indicating high underprediction using Meyerhof method. At the same embedment depth ratio, with the decrease of ϕ' to 30° , the breakout factor observed was 5.44 and 5.8 using Meyerhof (1973) and the present model respectively.

At this point, the results obtained by Basudhar and Singh (1994), who utilized lower bound procedure based on finite elements and non-linear programming will be compared with the results from the current study. In the research, Basudhar and Singh (1994) considered both smooth and rough anchors. However, it is unrealistic to think of a frictionless contact between anchor material and surrounding soil. Thus, the results considering rough interface will be considered here and are presented in Figure 5.9.

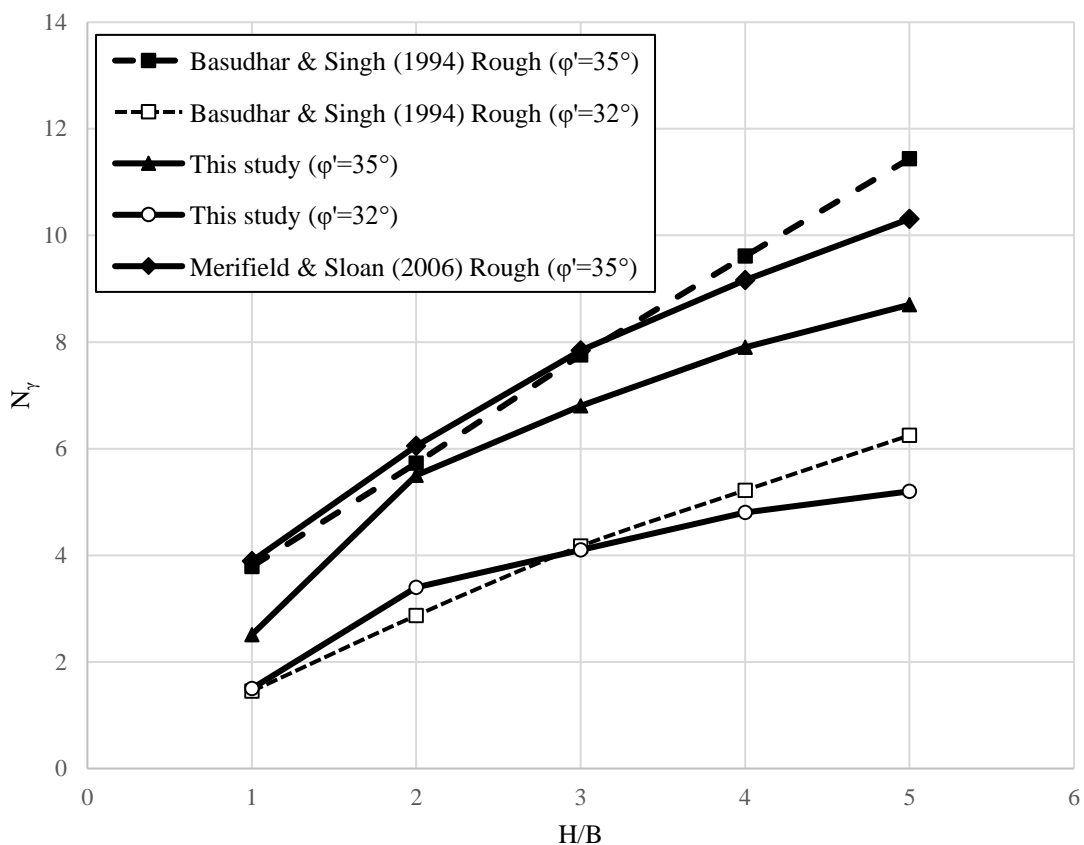


Figure 5.9 Comparison of breakout factors with Merifield and Sloan (2006), and Basudhar and Singh (1994)

It seems that at a friction angle of 32° , the predictions from the current investigation are in close agreement with the predictions of Basudhar and Singh (1994). Merifield and Sloan (2006) suggested that the algorithm of Basudhar and Singh (1994) is not based on properly extended stress field. Thus, it may provide optimistic results in situations where the friction angle is on the lower side.

The observation seems to be true in the present study as well. With the increase of the friction angle, the predictions from Basudhar and Singh (1994) seem to overpredict. At $\varphi' = 32^\circ$, a maximum discrepancy of 17% can be observed between the prediction from the current model and Basudhar and Singh (1994) at an embedment depth ratio of 5. However, the discrepancy increases to 34.7% at an embedment depth ratio of 5 corresponding to $\varphi' = 35^\circ$. To assess the observation of Merifield and Sloan (2006), the breakout factor corresponding to $\varphi' = 35^\circ$ is also presented in the same plot. The discrepancy between the predictions from present method with that of Merifield and Sloan (2006) is as much as 20.7% at an embedment depth ratio of 5. Nevertheless, it is understood that the predictions from the present study provided optimistic results for most of the embedment depths considered, which is important from reliability point of view.

5.4 Parametric Studies

In the next couple of sections, the influence of parameters like friction angle, aspect ratio, active pressure components, side flanks and angle of wall friction on the ultimate pullout capacity will be investigated.

5.4.1 Effect of Friction Angle on Pullout Capacity

Figure 5.10 presents the effect of friction angle on the force coefficient for an anchor with a height of 50 mm. It seems that with the increase of friction angle, the force coefficient increases. An increase of friction angle from 35° to 40° causes a 59.5% increase of force coefficient (at $H/B = 8$). However, this increase percentage decreases to 49.2% as the friction angle increases from 30° to 35° (at $H/B = 8$). The increase of force coefficient is 48.5%, when friction angle increases from 25° to 30° . It suggests that the increased friction angle has higher tendency to increase the pullout capacity with the increase of embedment depth ratio compared to the same anchor embedded in soils having less friction angle.

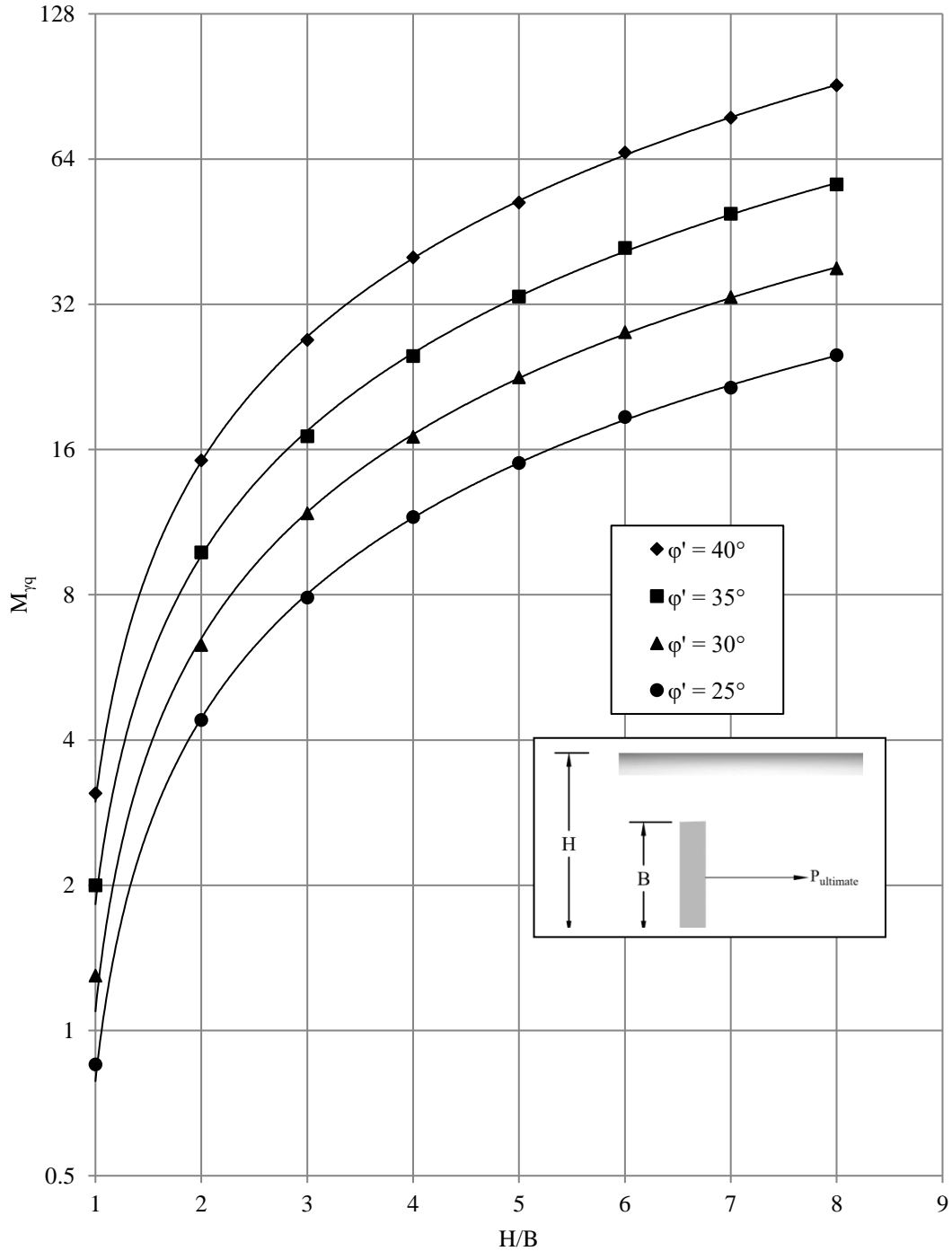


Figure 5.10 Effect of friction angle on the force coefficient for an anchor with a height of 50 mm

5.4.2 Effect of Aspect Ratio on Pullout Capacity

The effect of aspect ratio on the pullout capacity of a 50 mm model anchor embedded in a soil with friction angle of 40° is apparent from Figure 5.11. It seems that a square anchor has 36.1% higher force coefficient (corresponding to an embedment depth ratio of 8) than the anchor with same height, but with a L/B ratio of 2. In literature, it is suggested by

Das (1990) that an anchor with an aspect ratio of greater than 5 can be considered as a continuous anchor. However, in the present study, the increase of L/B ratio from 5 to 10 caused 8.5% decrease in force coefficient. Again, the increase of L/B ratio from 10 to 20 caused a maximum of 3.0% increase in force coefficient. As presented in Figure 5.11, increase of aspect ratio further to 100 didn't cause any considerable decrease in force coefficient. Thus, the conventional approach proposed by Das (1990) seems not to be applicable in the present study. An aspect ratio of 10 instead of 5 can be considered as the demarcation line between single anchor and continuous anchor.

5.4.3 Effect of Active Pressure Components on Pullout Capacity

In Figure 5.12, the effect of active pressure components on the breakout factor is demonstrated using the analytical model of the present study. To develop the figure, the anchor and soil parameters of Neely et al. (1973), Dickin and Leung (1983), Basudhar and Singh (1994) and Merifield and Sloan (2006) were used. However, pullout capacity was obtained using the present model. In some past studies it has been suggested that active earth pressure components do not play a significant role in the ultimate pullout capacity. Nevertheless, it is accepted that consideration of active pressure components provides a lower estimate of the ultimate pullout capacity. Although, the discrepancy is less at an embedment depth ratio below 2–2.5, at high embedment depth ratio, the discrepancy seems to be substantial. For instance, the increase of breakout factor corresponding to an embedment depth ratio of 8, for the test results of Dickin and Leung (1983) is 14.9% for neglecting the active pressure components. Again, the increase of breakout factor is only 4.25% for the same test corresponding to an embedment depth ratio of 1.

In Figure 5.13, the effect of active pressure components on the force coefficient is demonstrated using the results of Dickin and Leung (1985). The maximum increase of force coefficient for neglecting the active pressure components of a 50 mm model test is observed to be 26.1% corresponding to an embedment depth ratio of 8. In the similar fashion as the effect observed in Figure 5.11, the increase was only 2.1% for the same anchor placed at an embedment depth ratio of 1. Thus, it is understood that the active pressure components although play an insignificant role at an embedment depth ratio of less than 2.5, the effect is substantial thereafter.

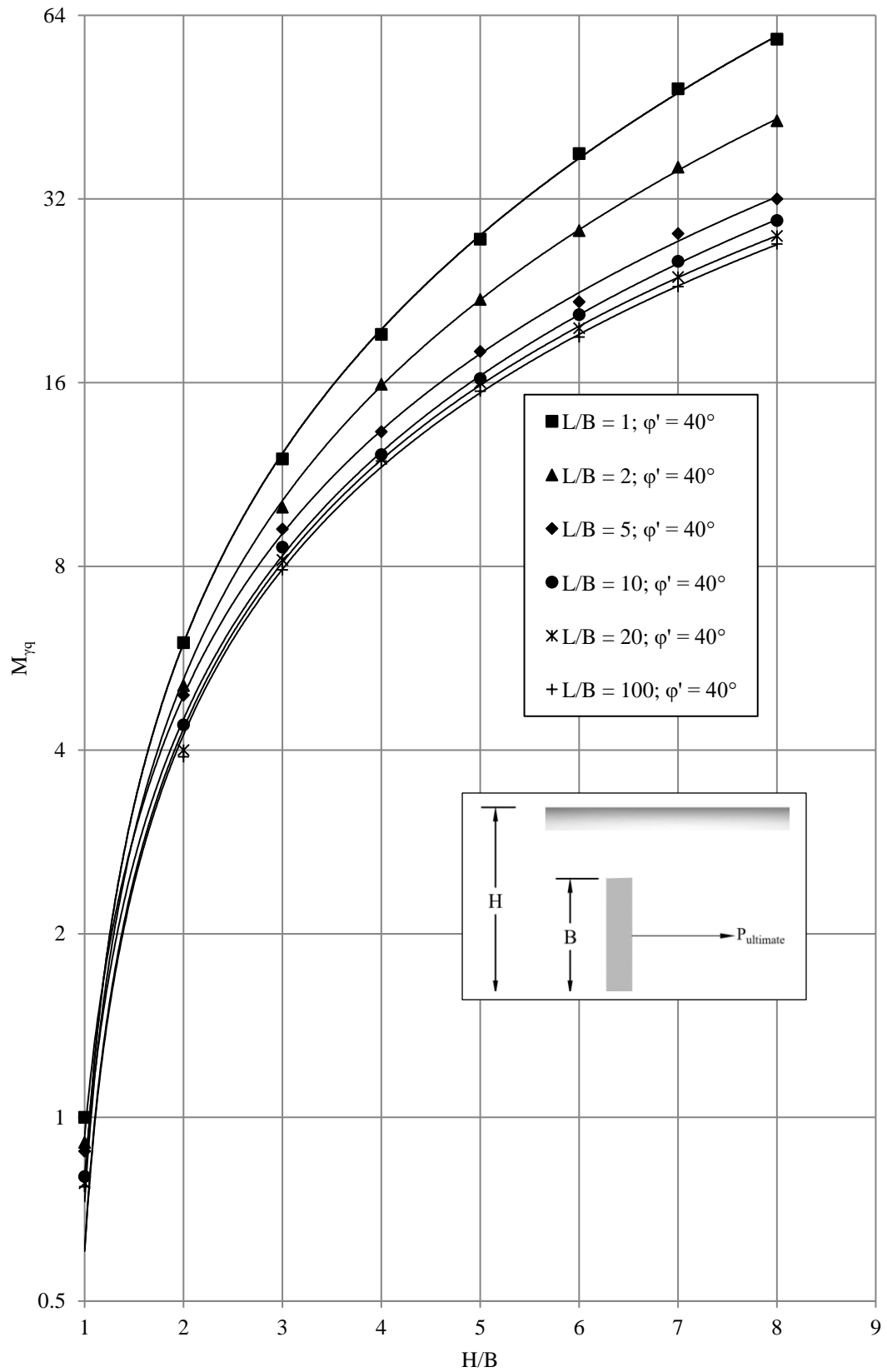


Figure 5.11 Effect of aspect ratio on the force coefficient for an anchor with a height of 50 mm

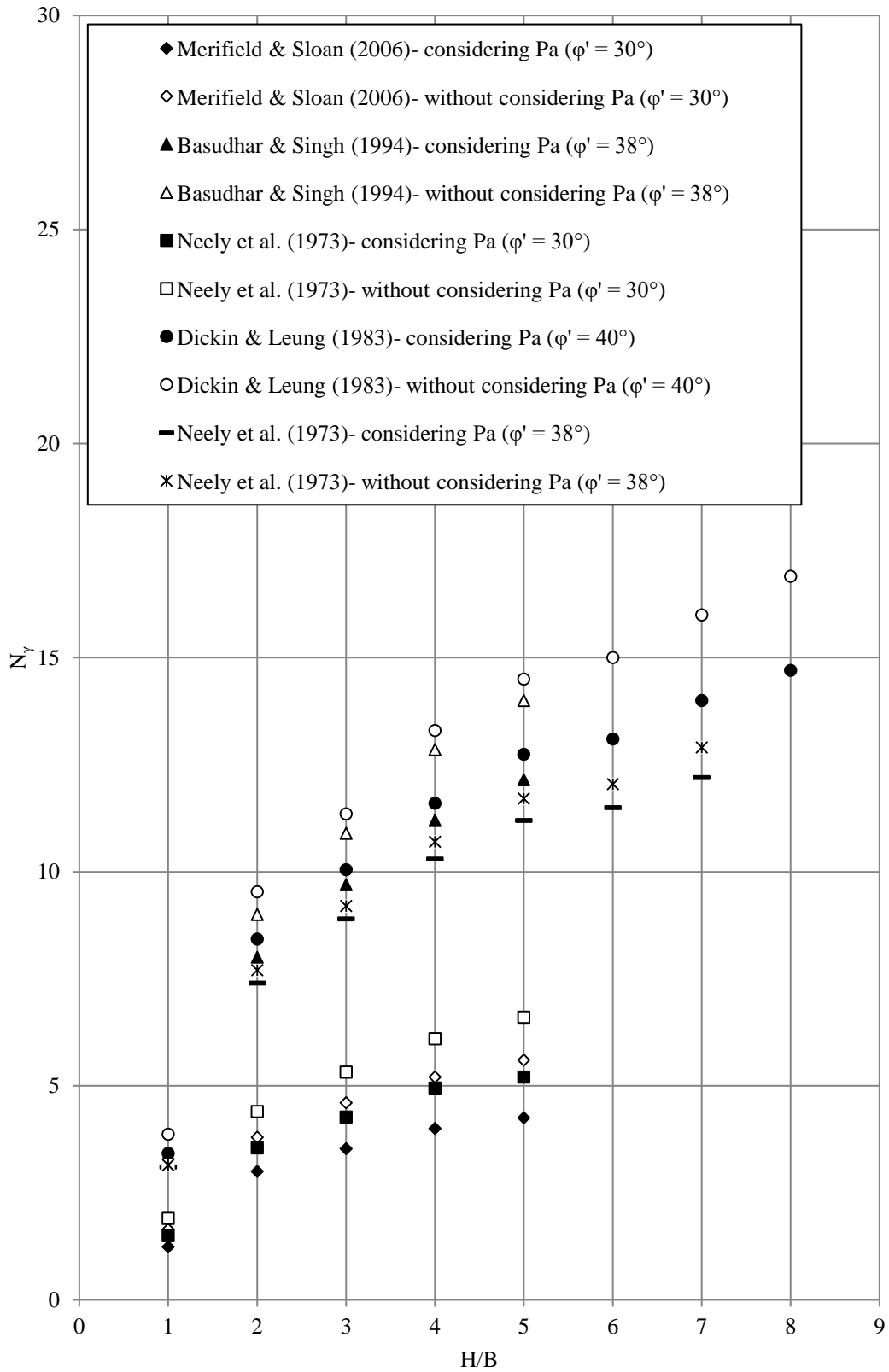


Figure 5.12 Effect of active pressure components on the breakout factor (P_a = active pressure components)

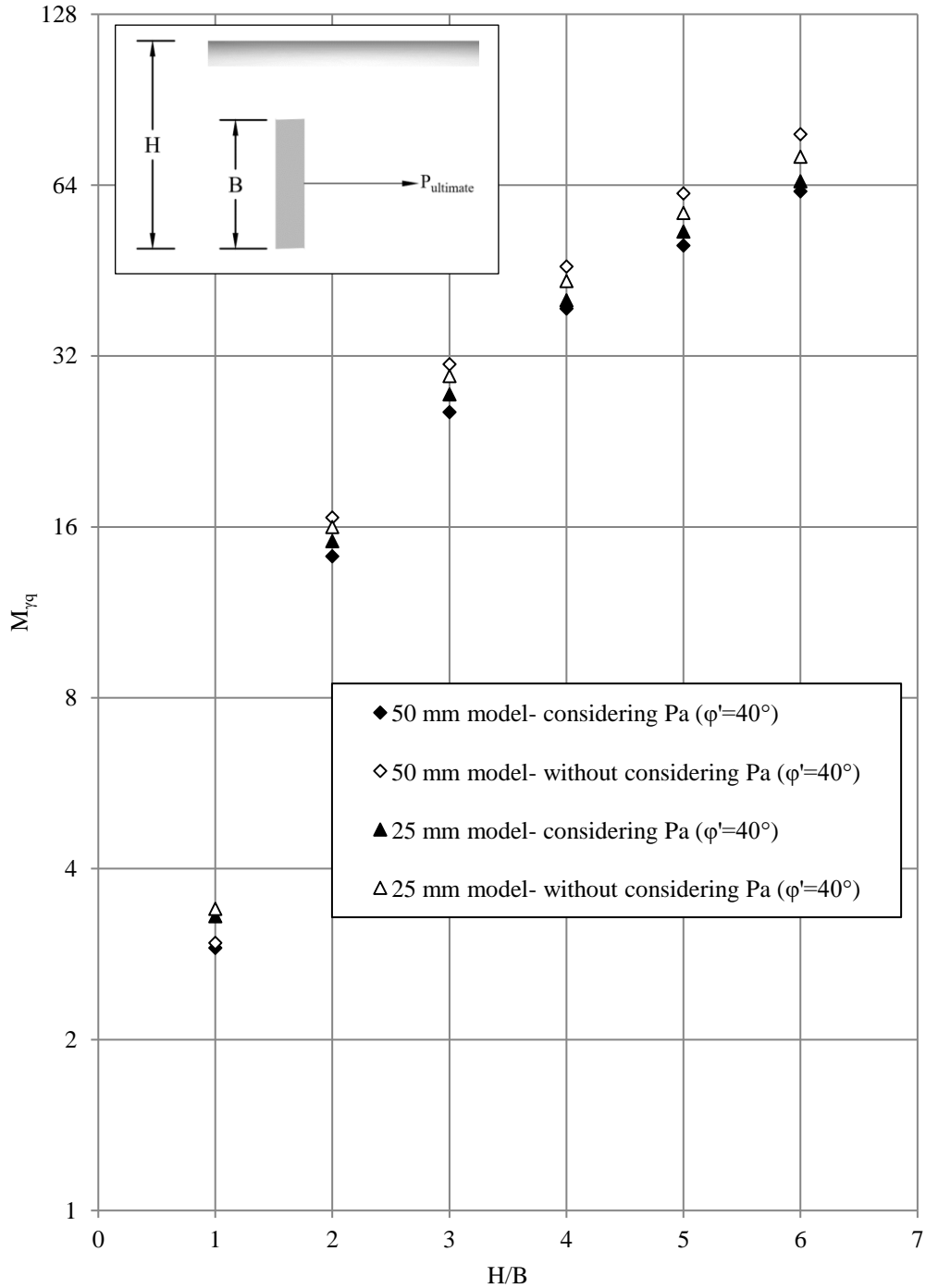


Figure 5.13 Effect of active pressure components on the force coefficient

It should also be noted that consideration of the active pressure components provides a reliable/conservative estimate of the pullout capacity.

5.4.4 Effect of Side Flank on Pullout Capacity

Figure 5.14 represents the effect of side flank on the force coefficient of an anchor of height 1m embedded at different depths from the ground surface, considering a soil

having a friction angle within the range of $30^\circ - 40^\circ$. It is apparent that consideration of side flank contribution increases the estimated pullout capacity. The effect seems to be prominent at high friction angles like 40° in the present case. In addition, the discrepancy between the force coefficients are not significant up to an embedment ratio up to 2, however, it is considerable thereafter. For instance, for soils having a φ' of 40° , the increase of force coefficient due to the consideration of side flank is 12.1% at an embedment depth ratio of 2, however, it is 37.4% at an embedment depth ratio of 8. Again, for soils having a φ' of 30° , the increase of force coefficient due to the consideration of side flank is 5.8% at an embedment depth ratio of 2, however, it is 21.1% at an embedment depth ratio of 8. Thus, the discrepancy seems to increase with the increase of the embedment depth ratio. Nevertheless, the effect seems to be considerable for soils with high friction angles, indicating a cautious selection of pullout capacity prediction model for highly frictional soils. In the present state-of-the-art, it is a common practice to consider plane strain case for the analysis of such structures. The present analysis indicates that the 3-D effect, which can be overlooked at low embedment depths (less than 3), however, is unavoidable in the cases when embedment depth ratio is higher than 3. Omission of such effects might result in an erroneous result in highly frictional soils and at an embedment depth ratio greater than 3.

5.4.5 Effect of Angle of Wall Friction on Pullout Capacity

Anchor roughness is one of the most important parameters for the analysis of anchor pullout capacity. To estimate the angle of wall friction, several charts are suggested by different researchers based on the anchor material. However, it is understood that the maximum possible value of δ depends on the roughness of the interface and properties of the soil. It is already discussed in Chapter 2 that the value of δ_{max}/φ' varies between 0 and 1 depending upon surface roughness, mean particle size of sand and method of installation (Tiwary et al., 2010). However, in the current study it is observed that δ is not constant for all the embedment depths. Figure 5.15 shows the relationship between H/B and δ/φ' for a 50 mm high anchor. It can be observed that δ/φ' increases as the embedment depth ratio increases. The increase is not uniform throughout. It is rapid up to an embedment depth ratio of 2. After this limit, the increase of δ/φ' is uniform. For instance, for a soil with $\varphi' = 40^\circ$, with the increase of H/B from 3 to 8, δ/φ' increases from 0.58 to 0.66.

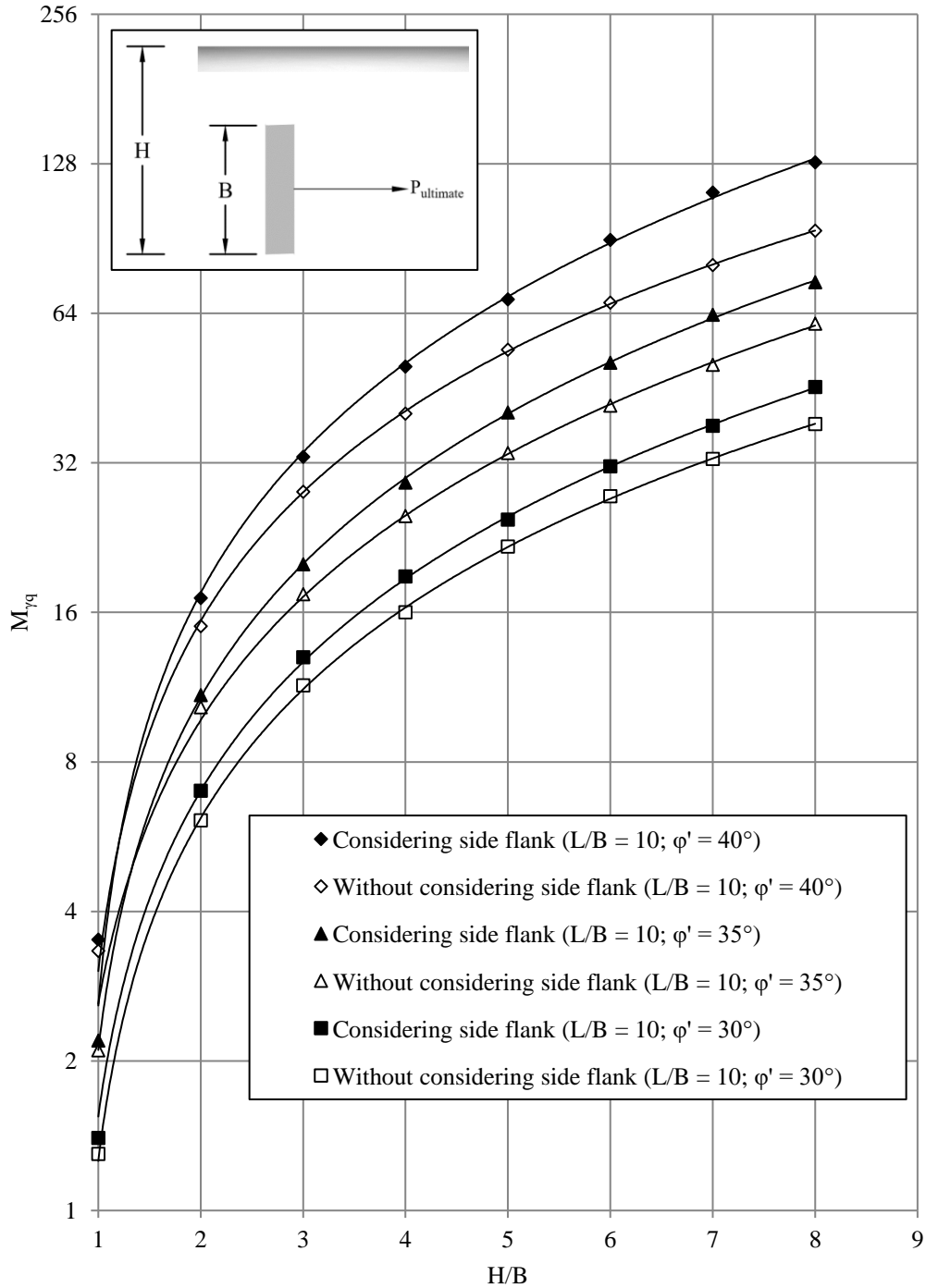


Figure 5.14 Effect of consideration of side flanks on the force coefficient

Again, the increase of δ/φ' is from 0.10 to 0.52 with the increase of H/B from 1 to 2, suggesting that at shallow depth (H/B up to 2), the factors causing the variation of δ are not completely mobilized. From Figure 5.15 it can also be observed that δ_{max}/φ' can be reported as 0.66 between the concrete anchor and the soil. In addition to that the effect of L/B is also apparent from the same plot. It seems that for an anchor with similar material, as the L/B ratio increases, δ/φ' also increases. For a square anchor, maximum δ/φ' was

observed to be 0.42, whereas for an anchor with L/B ratio of 10, maximum δ/φ' was 0.66. However, for an anchor with L/B ratio of 5 and 2, maximum δ/φ' was 0.65 and 0.59 respectively. Thus, it is understood that the increase of L/B ratio from 5 to 10 did not increase the δ/φ' substantially, suggesting the demarcation line between heavy and light anchor suggested by Duncan and Mokwa (2001).

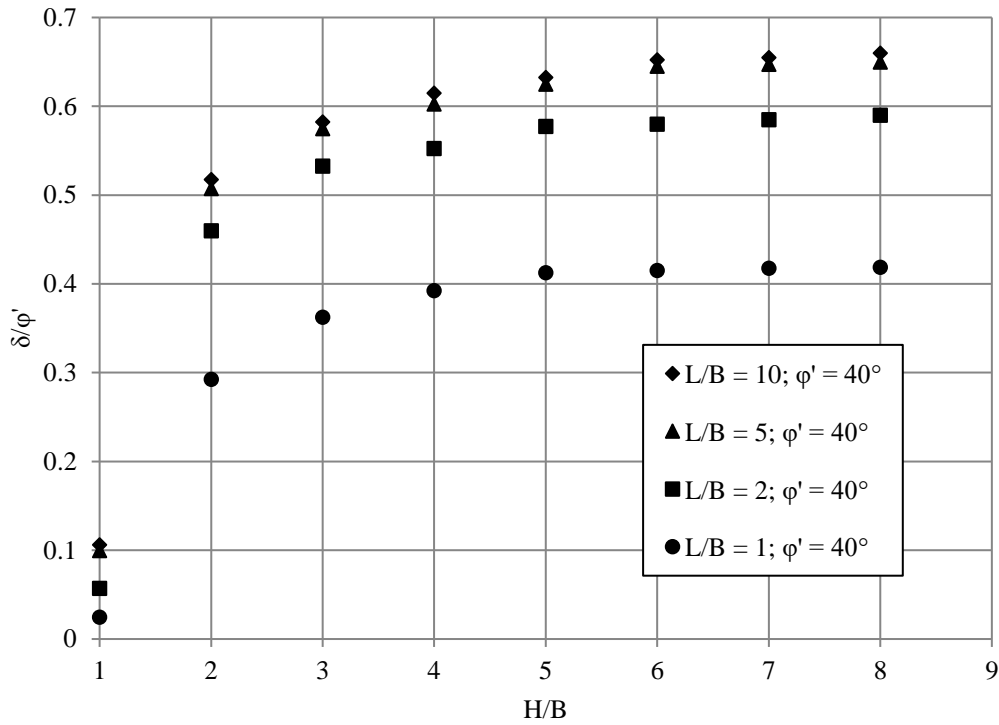


Figure 5.15 Change of δ/φ' with H/B and L/B for a typical concrete anchor of height 50 mm

Although in the study of Duncan and Mokwa (2001), the different behavior of light and heavy structure is discussed, no demarcation between light and heavy structure is suggested based on L/B ratio. It is apparent from this study that an L/B ratio of 5 can be used as a demarcation line. In addition to that, for surficial anchors, wall friction is not fully mobilized. And most importantly, it is perceived from this study that although δ/φ' is constant in the range of L/B from 5 to 10 and H/B from 3 to 8, the constant value of δ/φ' assumed in most cases for all the range of embedment depths and L/B to analyze the pullout capacity doesn't really hold true. Additionally, in the idea of Duncan and Mokwa (2001) a light structure is the one which has a L/B ratio of less than 5, and a heavy structure will have an L/B ratio beyond the aforementioned limit.

5.5 Why this Model?

It seems that the present model involves complex mathematical analyses to obtain the pullout capacity. In the existing literatures, some pullout capacity prediction models are available which are easier to use. Therefore, the question arises, why should someone prefer the current model. It is important to note that the main objective of this study was to obtain a more reliable and accurate estimate of pullout capacity. Subsequently, simplicity was not preferred over reliability. To clarify this, author took an attempt to show the predictive capability of existing pullout capacity prediction models using a single plot. The plot can be termed as reliability versus error plot. For developing the plot, the experimental results of Rowe and Davis (1982), who conducted 47 experiments on anchors having different geometry and soil parameters was considered as the base case. Reliability is defined as the percentage of cases for which the calculated pullout capacity is lower than or equal to the experimental value, with a value approaching 100 percent indicating the most desirable characteristics of reliability. Error in the system was expressed using Mean Absolute Percentage Error (MAPE). A MAPE value of zero indicates the best possible accuracy. In Figure 5.16, the available pullout capacity predictions are plotted along with the prediction from the current model.

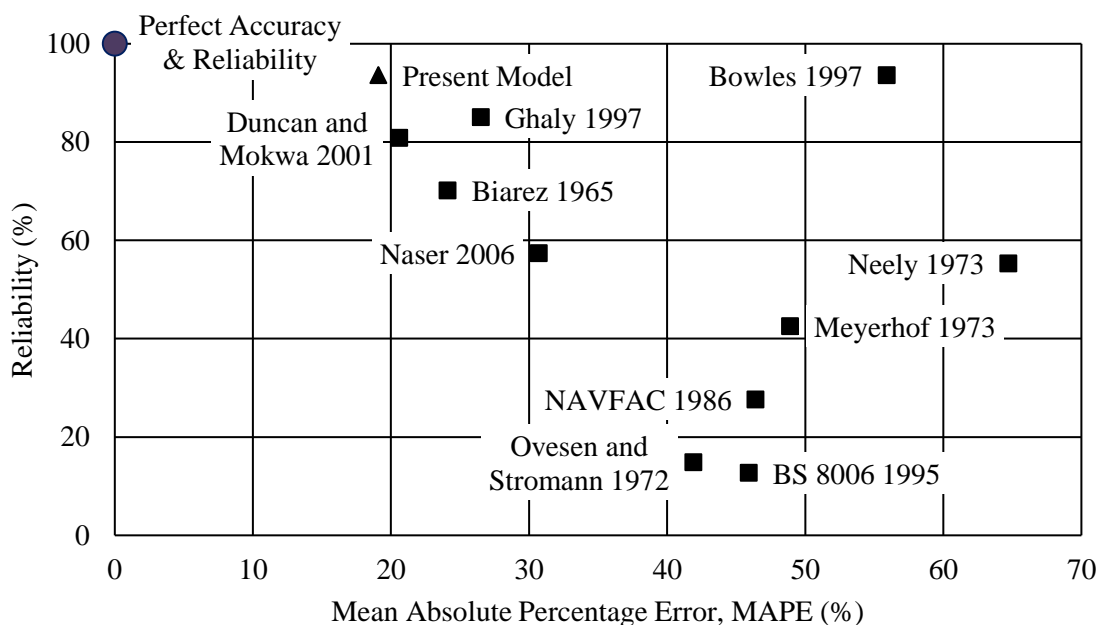


Figure 5.16 Evaluation of different methods with respect to reliability and MAPE

It seems that values of MAPE vary from 19.1% (most accurate) for the current model to 64.7% (least accurate) for the Neely's method. It can also be observed that maximum

reliability was observed to be 93.7% using current model and Bowles (1997) method. However, a minimum reliability of 12.8% was observed from BS 8006 (1995) method. The models of Duncan and Mokwa (2001), Ghaly (1997) and Biarez et al. (1965) provide a good combination of accuracy and reliability. From engineering point of view, reliability is a very important aspect in any design scheme. Thus, it is suggested not to prefer user-friendliness over reliability during the selection of suitable model during design practice. Nevertheless, considering the predictive capability of the available models, the current model seems to provide the best combination of accuracy and reliability, thus, suggested to be adopted in anchor design when it is laid at shallow and intermediate depth.

5.6 Summary

In this chapter, the validation of the proposed model was done with the theoretical and experimental investigations available in the existing literature. The presented data shows the accuracy of the prediction of pullout capacity of the proposed model. Its suitability for the estimation of pullout capacity shallow and intermediate anchors is also discussed. A parametric study was conducted and the effect of different influencing parameters on the pullout capacity was studied.

Chapter 6

CONCLUSIONS AND RECOMMENDATIONS

6.1 General

In the current study, a rigorous analytical investigation into the behavior of anchor is presented. The factors affecting the pullout capacity have properly been addressed. In addition, comparative assessment has been presented to illustrate the superiority of the proposed model. After that some parametric studies have also been shown. Finally, the author recommended some scope in further continuing the study.

6.2 Conclusions

The basic conclusions that can be drawn from the present study are-

- a) The ultimate pullout capacity of a shallow or intermediate anchor can accurately and reliably estimated by using Eq. (4.168). Comparison with existing experimental and theoretical studies suggests that the model is capable to consider variations in pullout capacity installed at an embedment depth ratio (H/B) up to 8 in frictional soils.
- b) One important feature of the proposed model is that the interface friction angle is obtained from the equilibrium of the forces in horizontal and vertical direction. However, in most of the pullout capacity prediction models, based on the type of anchor material, interface friction angle need to be assumed initially. Subsequently, the maximum possible value is inserted in the model to estimate the pullout capacity. Thus, the present analysis considers the feature that the interface friction angle not only depends on the interface roughness, but also on the weight of the anchor itself and the weight of soil mass contained within the failure surface.
- c) The force coefficient tends to increase with the increase of friction angle (φ'). The effect is prominent in anchors embedded in highly frictional soils, as the increase of pullout capacity increases significantly if the friction angle is increased from 35° to 40° compared to the increase from 30° to 35° . It

suggests, the denser the surrounding soils are, the more prominent will be the increase of the pullout capacity.

- d) The conventional approach proposed by Das (1990) that an aspect ratio (L/B) of more than 5 is sufficient to consider an anchor as a continuous one, seems not to be comprehensive in the present study. A L/B of 10 instead of 5 can be considered as the demarcation line between single anchor and continuous anchor.
- e) The present study suggests that the active pressure components although play an insignificant role at an embedment depth ratio of less than 2.5, the effect causes high discrepancy thereafter. It was also pointed out that the consideration of the active pressure components provides a reliable and conservative estimate of the ultimate pullout capacity.
- f) The present analysis indicates that the 3-D effect, which generates due to the formation of side flanks, can be overlooked at low embedment depths ($H/B < 2$). The effect is substantial in the cases when $H/B > 2$. Omission of such effects resulted in an erroneous result (a discrepancy of as much as 37.4%) in highly frictional soils ($\varphi' = 40^\circ$) and in the cases when the embedment depth ratio is greater than 2.
- g) It is perceived from this study that although δ/φ' is constant in the range of L/B from 5 to 10 and H/B from 3 to 8, the constant value of δ/φ' assumed in most cases for all the range of embedment depths and L/B to analyze the pullout capacity is not actually valid. Additionally, in the classification of retaining structure of Duncan and Mokwa (2001), a light structure is the one which has a L/B ratio of less than 5, and a heavy structure will have an L/B ratio beyond the aforementioned limit.

6.3 Recommendations for Future Study

During the course of theoretical analyses, there was always an urge to expand the scope of the study in order to gather more information and to achieve better approximations. Some of these future research prospects are recommended below-

- a) Although frictional soils are always preferred as a backfill material in general, sometimes cohesive soil may be encountered during backfilling. In such circumstances, design should be done considering cohesive soil and its relevant properties (Shahriar, 2016; Shahriar et al. 2018), which may be studied.
- b) Very high retaining wall may require multi-staged anchor system. The anchor in the lowest stage may be embedded at deeper depth. In that case, new theoretical approach may be developed to study the behavior of deep anchor. The present study predicts the pullout capacity up to an embedment depth ratio of 8 but not beyond.
- c) The effect of dynamic loading (e.g. earthquake or, liquefaction) on pullout capacity of anchor may be investigated. In addition, the applicability of the theory to foundation of different structures (like concrete, adobe) may be studied (Islam and Iwashita, 2010).
- d) Although the inclination of the present researchers is towards numerical analyses, there is no better alternative than field scale experimental tests. In existing state of art very few small-scale model tests are being observed to be existent, however, the extrapolation to field scale may incorporate significant errors. Thus, field scale model test need to be performed in order to better understand the actual mechanisms involved.

Thus, it is recommended for future study to work on the above-mentioned areas to consider most of the problems encountered in the field during the design and construction of anchor. Finally, it is expected that the present study will be useful to all those dealing with civil engineering projects and research works on anchored retaining wall. This research will also be useful to those who are involved in the development of standards on the determination of horizontal pullout capacity of anchor.

REFERENCES

- Adams, J.I., and Hayes, D.C. (1967). "The Uplift Capacity of Shallow Foundations." *Ontario Hydro Research Quarterly*, 19(1), pp. 1–13.
- Akinmusuru, J.O. (1978). "Horizontally Loaded Vertical Plate Anchors in Sand." *Journal of the Geotechnical Engineering Division, ASCE*, 104(2), pp. 283-286.
- Baker, W.H., and Kondner, R.L. (1966). "Pullout Load Capacity of Circular Earth Anchor Buried in Sand." *National Academy of Sciences, Highway Research Board, Report 108*, pp. 1–10.
- Balla, A. (1961). "The Resistance of Breaking-out of Mushroom Foundations for Pylons." *Proceedings of the 5th International Conference on Soil Mechanics and Foundation Engineering*, Paris, France. A.A. Balkema, Rotterdam, The Netherlands. Vol. 1, pp. 569–576.
- Basudhar, P.K., and Singh, D.N. (1994). "A Generalized Procedure for Predicting Optimal Lower Bound Break-out Factors of Strip Anchors." *Géotechnique*, 44(2), pp. 307-318.
- Biarez, I, Boucraut, L.-M., and Negre, R. (1965). "Limiting Equilibrium of Vertical Barriers Subjected to Transition and Rotational Forces." *Proceedings of the Sixth International Conference on Soil Mechanics and Foundation Engineering*. Montreal, Canada, pp. 368-372.
- Bhattacharya, P., and Kumar, J. (2014). "Pullout Capacity of Inclined Plate Anchors Embedded in Sand." *Canadian Geotechnical Journal*, 51(11), pp. 1365-1370.
- Bhattacharya, P., and Kumar, J. (2011). "Horizontal Pullout Capacity of a Group of Two Vertical Strip Anchors Plates Embedded in Sand." *Geotechnical and Geological Engineering*, 30(2), pp. 513-521.
- Bhattacharya, P., and Roy, A. (2016). "Variation of Horizontal Pullout Capacity with Width of Vertical Anchor Plate." *International Journal of Geomechanics, ASCE*, 10.1061/(ASCE)GM.1943-5622.0000639, 06016002.
- Bowles, J.E. (1997). "Sheet-pile Walls: Cantilevered and Anchored." *Foundation Analysis and Design* (5th ed.). pp. 778-780. The McGraw-Hill Companies, Inc., Singapore.
- BS 8006. (1995). Strengthened/Reinforced Soils and Other Fills, Section 6.6. *British Standard*. London.
- Choudhary, A.K., and Dash, S.K. (2016). "Load-Carrying Mechanism of Vertical Plate Anchors in Sand." *International Journal of Geomechanics, ASCE* 10.1061/(ASCE)GM.1943-5622.0000813, 04016116.

- Daniel, D.E., and Olson, R.E. (1982). "Failure of an Anchored Bulk-Head." *Journal of Geotechnical Engineering Division, ASCE*, 108(10), pp. 1318-1327.
- Das, B.M. (1975). "Pullout Resistance of Vertical Anchors." *Journal of the Geotechnical Engineering Division, ASCE*, 101(1), pp. 87–91.
- Das, B.M. (1990). *Earth Anchors*. Amsterdam, Netherlands Elsevier.
- Das, B.M. (2007). *Principles of Foundation Engineering* (6th ed.). Thomson Brooks/Cole, Ontario, Canada.
- Das, B.M., and Seeley, G.R. (1975). "Load-Displacement Relationships for Vertical Anchor Plates." *Journal of the Geotechnical Engineering Division, ASCE*, 101(GT7), pp. 711-715.
- Dewaikar, D.M., and Mohapatro, B.G. (2003). "Computation of Bearing Capacity Factor N_γ – Terzaghi's Mechanism." *International Journal of Geomechanics, ASCE*, 10.1061/(ASCE)1532-3641(2003)3:1(123), pp. 123–128.
- Dickin, E.A., and King, J.W. (1997). "Numerical Modelling of the Load-Displacement Behaviour of Anchor Walls." *Computers and Structures*, 63(4), pp. 849-858.
- Dickin, E.A., and Leung, C.F. (1983). "Centrifuge Model Tests on Vertical Anchor Plates." *Journal of Geotechnical Engineering, ASCE*, 109(12), pp. 1503-1525.
- Dickin, E.A., and Leung, C.F. (1985). "Evaluation of Design Methods for Vertical Anchor Plates." *Journal of Geotechnical Engineering, ASCE*, 111(4), pp. 500-520.
- Drucker, D.C., Greenberg, H.J., and Prager, W. (1952). "Extended Limit Design Theorems for Continuous Media." *Quarterly Journal of Applied Mathematics*, 9, pp. 381–389.
- Duncan, M., and Mokwa, R. (2001). "Passive Earth Pressures: Theories and Test." *Journal of Geotechnical and Geoenvironmental Engineering, ASCE*, 127(4), pp. 248-257.
- Ghaly, A.M. (1997). "Load-Displacement Prediction for Horizontally Loaded Vertical Plates." *Journal of Geotechnical and Geoenvironmental Engineering, ASCE*, 10.1061/(ASCE)1090-0241(1997)123:1(74), 123(1), pp. 74-76.
- Giampa, J.R., Bradshaw, A.S., and Schneider, J.A. (2016). "Influence of Dilation Angle on Drained Shallow Circular Anchor Uplift Capacity." *International Journal of Geomechanics, ASCE*, 10.1061/(ASCE)GM.1943-5622.0000725, 04016056.
- Gireesha, T., and Muthukkumaran, K. (2011). "Study on Soil-Structure Interface Strength Property." *International Journal of Earth Sciences and Engineering*, 4(6), pp. 89-93.
- Giffels, W.C., Graham, R.E., and Mook, J.F. (1960). "Concrete Cylinder Anchors Proved for 345-KV Tower Line." *Electrical World*, 154, pp. 46–49.
- Hanna, A., Rahman, F., and Ayadat, T. (2011). "Passive Earth Pressure on Embedded Vertical Plate Anchors in Sand." *Acta Geotechnica*, 6, pp. 21-29.

- Hansen, J.B. (1966). "Resistance of Rectangular Anchor Slab." *Danish Geotechnical Institute*, 21, pp. 12-13.
- Hijab, W.A. (1956). "A Note on the Centroid of a Logarithmic Spiral Sector." *Géotechnique*, 6(2), pp. 96-99.
- Hoshiya, M., and Mandal, J.N. (1984). "Some Studies of Anchor Plates in Sand." *Soils and Foundations*, 24(1), pp. 9-16.
- Hueckel, S. (1957). "Model Tests on Anchoring Capacity of Vertical and Inclined Plates." In *Proceeding 4th Inter-nation Conference on Soil Mechanics and Foundation Engineering*, 2, pp. 203-206. London, England Butterworths Scientific Publications.
- Islam, M.S., and Iwashita, K. (2010). "Earthquake Resistance of Adobe Reinforced by Low Cost Traditional Materials." *Journal of Natural Disaster Science*, 32(1), pp. 1-21.
- Jadid, R., Abedin, M.Z., Shahriar, A.R., and Arif, Z.U. (2018). "Analytical Model for Pullout Capacity of a Vertical Concrete Anchor Block Embedded at Shallow Depth in Cohesionless Soil" *International Journal of Geomechanics, ASCE*, 10.1061/(ASCE)GM.1943-5622.0001212.
- Jadid, R. (2016). "Modelling of Pullout Resistance of Concrete Anchor Block Embedded in Cohesionless Soil," M.Sc. Engg. Thesis, Department of Civil Engineering, Bangladesh University of Engineering and Technology.
- Jones, C. (1996). "Earth Reinforcement and Soil Structures." *Thomas Telford Services Ltd.*, London, UK.
- Kame, G.S., Dewaikar, D.M., and Choudhury, D. (2012a). "Pullout Capacity of a Vertical Plate Anchor Embedded in Cohesionless Soil." *Earth Science Research*, 1(1), pp. 27-56.
- Kame, G.S., Dewaikar, D.M., and Choudhury, D. (2012b). "Pullout Capacity of a Vertical Plate Anchor Embedded in Cohesionless Soil." *Geomechanics and Engineering, An International Journal*, 4(2), pp. 105-120.
- Kananyan, A.S. (1966). "Experimental Investigation of the Stability of Base of Anchor Foundations." *Soil Mechanics and Foundation Engineering (Moscow)*, 3(6), pp. 387-392.
- Khan, A.J., and Sikder, M. (2004). "Design Basis and Economic Aspects of Different Types of Retaining Walls." *Journal of Civil Engineering, IEB, CE* 32(1), pp. 17-34.
- Khan, A.J., Mostofa, G., and Jadid, R. (2017). "Pullout Resistance of Concrete Anchor Block Embedded in Cohesionless Soil." *Geomechanics and Engineering, An International Journal*, 12(4), pp. 675-688.
- Kötter, F. (1903). Die Bestimmung des Drucksangekrümmten Gleitflächen, eine Aufgabeaus der Lehrevom. 229-233. Berlin Univ.-Bibliothek Frankfurt am Main.

- Kouzer, K.M., and Kumar, J. (2009). "Vertical Uplift Capacity of Equally Spaced Horizontal Strip Anchors in Sand." *International Journal of Geomechanics, ASCE* 10.1061/ASCE1532-3641(2009)9:5(230), pp. 230-236.
- Kumar, J., and Sahoo, J.P. (2012). "Upper Bound Solution for Pullout Capacity of Vertical Anchors in Sand Using Finite Elements and Limit Analysis." *International Journal of Geomechanics, ASCE*, 12(3), pp. 333-337.
- Lin, C., Han, J., Bennett, C., and Parsons, R.L. (2014). "Analysis of Laterally Loaded Piles in Sand Considering Scour Hole Dimensions." *Journal of Geotechnical and Geoenvironmental Engineering, ASCE*, 140(6), pp. 1-13.
- Lyamin, A.V., and Sloan S.W. (2002). "Upper Bound Limit Analysis Using Finite Elements and Non- Linear Programming." *International Journal for Numerical and Analytical Methods in Geomechanics*, 26, pp. 181–216.
- Merifield, R.S., and Sloan, S.W. (2006). "The Ultimate Pullout Capacity of Anchors in Frictional Soils." *Canadian Geotechnical Journal*, 43, pp. 852-868.
- Meyerhof, G.G. (1973). "Uplift resistance of inclined anchors and piles." In *Proceedings of the 8th International Conference on Soil Mechanics and Foundation Engineering*, Moscow. A.A. Balkema, Rotterdam, The Netherlands. Vol. 3, pp. 167–172.
- Mors, H. (1959). "The Behavior of Mast Foundations Subjected to Tensile Forces." *Bautechnik*, 10, pp. 367–378.
- Mostofa, M.G. (2013). "Horizontal Pullout Resistance of Concrete Anchor Blocks in Sand Backfill," M.Sc. Engg. Thesis, Department of Civil Engineering, Bangladesh University of Engineering and Technology.
- Murray, E.J., and Geddes, J.D. (1989). "Resistance of Passive Inclined Anchors in Cohesionless Medium." *Géotechnique*, 39(3), pp. 417-431.
- Naser, A.S. (2006). "Pullout Capacity of Block Anchor in Unsaturated Sand." *Unsaturated Soils 2006 (GSP 147), Proceedings of the Fourth International Conference on Unsaturated Soils, ASCE*. (pp. 403-414). Arizona.
- NAVFAC DM (1986). "Foundations and Earth Structures." In *Naval Facilities Engineering Command* (pp. 91-92). Alexandria, Virginia.
- Neely, W.J., Stuart, J.G., and Graham, J. (1973). "Failure Loads of Vertical Anchor Plates in Sand." *Journal of the Geotechnical Engineering Division, ASCE*, 99(9), pp. 669-685.
- Ovesen, N.K. (1964). "Passive Anchor Slabs: Calculation Methods and Model." *Danish Geotechnical Institute*, 4, pp. 5-39.
- Ovesen, N.K. (1981). "Centrifuge Tests of the Uplift Capacity of Anchors." *Proceedings of the 10th International Conference on Soil Mechanics and Foundation Engineering*, 1, pp. 717-722. Stockholm, A.A. Balkema, Rotterdam, The Netherlands.

- Ovesen, N.K., and Stromann, H. (1972). "Design Methods of Vertical Anchor Slabs in Sand." *Proceedings, Specialty Conference on Performance of Earth and Earth-Supported Structures, American Society of Civil Engineers*, 2.1, pp. 1481-1500.
- Patki, M.A., Mandal, J.N., and Dewaikar, D.M. (2015). "Determination of Passive Earth Pressure Coefficients Using A Limit Equilibrium Approach Coupled with the Kötter's Equation." *Canadian Geotechnical Journal*, 52(9), pp. 1241–1254.
- Patki, M.A., Dewaikar, D.M., and Mandal, J.N. (2017). "Numerical Study on Passive Earth Pressures Using Kötter's Equation." *International Journal of Geomechanics, ASCE*, 17(2), 06016015.
- Potyondy, J.G. (1961). "Skin Friction between Various Soils and Construction Materials." *Géotechnique*, 11(1), pp. 339-353.
- Reese, L.C., Cox, W.R., and Koop, F.D. (1974). "Analysis of Laterally Loaded Piles in Sand." *Sixth Annual Offshore Technology Conference*, pp. 473-480. Houston, Texas OTC 2080.
- Rowe, R.K. (1978). Soil Structure Interaction Analysis and Its application to the Prediction of Anchor Behavior, *PhD Thesis*, University of Sydney, Department of Civil Engineering, Sydney, Australia
- Rowe, R.K., and Davis, H. (1982). "The Behaviour of Anchor Plates in Sand." *Géotechnique*, 32(1), pp. 25-41.
- Shahriar, A.R. (2016). "Thixotropic Hardening of Clay-Water System," B.Sc. Engineering Thesis. Department of Civil Engineering, Bangladesh University of Engineering and Technology, Dhaka.
- Shahriar, A.R., Abedin, M.Z., and Jadid, R. (2018). "Thixotropic Aging and its Effect on 1-D Compression Behavior of Soft Reconstituted Clays," *Applied Clay Science*, 153, pp. 217-228.
- Shahriar, A.R. (2015). "Effect of Moisture Content on the Thixotropic Strength Recovery of Dhaka Clays," *Proceedings of the First International Conference on Advances in Civil Infrastructures and Construction Materials*, (pp. 722-729). Dhaka.
- Sloan, S.W. (1988). "Lower Bound Limit Analysis Using Finite Elements and Linear Programming." *International Journal for Numerical and Analytical Methods in Geomechanics*, 12, pp. 61-67.
- Sloan S.W. (1989). "Upper Bound Limit Analysis Using Finite Elements and Linear Programming." *International Journal for Numerical and Analytical Methods in Geomechanics*, 13, pp. 263–282.
- Sloan, S.W., and Kleeman, P.W. (1995). "Upper Bound Limit Analysis Using Discontinuous Velocity Fields." *Computer Methods in Applied Mechanics and Engineering*, 127, pp. 293–314.

- Sloan, S.W., and Randolph, M.F. (1982). "Numerical Prediction of Collapse Loads Using Finite Element Methods." *International Journal for Numerical and Analytical Methods in Geomechanics*, 6(1), pp. 47–76.
- Smith, J.E. (1962). *Deadman Anchorages in Sand*. Washington, D.C. U.S. Naval Civil Engineering Laboratory.
- Smith, C.S. (1998). "Limit Loads for an Anchor/Trapdoor Embedded in an Associated Coulomb Soil." *International Journal for Numerical and Analytical Methods in Geomechanics*, 22, pp. 855–865.
- Teng, W.C. (1962). *Foundation Design* (1st ed.). Prentice Hall Inc., USA.
- Terzaghi, K. (1948). *Soil Mechanics in Engineering Practice*. New York Wiley.
- Tiwari, B., and Al-Adhadh, A.R. (2014). "Influence of Relative Density on Static Soil–Structure Frictional Resistance of Dry and Saturated Sand." *Geotechnical and Geological Engineering*, 32, pp. 411-427.
- Toh, C.T., and Sloan, S.W. (1980). "Finite Element Analysis of Isotropic and Anisotropic Cohesive Soils with A View to Correctly Predicting Impending Collapse." *International Journal for Numerical and Analytical Methods in Geomechanics*, 4, pp. 1-23.
- Turner, E.Z. (1962). "Uplift Resistance of Transmission Tower Footings." *Journal of the Power Division, ASCE*, 88(2), pp. 17–34.
- Zhao, L., Li, L., Yang, F., and Liu, X. (2011). "Joined Influences of Nonlinearity and Dilation on the Ultimate Pullout Capacity of Horizontal Shallow Plate Anchors by Energy Dissipation Method." *International Journal of Geomechanics*, 11(3), pp. 195-201.

APPENDIX A

Simple integrations performed to obtain the close form solution from Eq. (4.60) and Eq. (4.71) are presented below.

$$\begin{aligned}
 I &= \int e^{mx} \sin x \, dx \\
 &= \sin x \int e^{mx} \, dx - \left\{ \frac{d}{dx} (\sin x) \int e^{mx} \, dx \right\} dx \\
 &= \sin x \frac{1}{m} e^{mx} - \int \cos x \frac{e^{mx}}{m} \, dx \\
 &= \frac{1}{m} e^{mx} \sin x - \frac{1}{m} \int e^{mx} \cos x \, dx \\
 &= \frac{1}{m} e^{mx} \sin x - \frac{1}{m} \left[\cos x \int e^{mx} \, dx \right. \\
 &\quad \left. - \int \left\{ \frac{d}{dx} (\cos x) \int e^{mx} \, dx \right\} dx \right] \\
 &= \frac{1}{m} e^{mx} \sin x - \frac{1}{m} \left[\cos x \frac{e^{mx}}{m} + \int \frac{\sin x e^{mx}}{m} \, dx \right] \\
 &= \frac{1}{m} e^{mx} \sin x - \frac{1}{m} \left[\cos x \frac{e^{mx}}{m} + \frac{1}{m} \int \sin x e^{mx} \, dx \right] \\
 &= \frac{1}{m} e^{mx} \sin x - \frac{1}{m^2} e^{mx} \cos x - \frac{1}{m^2} I
 \end{aligned}$$

Using some side change simplification,

$$\begin{aligned}
 I + \frac{1}{m^2} I &= \frac{1}{m} e^{mx} \sin x - \frac{1}{m^2} e^{mx} \cos x \\
 \left(1 + \frac{1}{m^2} \right) I &= e^{mx} \left(\frac{1}{m} \sin x - \frac{1}{m^2} \cos x \right) \\
 \therefore I &= \frac{m^2}{m^2 + 1} e^{mx} \left(\frac{\sin x}{m} - \frac{\cos x}{m^2} \right)
 \end{aligned}$$

Now putting the limits of angle, we get,

$$\begin{aligned}
 \int_0^{\theta_m} e^{mx} \sin x \, dx &= \frac{m^2}{m^2 + 1} \left[e^{m\theta_m} \left(\frac{\sin \theta_m}{m} - \frac{\cos \theta_m}{m^2} \right) - \frac{1}{m^2} \right] \\
 \therefore \int_0^{\theta_m} e^{mx} \sin x \, dx &= \frac{m^2}{m^2 + 1} \left[e^{m\theta_m} \left(\frac{\sin \theta_m}{m} - \frac{\cos \theta_m}{m^2} \right) \right] - \frac{1}{m^2 + 1}
 \end{aligned}$$

Here $m = \tan \varphi'$ or, $-\tan \varphi'$.

$$\int e^{2\theta \tan \varphi'} \sin 2\theta \, d\theta$$

$$\text{Let, } 2\theta = x$$

$$\therefore 2d\theta = dx$$

$$\therefore \frac{1}{2} \int e^{x \tan \varphi'} \sin x \, dx = \frac{1}{2} I$$

If, $m = \tan \varphi$ then, $I = I_1$ and if, $m = -\tan \varphi'$ then, $I = I_2$

The charts corresponding to I_1 and I_2 are provided in the later part of the Appendix.

Again,

$$\begin{aligned} J &= \int e^{mx} \cos x \, dx \\ &= \cos x \int e^{mx} \, dx - \int \left\{ \frac{d}{dx} (\cos x) \int e^{mx} \, dx \right\} dx \\ &= \cos x \frac{e^{mx}}{m} + \int \sin x \frac{e^{mx}}{m} \, dx \\ &= \frac{1}{m} e^{mx} \cos x + \frac{1}{m} \int e^{mx} \sin x \, dx \\ &= \frac{1}{m} e^{mx} \cos x + \frac{1}{m} \left[\sin x \int e^{mx} \, dx \right. \\ &\quad \left. - \int \left\{ \frac{d}{dx} (\sin x) \int e^{mx} \, dx \right\} dx \right] \\ &= \frac{1}{m} e^{mx} \cos x + \frac{1}{m} \left[\frac{\sin x e^{mx}}{m} - \int \frac{\cos x e^{mx}}{m} \, dx \right] \\ &= \frac{1}{m} e^{mx} \cos x + \frac{1}{m^2} e^{mx} \sin x - \frac{1}{m^2} \int e^{mx} \cos x \, dx \\ &= \frac{1}{m} e^{mx} \cos x + \frac{1}{m^2} e^{mx} \sin x - \frac{1}{m^2} J \end{aligned}$$

Using some side change simplification,

$$\begin{aligned} J + \frac{1}{m^2} J &= e^{mx} \left(\frac{\cos x}{m} + \frac{\sin x}{m^2} \right) \\ \left(1 + \frac{1}{m^2} \right) J &= e^{mx} \left(\frac{\cos x}{m} + \frac{\sin x}{m^2} \right) \end{aligned}$$

$$\therefore J = \frac{m^2}{m^2 + 1} e^{mx} \left(\frac{\cos x}{m} + \frac{\sin x}{m^2} \right)$$

Now putting the limits of angle, we get,

$$\int_0^{\theta_m} e^{mx} \cos x \, dx = \frac{m^2}{m^2 + 1} \left[e^{m\theta_m} \left(\frac{\cos \theta_m}{m} + \frac{\sin \theta_m}{m^2} \right) - \frac{1}{m^2} \right]$$

$$\therefore \int_0^{\theta_m} e^{mx} \cos x \, dx = \frac{m^2}{m^2 + 1} \left[e^{m\theta_m} \left(\frac{\cos \theta_m}{m} + \frac{\sin \theta_m}{m^2} \right) \right] - \frac{m}{m^2 + 1}$$

Here, $m = \tan \varphi'$ or $-\tan \varphi'$

$$\int e^{2\theta \tan \varphi'} \cos 2\theta \, d\theta$$

$$\text{Let, } 2\theta = x$$

$$2d\theta = dx$$

$$\therefore \frac{1}{2} \int e^{x \tan \varphi'} \cos x \, dx = \frac{1}{2} J$$

If, $m = \tan \varphi'$ then, $J = J_1$ and if, $m = -\tan \varphi'$ then, $J = J_2$

The charts corresponding to I_1 and I_2 are provided in Appendix C.

Area calculation of Zone *ODE* in Figure 4.7

$$A = \int_0^{\theta_m} \frac{1}{2} r (r d\theta) \quad (4.121)$$

$$= \frac{1}{2} \int_0^{\theta_m} r^2 d\theta$$

$$= \frac{1}{2} \int_0^{\theta_m} r_0^2 e^{2\theta \tan \varphi'} d\theta \quad [\because r = r_0 e^{\theta \tan \varphi'}]$$

$$= \frac{1}{2} r_0^2 \left[\frac{e^{2\theta \tan \varphi'}}{2 \tan \varphi'} \right]_0^{\theta_m}$$

$$= \frac{r_0^2}{4 \tan \varphi'} [e^{2\theta \tan \varphi'} - 1]$$

$$= \frac{r_0^2 e^{2\theta \tan \varphi'} - r_0^2}{4 \tan \varphi'}$$

$$\therefore A = \frac{r_1^2 - r_0^2}{4 \tan \varphi'} \quad (4.122)$$

α' can be determined using the following procedure.

$$OA^2 + \bar{m}^2 = \bar{n}^2 + OC^2 \quad (4.139)$$

$$\text{or, } \frac{\bar{m}^2}{(\tan \alpha')^2} + \bar{m}^2 = \frac{\bar{n}^2}{\{\tan(\theta_m - \alpha')\}^2} + \bar{n}^2$$

$$\text{or, } \bar{m}^2 \left\{ 1 + \frac{1}{(\tan \alpha')^2} \right\} = \bar{n}^2 \left[1 + \frac{1}{\{\tan(\theta_m - \alpha')\}^2} \right]$$

$$\text{or, } \bar{m}^2 \left\{ \frac{1 + (\tan \alpha')^2}{(\tan \alpha')^2} \right\} = \bar{n}^2 \left[\frac{1 + \{\tan(\theta_m - \alpha')\}^2}{\{\tan(\theta_m - \alpha')\}^2} \right]$$

$$\text{or, } \bar{m}^2 \frac{1}{(\sin \alpha')^2} = \bar{n}^2 \frac{1}{\{\sin(\theta_m - \alpha')\}^2}$$

$$\text{or, } \frac{\{\sin(\theta_m - \alpha')\}^2}{(\sin \alpha')^2} = \frac{\bar{n}^2}{\bar{m}^2}$$

$$\text{or, } \frac{\{\sin(\theta_m - \alpha')\}}{(\sin \alpha')} = \frac{\bar{n}}{\bar{m}}$$

$$\text{or, } \frac{\sin \theta_m \cdot \cos \alpha' - \cos \theta_m \cdot \sin \alpha'}{\sin \alpha'} = \frac{\bar{n}}{\bar{m}}$$

$$\text{or, } \frac{\sin \theta_m}{\tan \alpha'} - \cos \theta_m = \frac{\bar{n}}{\bar{m}}$$

$$\text{or, } \frac{\bar{n}}{\bar{m}} + \cos \theta_m = \frac{\sin \theta_m}{\tan \alpha'}$$

$$\text{or, } \alpha' = \tan^{-1} \left[\frac{\sin \theta_m}{\frac{\bar{n}}{\bar{m}} + \cos \theta_m} \right] \quad (4.142)$$

APPENDIX B

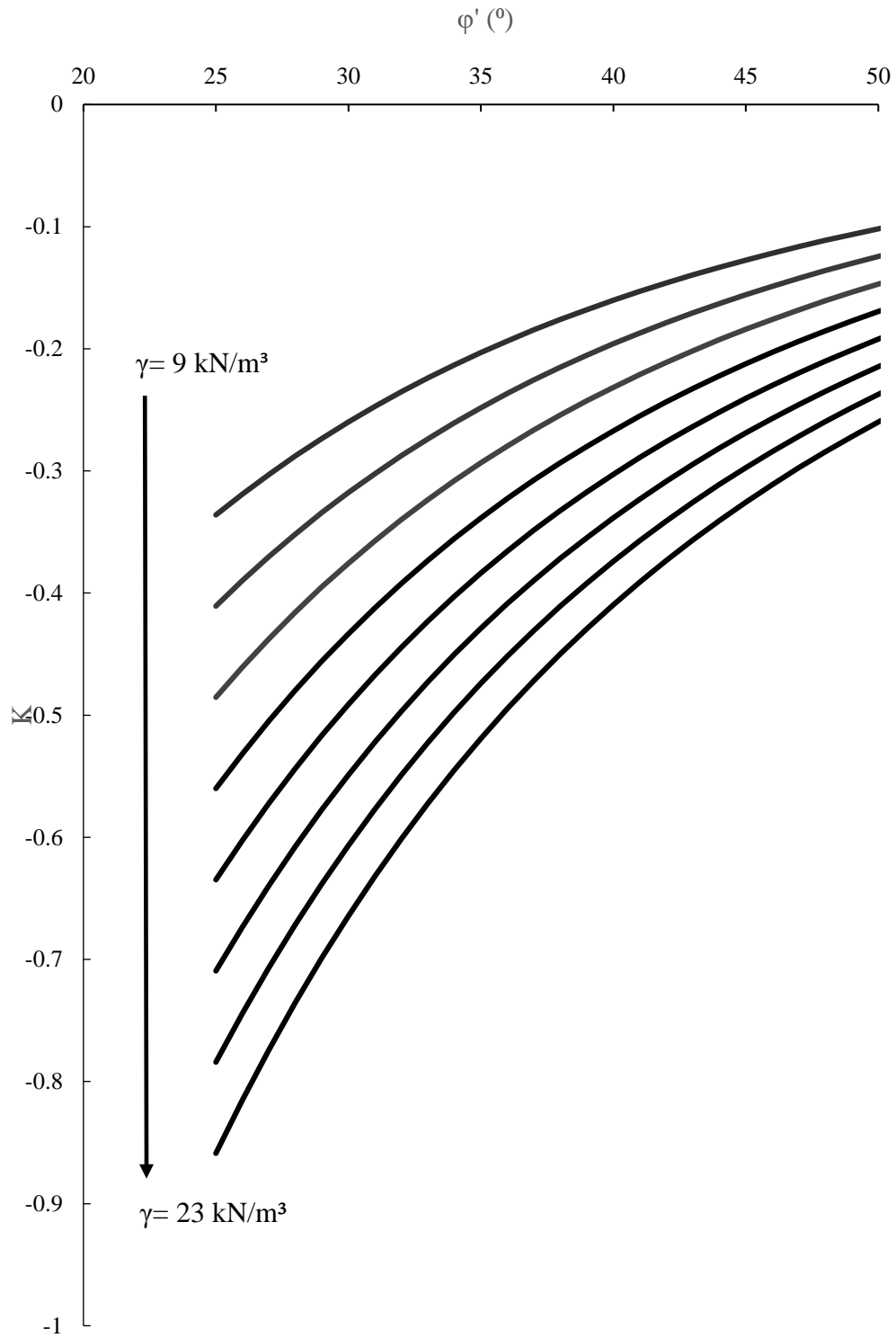


Figure B-1 Variation of K with the change of ϕ' and γ for a 0.1m high anchor

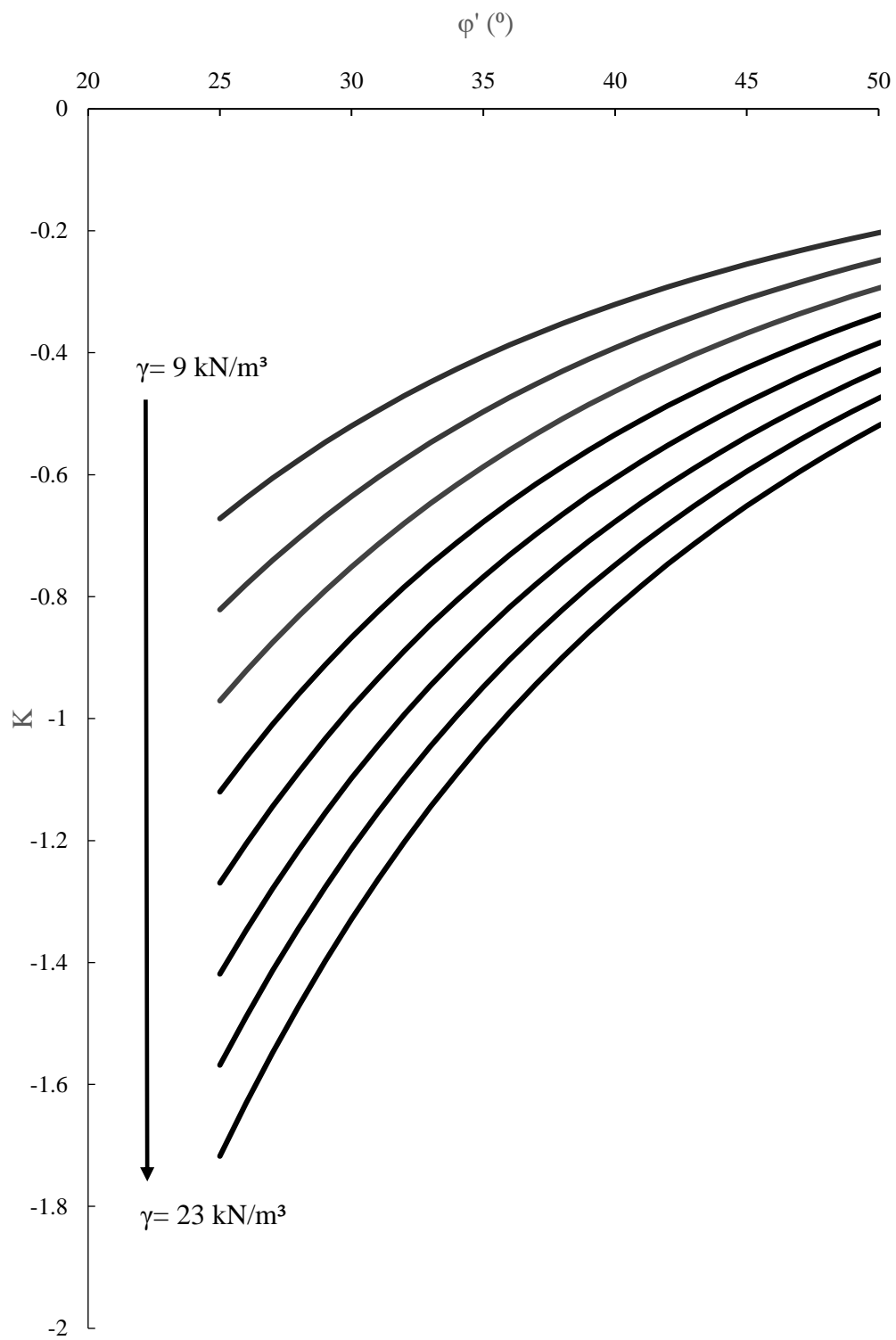


Figure B-2 Variation of K with the change of ϕ' and γ for a 0.2m high anchor

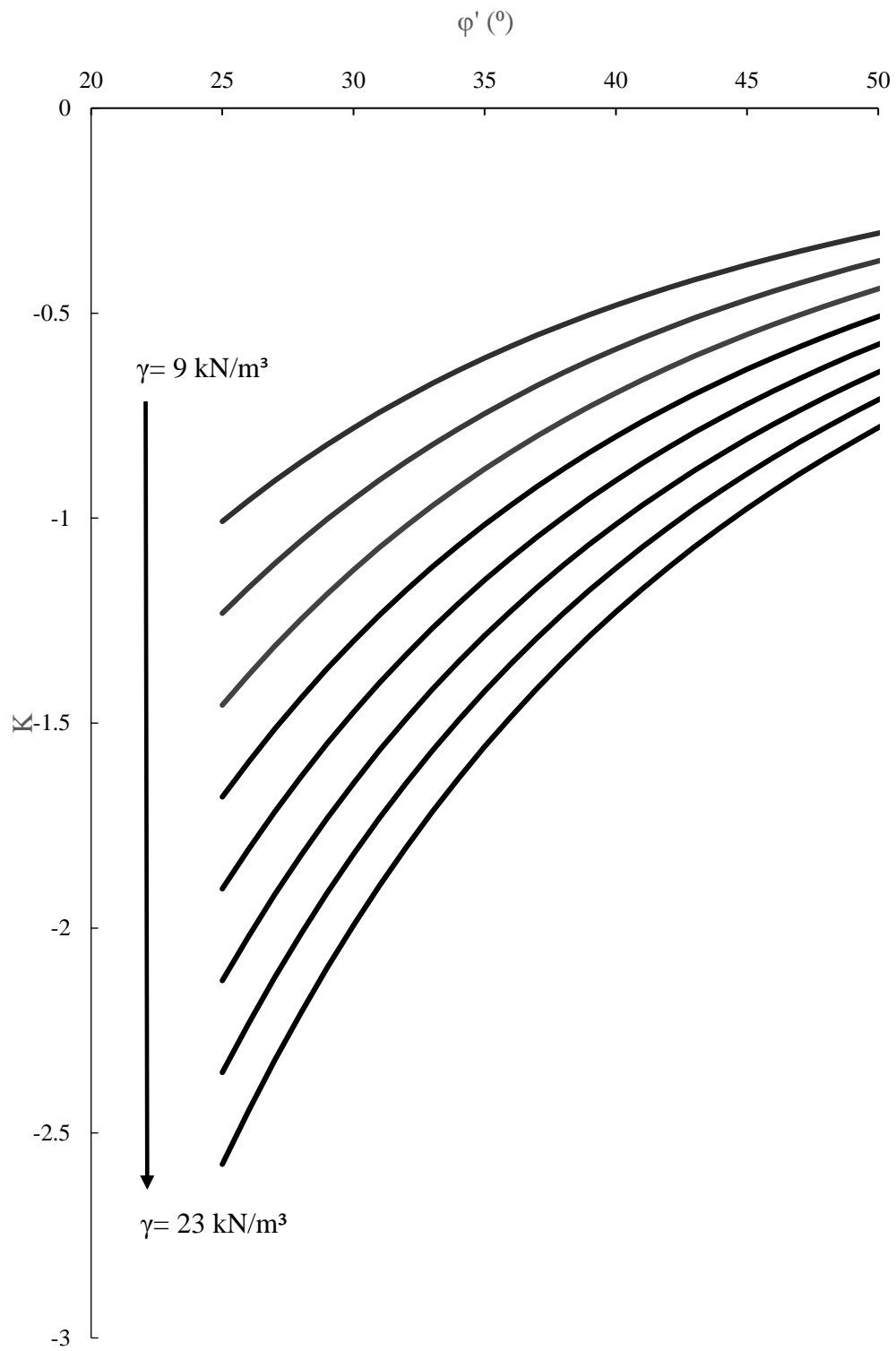


Figure B-3 Variation of K with the change of ϕ' and γ for a 0.3m high anchor

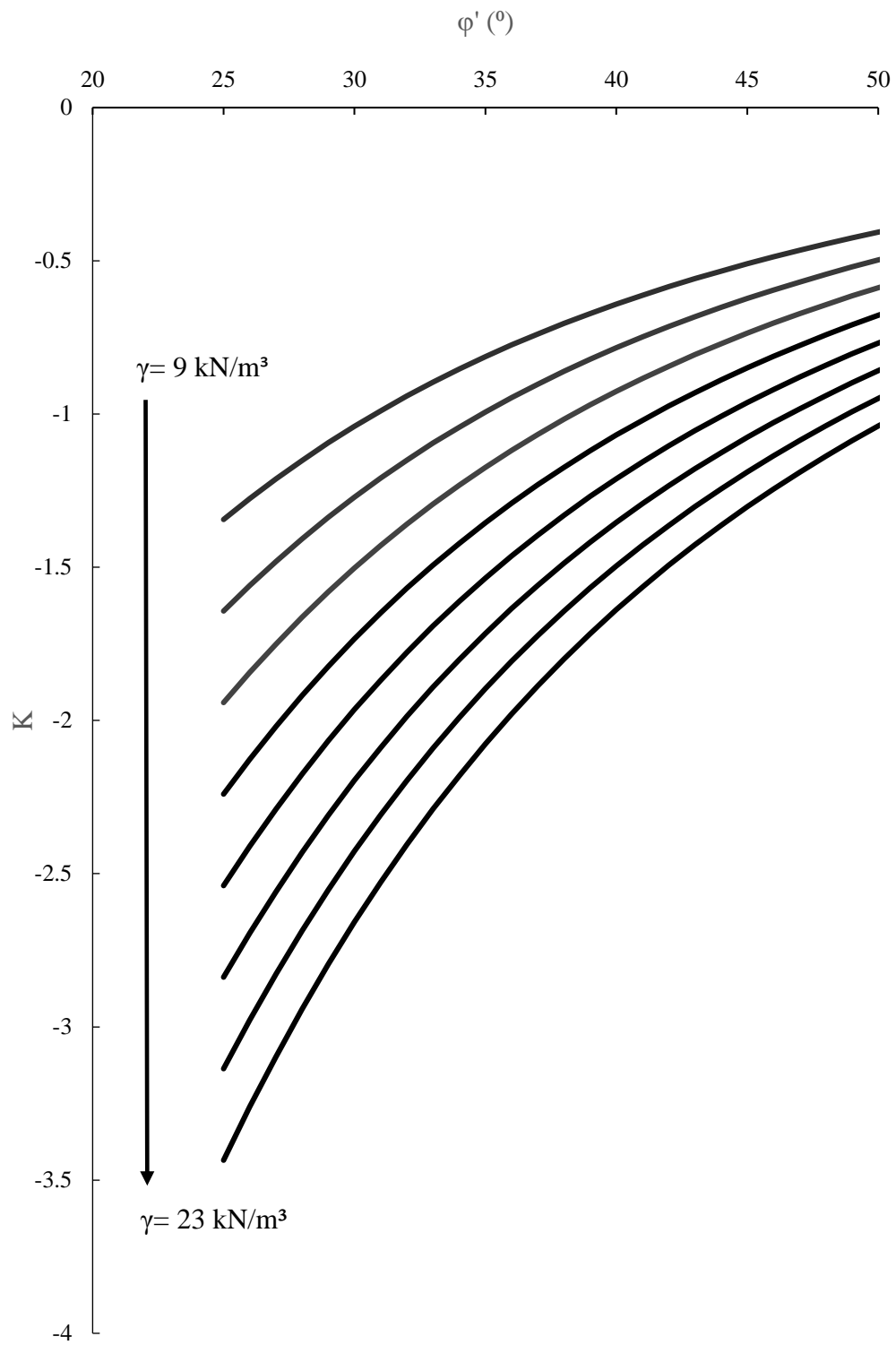


Figure B-4 Variation of K with the change of ϕ' and γ for a 0.4m high anchor

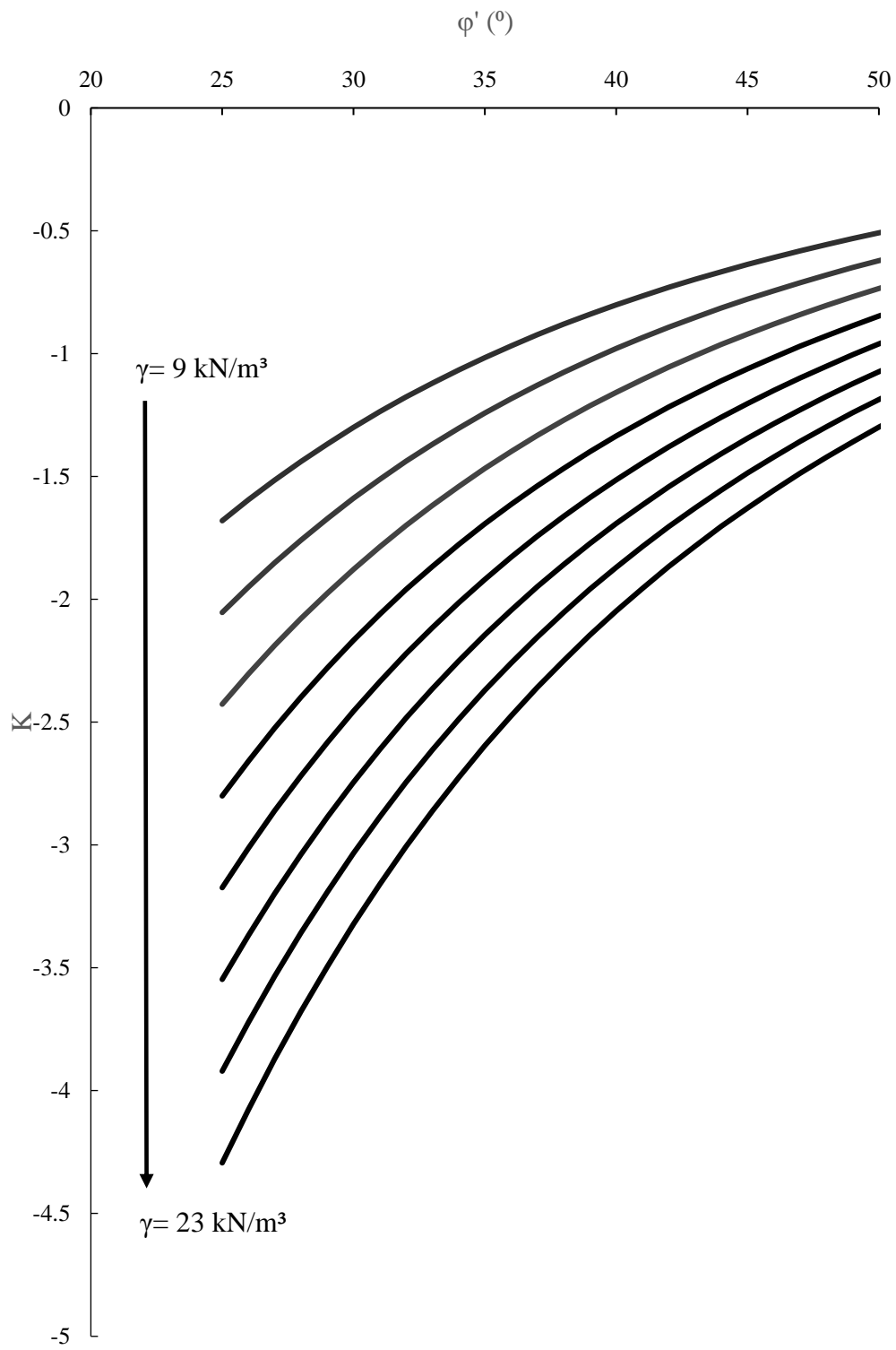


Figure B-5 Variation of K with the change of ϕ' and γ for a 0.5m high anchor

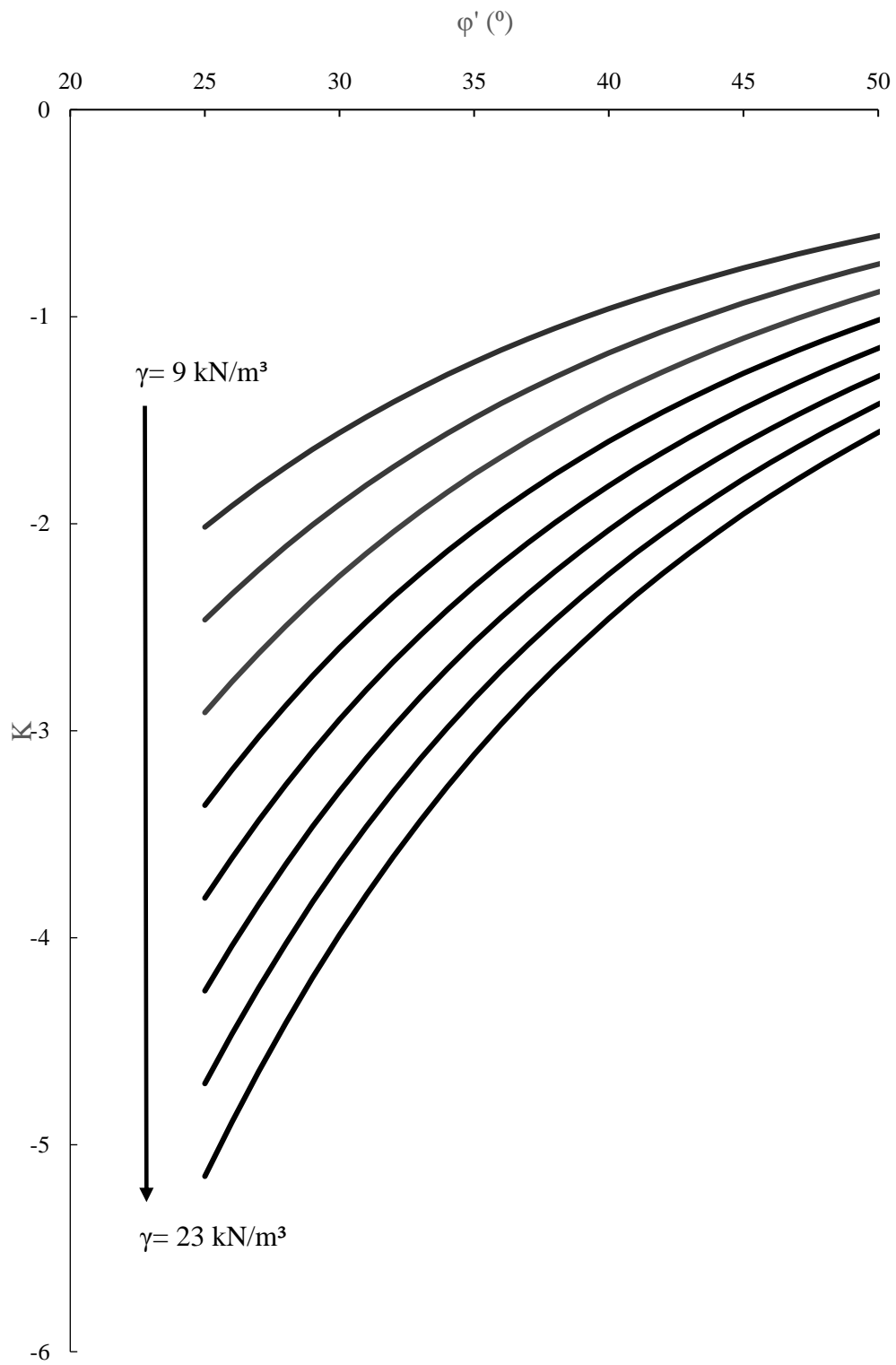


Figure B-6 Variation of K with the change of ϕ' and γ for a 0.6m high anchor

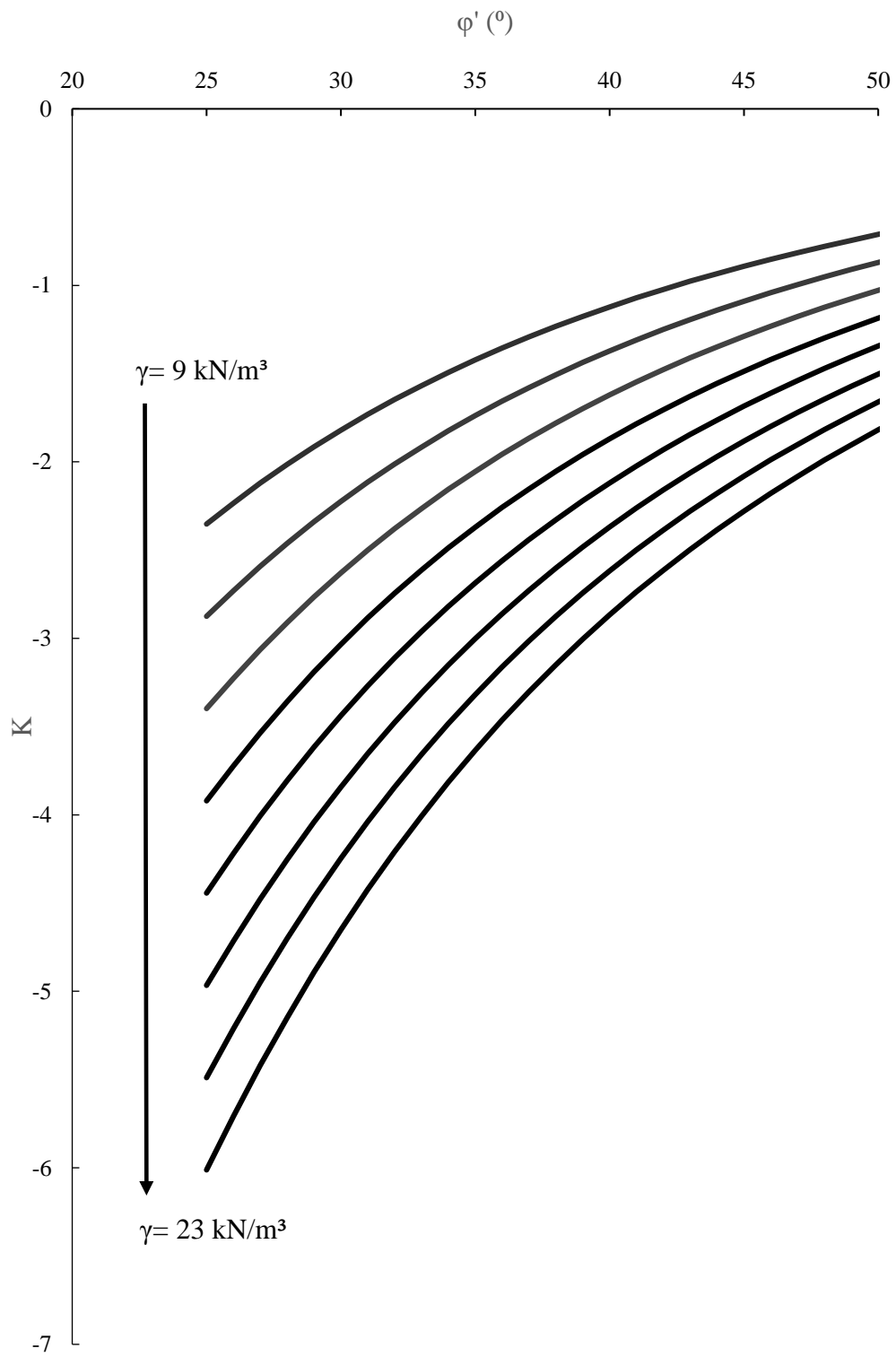


Figure B-7 Variation of K with the change of ϕ' and γ for a 0.7m high anchor

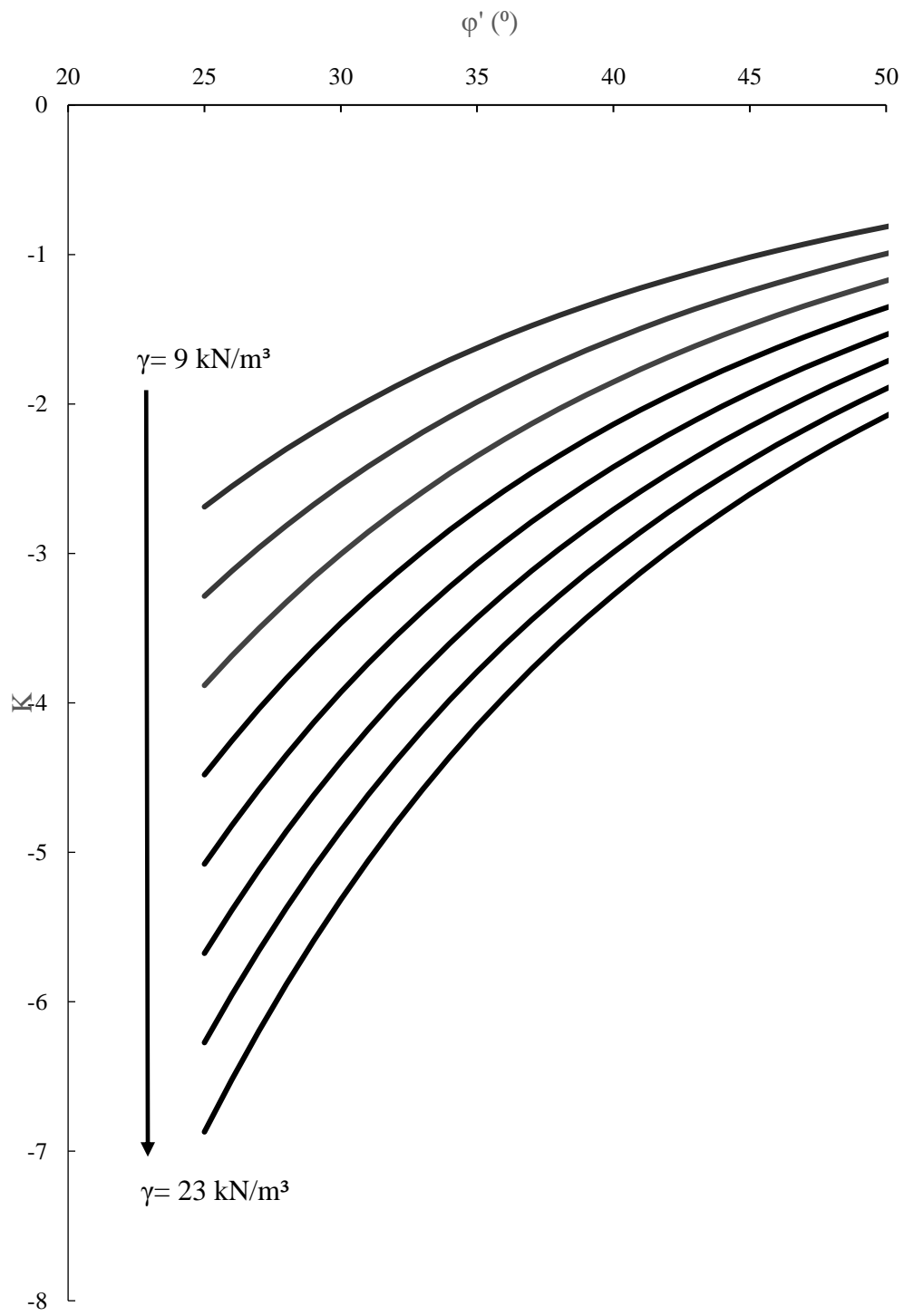


Figure B-8 Variation of K with the change of ϕ' and γ for a 0.8m high anchor

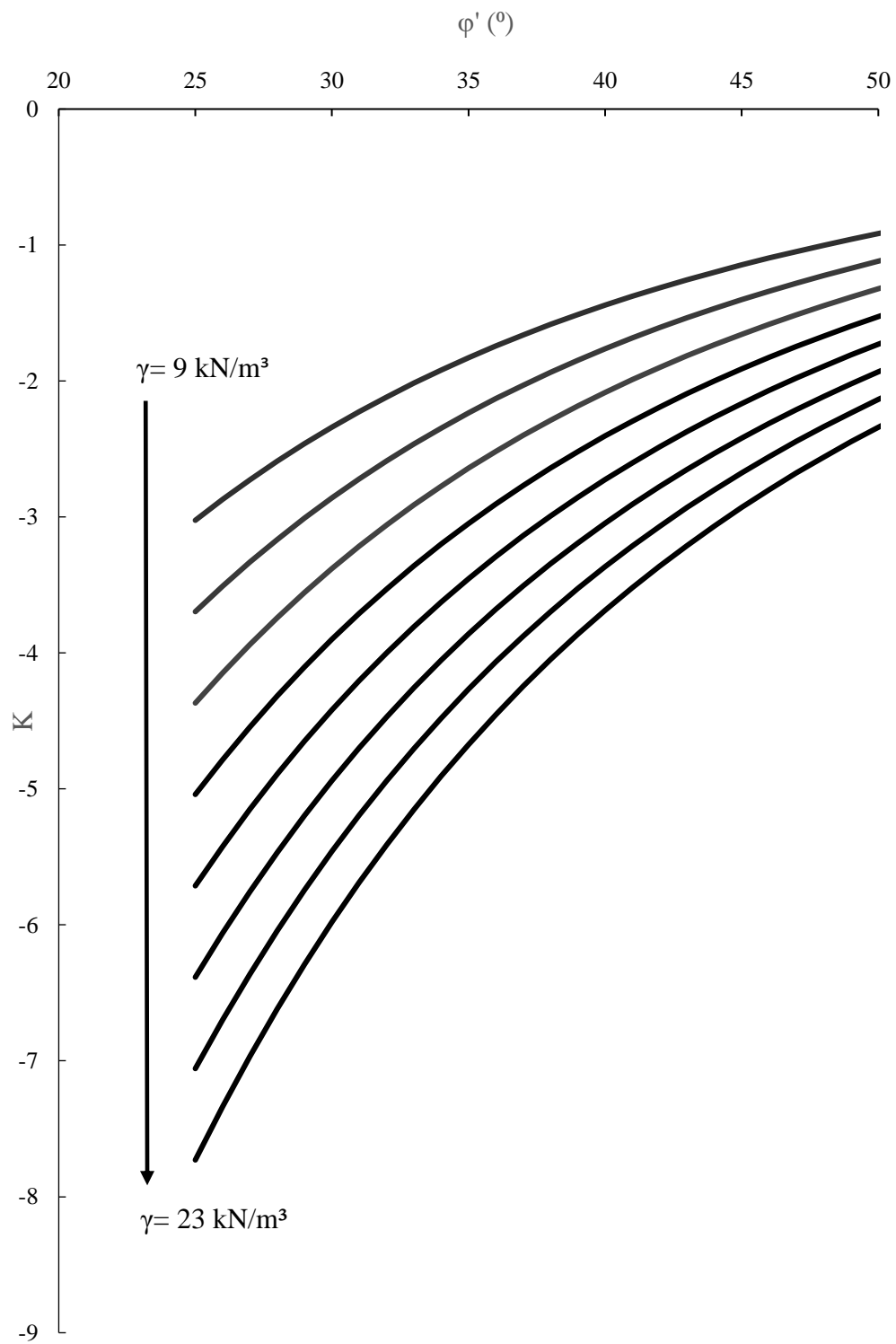


Figure B-9 Variation of K with the change of ϕ' and γ for a 0.9m high anchor

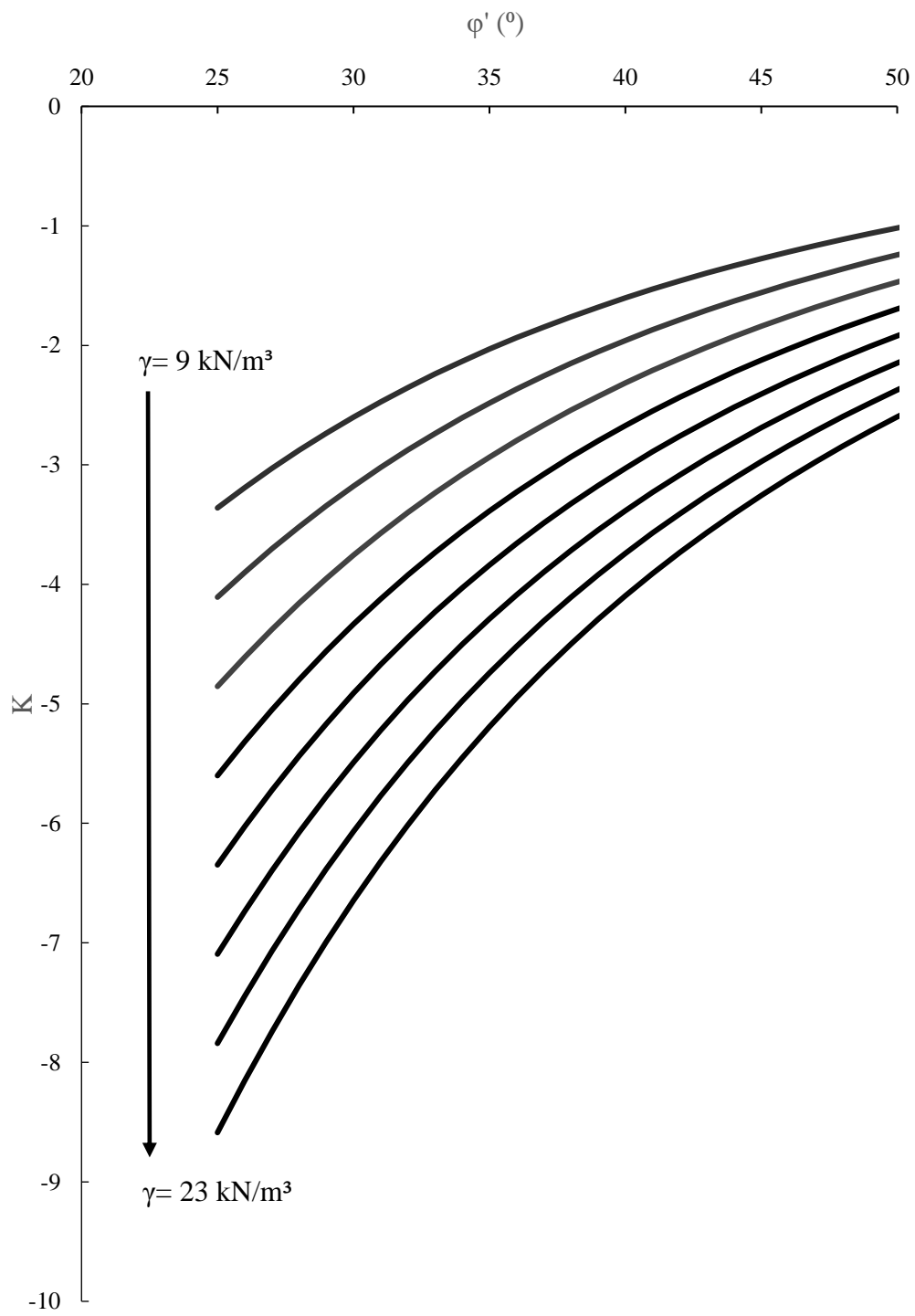


Figure B-10 Variation of K with the change of ϕ' and γ for a 1.0m high anchor

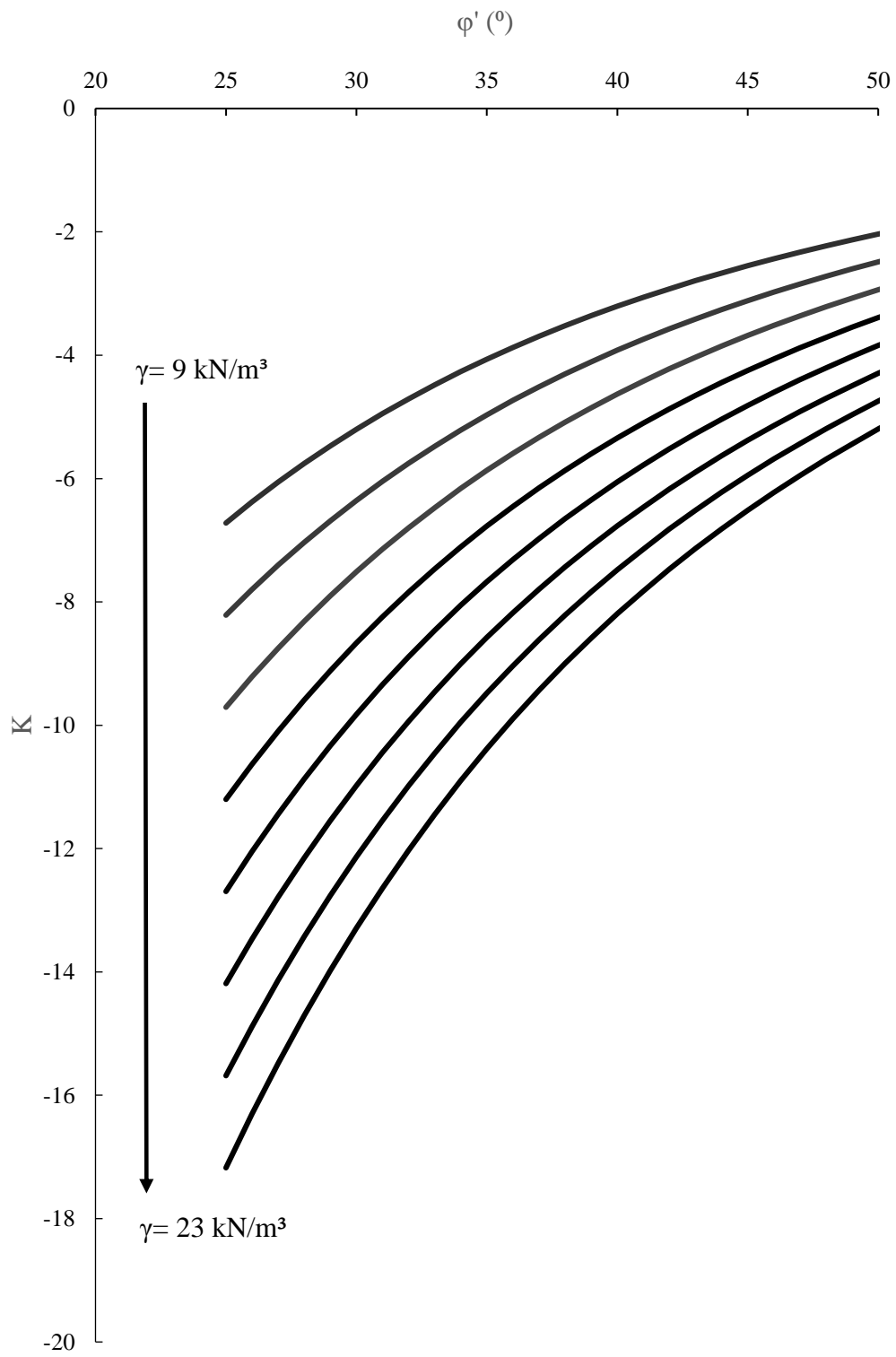


Figure B-11 Variation of K with the change of ϕ and γ for a 2.0m high anchor

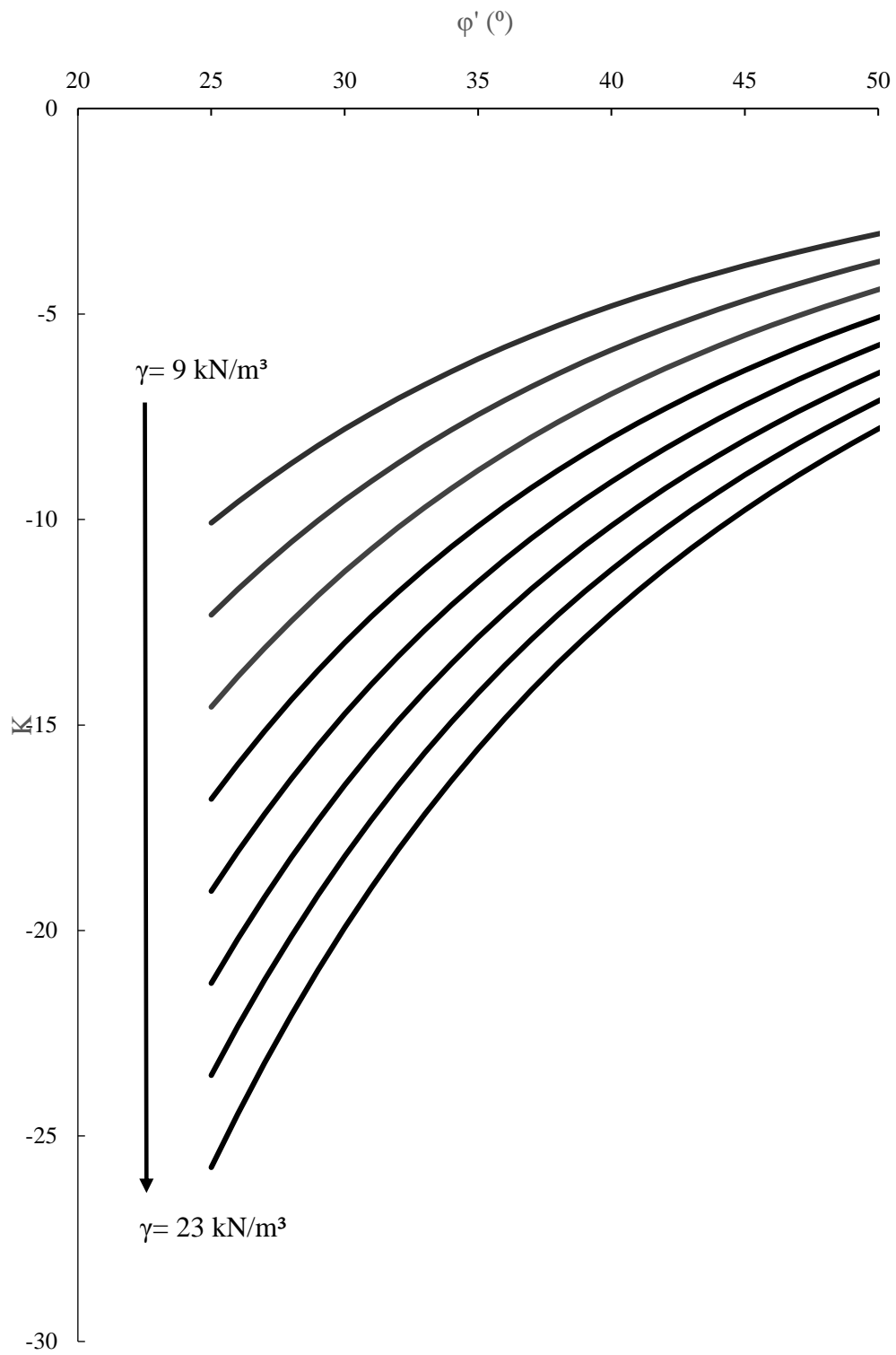


Figure B-12 Variation of K with the change of ϕ' and γ for a 3.0m high anchor

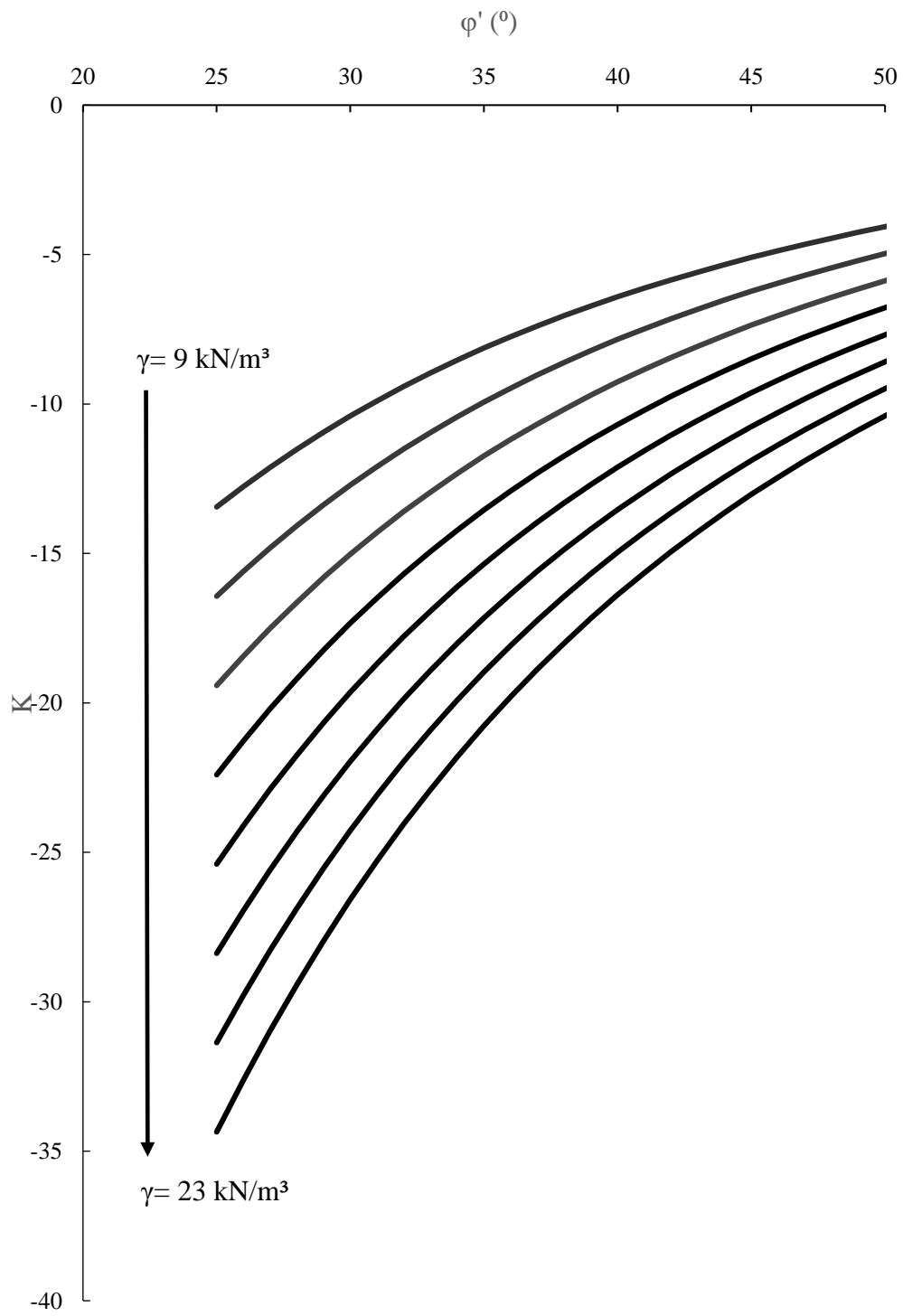


Figure B-13 Variation of K with the change of ϕ' and γ for a 4.0m high anchor

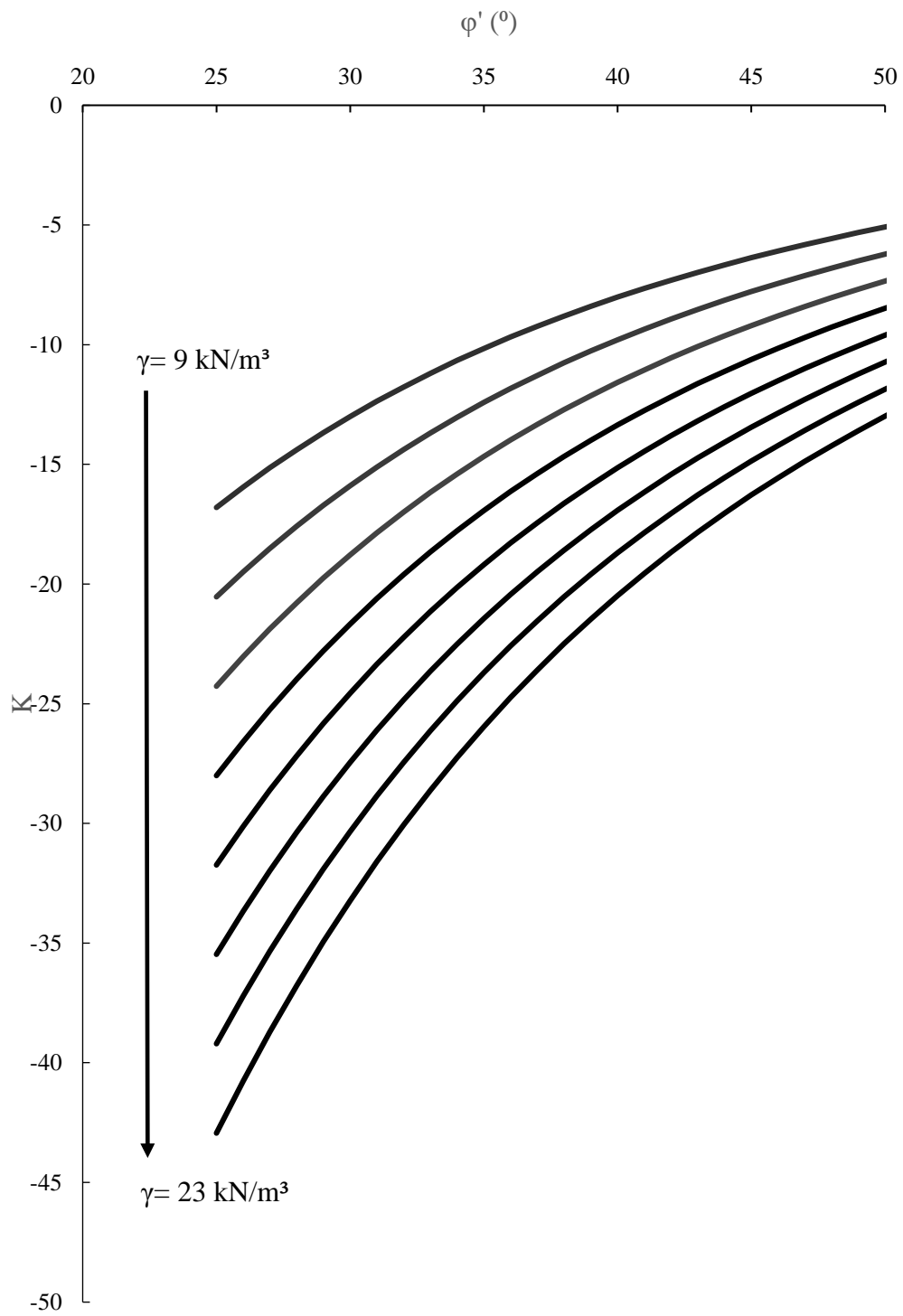


Figure B-14 Variation of K with the change of ϕ' and γ for a 5.0m high anchor

APPENDIX C

Table C-1 Integrals and k value corresponding to a given φ'

φ' (°)	J_1	I_1	J_2	I_2	k
25	1.052	-1.010	0.68799	-1.30010	1.59593918
26	1.071	-0.962	0.68471	-1.27305	1.63752982
27	1.090	-0.912	0.68122	-1.24545	1.68146203
28	1.110	-0.859	0.67754	-1.21733	1.72792304
29	1.131	-0.806	0.67365	-1.18874	1.77711966
30	1.152	-0.750	0.66956	-1.15972	1.82928083
31	1.175	-0.692	0.66527	-1.13030	1.88466048
32	1.198	-0.633	0.66078	-1.10053	1.94354099
33	1.222	-0.571	0.65608	-1.07045	2.00623702
34	1.247	-0.507	0.65118	-1.04010	2.07310012
35	1.273	-0.442	0.64607	-1.00952	2.14452406
36	1.301	-0.373	0.64075	-0.97876	2.22095106
37	1.330	-0.302	0.63522	-0.94787	2.30287913
38	1.360	-0.229	0.62948	-0.91688	2.39087078
39	1.391	-0.153	0.62353	-0.88585	2.48556329
40	1.425	-0.073	0.61737	-0.85481	2.58768094
41	1.460	0.009	0.61099	-0.82381	2.69804971
42	1.497	0.096	0.60440	-0.79289	2.81761481
43	1.536	0.186	0.59759	-0.76211	2.94746192
44	1.578	0.280	0.59056	-0.73151	3.0888429
45	1.622	0.379	0.58331	-0.70112	3.24320714
46	1.669	0.483	0.57583	-0.67100	3.41223998
47	1.720	0.593	0.56813	-0.64118	3.59791001
48	1.774	0.710	0.56021	-0.61172	3.80252775
49	1.832	0.833	0.55205	-0.58265	4.02881885
50	1.895	0.965	0.54366	-0.55401	4.28001601
51	1.963	1.107	0.53504	-0.52585	4.55997526
52	2.037	1.259	0.52618	-0.49821	4.87332411